NASA CONTRACTOR REPORT

NASA CR-1831

NASA CR-1831

THE THEORETICAL AND EXPERIMENTAL INVESTIGATIONS ON MULTIPLE PURE TONE NOISE – PART I

by R. A. Kantola and M. Kurosaka

Prepared by
GENERAL ELECTRIC RESEARCH AND DEVELOPMENT CENTER
Schenectady, N.Y.
for

NATIONAL AERONAUTICS AND SPACE ADMINISTRATION • WASHINGTON, D. C. • NOVEMBER 1971

1. Report No. NASA CR-1831	2. Government Accession No.	3. Recipient's Catalog No.
4. Title and Subtitle THE THEORETICAL AND EXPERIMENTAL INVESTIGATIONS ON MULTIPLE PURE TONE NOISE - PART I		5. Report Date November 1971 6. Performing Organization Code
7. Author(s) R. A. Kantola and M. Kurosaka		8. Performing Organization Report No. 10. Work Unit No.
9. Performing Organization Name and Address General Electric Research and Development Center Schenectady, New York		11. Contract or Grant No. NASW-1922
12. Sponsoring Agency Name and Address National Aeronautics and Space Administration Washington, D. C., 20546		13. Type of Report and Period Covered Contractor Report 14. Sponsoring Agency Code

15. Supplementary Notes

Part II "The Calculation of Optimal Linings for Jet Engine Inlet Ducts" by J.P.D. Wilkinson - NASA CR-1832

16. Abstract

A theoretical and experimental investigation is described on multiple pure tone noise. Based on a two-dimensional and inviscid flow model, an analysis is developed to predict the generation and subsequent evolution of multiple pure tone noise from prescribed blade-to-blade nonuniformities in the rotor geometry. The results show that even small nonuniformities within manufacturing tolerances can cause a significant amount of multiple pure tone noise. Among the different kinds of nonuniformities investigated, errors in blade spacings are a weaker generator of multiple pure tone noise than errors in blade stagger or blade contours. Experimental investigations of the effects of the rotor relative Mach number, incidence angle and length of the inlet duct on the evolution of the multiple pure tone noise are conducted with a known distribution of rotor nonuniformities. The model fan is operated, in Freon 12, in a closed loop acoustical facility. In order to compare the analysis with the experimental results, the MPT distributions are computed from the known blade nonuniformities of the model fan. Due to the difficulty of measuring the blade contour on blades only 0.59 inches long, the important MPT contribution due to contour nonuniformity is not included. For this reason an exact comparison between theoretical and experimental results is not achieved. However, the computed result correctly predicts the position of the maximum peak of multiple pure tones in the frequency spectrum and predicts a sound pressure of the blade passing frequency noise that is in the same range as the experimental values.

17. Key Words (Suggested by Author(s))	18. Distribution Statement
Noise, Fan engines	Unclassified - Unlimited

19. Security Classif. (of this report)	20. Security Classif. (of this page)	21. No. of Pages	22. Price*
Unclassified	Unclassified	157	$3.00

*For sale by the National Technical Information Service, Springfield, Virginia 22151

FOREWORD

This report was prepared under Contract No. NASW-1922 for NASA Headquarters, Office of Advanced Research and Technology, Research Division, under the technical direction of Mr. I. R. Schwartz. The work was conducted at the Mechanical Engineering Laboratory, General Electric Research and Development Center in Schenectady, New York.

TABLE OF CONTENTS

LIST OF FIGURES

LIST OF TABLES

1.0 INTRODUCTION

In recent years the reduction of jet engine noise has been dramatic. These improvements have largely been concentrated on the blade passing frequencies and their higher harmonics. The contributions of these components has been so reduced that attention is now being focused on the next most objectionable sound emanating from the jet engine, that is, the multiple pure tone sound.

Multiple pure tone sound from aircraft engines is characterized by its noise spectra containing numerous spikes at shaft rotational frequency. Often some of the spikes prevail over the spikes at blade passing frequency and are thus quite audible. The response of human ears to multiple pure tone sound (abbreviated as MPT sound) is distinctly different from the response to blade passing frequency sound. Most people hear blade passing frequency sound as a shrill whine. MPT is perceived as a much lower tone and more ragged type of sound. MPT is also called "buzz saw" sound because it is allegedly similar to the sound from a circular buzz saw.

Recently published works of Kester (Ref. 1), Sofrin and Pickett (Ref. 2) and Philpot (Ref. 3) experimentally established the essential features of the MPT. First, the MPT sound from the current fan begins to dominate over the blade passing frequency sound when the relative tip speed of the fan exceeds sonic velocity. Second, it radiates only from the inlet duct of the fan and not out of the discharge duct. Third, and most important of all, the MPT signal is highly repetitive over each revolution of the rotor. These observed characteristics of the MPT suggests strongly that bow shock waves from fan tip are responsible for the generation of the MPT. Refs. 1 and 2 present convincing evidence that this is indeed the cause.

When the relative Mach number of the fan tip exceeds unity, bow shocks emanate from the leading edge of each blade and, as long as the axial velocity remains subsonic, one branch of bow shocks propagates away from and upstream of the rotor. These bow shocks are locked to and spinning with the rotor. In the absence of any geometric aberration of the blade, the bow shocks would be spatially uniform in strength and spacing (except for the monotonic attenuation with distance from the rotor). However, references 1 and 2 report that the pressure pattern in the compressor casing indicates an increasingly nonuniform shock pattern with increasing axial distance upstream of the rotor plane. Since the shock waves are spinning with the rotor, a stationary observer is swept by this shock pattern irregular both in spacings and strength but repetitive at each revolution of rotor. Thus the fundamental harmonic of such a sound is at the rotor frequency.

Were the shock patterns uniform, the fundamentals would be at the blade passing frequency. The causes of such irregular shock pattern amplification has been suggested to be the nonuniformity in the geometry of the blades in an actual fan. Although this is the most plausible explanation, it appears not to be positively confirmed. Manufacturing tolerances of conventional fans are usually very small and it is therefore a legitimate question to ask whether such small nonuniformities in the blades could be responsible for the generation and evolution of MPT. MPT sound does exist even in subsonic fans if the fan blades are designed deliberately to be nonuniform. However, in order to obtain substantial MPT sound, the nonuniformity of the blade has to be so large that sometimes they impair the other requirements.

The specific objectives of the present investigation are as follows:

(1) First, to confirm both analytically and experimentally, whether the lack of uniformity of blade geometry within the manufacturing tolerances are responsible for the MPT sound.

(2) Second, to determine whether different types of nonuniformities can be characterized by their effect on the generation of the MPT sound.

(3) Third, to determine the effect of the relative Mach number and the flow angle on the evolution of the MPT sound.

(4) Fourth, to determine the effect of the inlet duct length on the MPT sound generation.

In the section immediately following, section 2, the analytical method of MPT prediction is described. Section 3 presents the results based on the analysis. Section 4 discusses the experimental approach and facilities. Section 5 presents the conclusions and recommendation for future work.

2.0 ANALYSIS

2.1 Problem Statement and Assumptions

The problem to be analyzed may be posed as follows:

Given a rotor with blades of known geometrical non-uniformities, compute the pressure field upstream of the rotor.

To repeat the final objective, the goal is to examine if the small errors within the manufacturing tolerances are responsible for the MPT.

Needless to say, simplifications are needed to grapple with the above problem and the following assumptions are adopted:

(1) There are no inlet guide vanes.

(2) The bow shocks are attached to the leading edges of the blades.

(3) The flow field can be approximated by a two-dimensional model.

(4) The diffusive effects due to viscosity and heat conductivity are neglected.

Some remarks are needed to justify assumptions (3) and (4). A question might be raised as to the validity of two-dimensional assumption (3) in the conventional supersonic fan design where relative Mach number near the hub is still subsonic. According to the theoretical study performed by McCune (Refs. 4 and 5), the three-dimensional effects for such fans are so large that strip theory is hardly adequate. However, diagonally opposite experimentally evidence, which seems to lend support to the present assumption, was presented in Ref. 2 where three-dimensional effects were investigated. By inserting an annular sleeve in the vicinity of the tip, they eliminated interference in the radial direction. Comparison between the shock patterns with the evolution of irregular shock patterns. Support of assumption (4) is also found in Ref. 2. According to their measurements, starting from a chord length or so away from the rotor, the decay rate of average shock strength was found to be inversely proportional to the axial distance. According to Blackstock (Ref. 6) this decay rate is precisely that which can be predicted by treating the flow everywhere as nondissipative (with the exception of inside the shock wave) provided the axial distance from the rotor is not too large; whereas a dissipative model should show exponential decay. Therefore it seems that assumption (4) is valid provided the attention

is restricted to the near and intermediate field region of the rotor. It is a fortuitous circumstance that despite the fact that the wall boundary layer along the outer casing exists in the vicinity of the tip shock, these dissipative effects on the shock decay at the outer edge of the boundary layers are negligible.

2.2 Outline of Analysis

Basically the whole analysis consists of the construction of shock-expansion wave diagram upstream of rotor. Complications arise because of mutual interference between blades. Before considering how to estimate the effects of blade nonuniformity on the wave system, it is instructive to consider the wave system for the ideal rotor without any asymmetry. Fig. 1 shows the wave system for such an idealized rotor and the description of the wave system is given in Reference 7. Since the grasp of the wave system for the idealized rotor is vital to the understanding of the next step, it is summarized below. As seen in Figure 1, part of the expansion fans emanating from the suction surface between A and C interact with the shock wave generated from the same blade, while the rest of the expansion fans between C and B interact with the shock wave emerging from the adjacent blade. The dividing Mach line C - C is the only wave not intercepted by the shock and extends to infinity. Point C is that location on the blade the tangent of which is parallel to the velocity direction at infinity. If we cannot find a surface tangent parallel to the velocity direction at infinity, this is an unsteady condition and after the transient emission of an expansion fan at the leading edge, the velocity at infinity adjusts itself until the proper conditions are established on the suction surface. The trajectory of the curved shock can be determined by locally applying oblique shock relations. The conditions ahead and behind the shock are known from the Prandtl-Meyer relation.

Having once grasped the above, it is immediately clear how to examine the nonuniform blade arrangement. We need only identify the change of position C from one blade to another due to the change in the geometry between blades. The rest is exactly the same as the idealized symmetrical rotor.

A computer program was written with which the wave diagram may be constructed. As the sources of nonuniformity, the following blade-to-blade errors were considered.

(1) Spacing between blades,

(2) Stagger angle, and

(3) Blade contour near the leading edge.

Given the distribution of these errors and the flow conditions far upstream as inputs, the program provides such outputs as the pressure distribution, its harmonic components and bow shock trajectories as functions of axial distance. The detailed description of the program is given in Appendix 1. We will present here only a few points pertinent to the wave construction procedure utilized.

Referring to Fig. 1 again, once point C is located on the first blade, the expansion fans between C and B can be constructed immediately. The expansion fan B intersects the leading edge of the 2nd blade, A'. From the wedge angle of the second blade, the initial shock shape can be constructed as A'P'. The flow immediately downstream of the shock (in the region 1) is also known. Now, according to the considerations at the beginning of this section, the flow in region 1 must accelerate and attain Mach number at infinity at point C' where again the tangent to the blade is parallel to the velocity far upstream. This might seem to be true only if the shock is extremely weak. However it turns out that this holds true even if the wedge angle is moderately large, say, 10 degrees or so. This results from the fact that reflection of the expansion wave by the shock is small and confirms the validity of locating point C' (and C) by the aforementioned principle. Resuming the procedure of determining bow shock trajectory, the next segment P'Q' can be determined by finding the oblique shock satisfying the known upstream and downstream conditions. The same process determines the complete wave system between two adjacent blades. There is one small salient point to be made here. In as much as in the downstream region (say, region 2) not only the flow direction but the velocity is known and the shock is determined solely by specifying either one of them, it appears that the problem is overdetermined and some conflicting results might show up by the particular choice of downstream condition between the two. Actually it turns out the choice is insignificant so long as the shock remains moderate in strength. In the computer program, the flow direction is taken as the known downstream condition.

2.3 Comparison with Hawkings' Method

After the completion of the present investigation, a recently published analysis of MPT by Hawkings (Ref. 8) came to the attention of the present investigators. Although the basic physical model of the shock-expansion fan interference and the assumptions are the same, there appears to be distinct differences between the two approaches. Hawkings' approach is essentially a one dimensional (plane), unsteady shock analysis, whereas the present method is a two-dimensional (non-planar), steady shock analysis. According to Hawkings, if one takes a direction normal to the average shock fronts,

theory of one-dimensional shock propagation is then applied to describe their time history. The time, of course, is related to the axial distance. In the present analysis, the shock is treated as two-dimensional. Although the shocks are actually two-dimensional because of their curvatures and blade-to-blade differences, one-dimensional assumption of Hawkings is probably a reasonably good one. Such an approach has the advantage of being able to preserve the analytical expressions up to the advanced stages of computation. The most crucial difference between the two methods are the following: In the Hawkings' analysis, the initial nonuniformity of pressure profile has to be specified in order to obtain the history of shock propagation and the relation between the nonuniform pressure profile and the nonuniform blade geometry has to be guessed by some indirect means. In the present analysis, it is unnecessary to specify the initial pressure profile which results as a part of the answer once the nonuniformity of blade geometry is specified. Since, as emphasized before, the kernel of the supersonic MPT problem is to investigate whether small errors within the manufacturing tolerances are really responsible for MPT generation, it would seem that the present analysis answers the question in a more direct way.

3.0 RESULTS OF THE ANALYSIS

Utilizing the analysis described in Section 2, sample computations were conducted and these will be presented herein. The cascade geometry and the blade shape chosen is given in Table 1.

3.1 Ideal Uniform Blades -- Decay Rate of Shock Strength

As far as the MPT sound is concerned, the case of the uniform bladed rotor is of no particular consequence. However such an idealized case provides a good check on the entire analysis. Figure 2 is a plot of the decay of the shock strength for an ideally uniform cascade versus axial distance. It is readily observed that there is a change over in the decay rate. In the vicinity of the rotor the decay is gradual, at a rate approximately proportional to the inverse square root of the distance. After a transition in the neighborhood of one blade spacing ahead of the rotor, the decay rate becomes approximately inversely proportional to distance. According to Blackstock, (Ref. 6), this inverse decay rate is what can be expected with the inviscid model in the intermediate region between the close near field of the rotor and the far field. An interesting comparison can be made between Figure 2 and Figure 14 of Ref. 2, which is reproduced here as Figure 3. In Figure 3, the shock strength is an average shock strength measured from the actual fan. Thus the measured decay rate of an individual shock reflects the blade-to-blade nonuniformity but the average decay rate can be considered to be close to the ideal uniform blade case. The nominal spacing of the fan blades is about 2.8 inches. It is seen that the two different decay rate and their transitional point agrees quite well with the computed results.

3.2 Nonuniform Blade Geometry

3.2.1 Effects of Blade Spacing Errors

At this point only the effect of blade spacing errors in the absence of other nonuniformities will be considered. Figure 4 shows the growth of MPT in the two cases of spacing error distribution. The two different error distributions are given in Table 2. It is easily seen that even at a distance of five blade spacings ahead of the rotor, the MPT is still less than the blade passing frequency in intensity. Since the experimental results show that MPT intensities exceed BPF at about two or three blade spacings ahead of rotor, it would appear that spacing errors per se are insignificant in MPT generation. This is in contradiction to the speculation of Ffowcs-Williams (Ref. 9), where the error in circumferential positioning is one of the essential features of MPT. The answer to the question as to which is correct cannot be provided by the experimental fan simply because actual fans contain

other nonuniformities which tend to mask, as will be seen shortly, the spacing error effects.

3.2.2 Effects of Stagger Errors

Figure 5 shows the effect of stagger errors in the two cases of stagger error distributions. The two different error distributions are given in Table 3. At three blade spacing ahead of rotor, some MPT harmonics begin to prevail over BPF harmonics and this trend agrees with the observations (Refs. 1 and 2). The plot of pressure profiles, Figure 6, shows the change of pressure profiles at three different axial locations. Close to the rotor, the shocks are more or less uniform both in strength and spacings but away from the rotor, they become very irregular. Such a trend is also well established by experiments (Refs. 1 and 2). Therefore it would seem safe to conclude that stagger errors are important MPT generators. Physically there are two mechanisms of MPT generation. First, since the airfoil shape of the supersonic fan is nearly a flat plate, even a small change in the stagger can cause appreciable positional change of point C of Figure 1 along the suction surface. This positional change of C in turn induces the blade-to-blade changes in the initial shocks both in strength and direction. Second, the initial difference in the shock direction amplifies the shock-to-shock spacing nonuniformity as the shocks propagate upstream. Therefore seemingly small stagger errors result in substantially irregular shock patterns. Philpot (Ref. 3) appears to be the first to speculate the importance of stagger errors for MPT. The blade contour errors would also be a strong generator of MPT due to their effects similar to stagger angle errors. The control of such errors, however, is extremely difficult to achieve because of the buffing practice in manufacture and deposition of foreign materials during flight service.

4.0 MPT EXPERIMENTS

4.1 Introduction

Previous investigators (Ref. 1, 2 and 3) have studied the growth of the multiple pure tones in full-sized compressors. In most of these cases the flow geometry upstream of the rotor plane was rapidly diverging, i.e. an inlet bellmouth was used. Only a very limited amount of data (Ref. 2) was taken in a constant area annulus. In this investigation, to establish the connection between blade defects and MPT generation, the rotor nonuniformities are measured and used to predict the MPT generation. To allow a reasonably valid comparison between the predictions and experiments a constant area inlet annulus of approximately 9 rotor blade spacings is used. The evolution of the wave pattern in this long inlet is investigated by placing piezoelectric pressure transducers in the outer wall at three upstream locations. Measurements of the noise emanating from the compressor inlet are simulated by using a traversing microphone in an inlet-acoustical plenum chamber. The effect of the length of the inlet duct on this sound emission will be investigated by using two different duct lengths.

The effect of the flow variables that are of interest, the relative Mach number and the inlet flow angle, will also be determined. By running the compressor at three speeds and three different discharge load settings at each speed the effect of these variables on the MPT evolution can be determined.

4.2 Test Compressor

The test rotor is a model of a first state fan rotor from the G.E. TF-39, scaled to a 6 inch O.D. and operated in a closed-compressor acoustic test loop. Freon 12 is used as the working fluid to reduce the running speed at any given Mach number.

The compressor consists of a single stage 40-blade rotor and a 72-blade outlet guide vane. The rotor blade chord length is 0.6 inch. Figure 7 is a photograph of the rotor and Figure 8 shows the typical blade geometry.

The compressor inlet section is made of two sections, a constant area annulus and an inlet bellmouth, as shown in Figure 9. By removing the annular piece the inlet bellmouth can be brought right up to the rotor inlet plane. In this manner the effect of the inlet duct length on the inlet noise emission can be determined.

To study the generation of the MPT's it is necessary to remove all other possible noise sources, if possible. For

these tests the inlet guide vanes, IGV's, were removed and the struts (2 sets of 8 holding the inlet center body) made very small, 0.047" thick , and placed as far upstream of the rotor as practical. This will reduce the disruption of the wave pattern to a minimal amount. Also the noise produced by the rotor intercepting the waves from the struts will be reduced. To reduce any noise due to the viscous wakes from the rotor impinging on the stator and any potential interaction between the rotor and the stator, the stator is placed about 1.3 rotor blade chords downstream of the rotor.

4.3 Experimental Facility

4.3.1 Test Loop

The model compressor fits into a test loop which was designed to determine the acoustic and monitor the aerodynamic performance of a compressor.

The compressor is coupled to a variable speed eddy current clutch electrical drive which can deliver 100 hp at a maximum 22,500 rpm. A running shaft carbon face seal and static elastomer seals isolate the test gas from the external environment. To isolate the plenum chamber and the piping from the compressor vibrations thick rubber gaskets are used as shear-type connections on the inlet and exhaust.

Figure 10 presents a layout drawing of the compressor test loop with the reverberation chamber located upstream of the compressor. The volume of the plenum chamber is approximately 60 cubic feet with a 16.8 sq. ft. cross-section. The inlet duct of the compressor is coupled to the side of the lower portion of the chamber.

The compressor annulus has a 0.092 sq. ft. cross section for an inlet contraction area ratio of 182.6. Following the compressor blade rows, the annular flow path diffuses over an area ratio of about 2.7 and is then collected in an 8 inch diameter duct. The flow on leaving the compressor passes through a ball valve, a heat exchanger, an ASME metering nozzle, and an acoustic muffler before returning to the plenum. A minimum of 30 db of attenuation is effected by the muffler at frequencies above 2 KHz. On entering the plenum the flow is conditioned through a set of diffusing screens followed by a honeycomb straightener.

Weight flow through the compressor is determined by measuring pressure drop across a calibrated flow nozzle in the 8-inch pipe (see Figure 10). At the start of a test, air is evacuated from the system, and then enough Freon added to bring the pressure slightly above atmospheric pressure. To maintain this condition during tests - thus minimizing possible leakage of air into the system - the Freon tank is left connected to the loop, with the valve open slightly. Gas test samples were taken before and after compressor tests, showing the Freon to be at a very high level of purity throughout the test program.

In a previous program (Ref. 4), the sound levels produced by the drive motor and gear box employed to operate the model compressor were measured and found to be well below the levels to be expected from the compressor. Hence, no acoustic isolation was required.

4.3.2 Aerodynamic Instrumentation

For the tests described in this report only overall compressor performances data are taken. In the inlet annulus total temperature, total pressure and static pressure are measured. In the exhaust duct similar measurements are taken. The total temperature is measured with a TC - type 1/8 inch total temperature probe, manufactured by United Sensor and Control. The total pressure is measured using an 1/8 inch Kiel probe. Static pressure is measured with a wall static tap.

In addition to the above meauurements, the pressure in the acoustic chamber (wall static tap), the pressure drop across the nozzle (wall static taps), and the gas temperature at the nozzle (bare-wire thermocouple probe) were also recorded. All these pressure measurements were taken with electronic pressure transducers, Pace Model KP-15.

The compressor speed was sensed by an electromagnetic pickup mounted at the coupling and the speed pulses counted by means of an electronic counter. The flow was measured with an ASME long-radius nozzle of five-inch diameter.

The signals obtained from these sensors are fed into a Hewlett Packard Data-Logger and read sequentially into a teletype console for printout and recording on paper tape for subsequent use in performance evaluation computer programs.

4.3.3 Acoustic Instrumentation

Inlet wave patterns are measured with piezoelectric pressure transducers manufactured by Kistler Instruments, Model 601L1. These probes are acceleration compensated and have a sensitivity to acceleration of 0.002 psi/g. The probes are mounted so that the sensitive portion is flush with the outer radius of the inlet annulus. These probes are located at 0.61, 1.76 and 3.01 rotor blade chords ahead of the rotor.

The microphone in the inlet plenum is mounted on a motor-driven traversing mechanism that causes an oscillating motion of the microphone, back and forth across the chamber, on a circular arc in a plane not parallel to any of the chamber walls. The center of this path is along the compressor axis close to its inlet with a distance from the compressor inlet to the microphone of approximately 2 ft.

This motion takes 26 seconds to transverse completely in both directions. The walls of the inlet plenum chamber are hard metal. Hence, with proper calibration and instrumentation it may be used as a reverberation chamber to determine the acoustic power radiated from the compressor inlet. The details of the instrumental and calibration technique have previously been described in reference (3). Briefly, the procedure is to calibrate the chamber using the "integrated tone-burst method" developed by Schroeder (11). During compressor tests, measurements were made by a 1/8 in. Bruel and Kjaer Model 4138 condenser microphone which had previously been calibrated in Freon 12 gas using an electro-static actuator (3).

Signals from these probes are amplified and fed to a 7 channel instrument tape recorder manufactured by the Norelco Corporation. These magnetic tapes are then analyzed in a spectral analyzer, using a 10 Hz bandwidth. This analyzer uses a time averaging scheme to yield time steady frequency spectrums of the signals. The advantage of this analysis technique is that the time average of the signals is presented and not an instantaneous reading. This reduces the data scatter and produces very clear spectrogram, particularly if the signals have a high random noise content.

4.4 Experimental Results

4.4.1 Rotor Imperfections

Figure 8 shows the typical blade geometry of the rotor as specified on the drawings. To obtain a description of the rotor defects, as an input to the analysis described previously, the assembled rotor was measured prior to testing. The chord angle and the blade spacing were measured at the tip. The blade profiles were inspected, but not measured, and were found to be without major perturbations. Figure 11 shows the variation in chord angle and the blade spacing as measured at the tip leading edge. The average chord angle is measured to be 60.1 degrees, this combined with the angle between the chord line and the tangent to the mean camber line at the tip leading edge of 1.6° yields a stagger angle of 61.7°. The major perturbations occur between blades 7 and 8, and between blades 25 and 26. The stagger angle variations are on the order of ± 1 degree while the spacing variation is within ± 0.017 inch. On the full size fans the stagger angle variation is usually ± 1/2 to ± 3/4 degrees. Because centrifugal force is used to fix the blades in the dovetail grooves, in the full size machines, the relative magnitude of the spacing error is difficult to estimate. However the stagger angle error is the most critical, and it is expected that due to the large variations in stagger angle the MPT content will be very large when compared to full size results.

4.4.2 Aerodynamic Performance

In order to establish the velocity diagrams of this blading, a series of speed lines are run. Figure 12 illustrates the performance data for the conditions as used in the acoustic testing, where P_{T1} and P_{T5} are the isentropic inlet and exhaust total pressures, W the compressor weight flow, θ the inlet temperature correction and δ the inlet pressure correction using 518.6°R and 2116 lb/ft^2 as a base respectively. A more extensive series of tests were conducted, but are not pertinent to this study. From the performance data, the relative tip Mach number and the incidence angle, can be found from the axial flow velocity, the rotor tip speed and the blade stagger angle. Figure 13 shows the variation of incidence angle, α, with the relative Mach number, M_r, for three different speeds and three different discharge valve settings. The variation of incidence angle is less over the speed range than the load range, with a maximum variation of 2 degrees from 19,000 rpm to 22,700 rpm, while a maximum variation of 3.5 degrees occurs when changing from the least discharge resistance to near stall. The relative Mach change with discharge setting is quite small, (for a fixed speed) about 3% or less.

4.4.3 Acoustic Tests

4.4.3.1 Microphone Calibration

In condensor microphones the motion of the diaphragm depends on the dynamic and dissipative affects of the ambient. Since the microphone used in this study is designed for use in air, a calibration of the frequency response characteristics in the Freon 12 environment is conducted. In this test the microphone and electrostatic actuator are placed in a small glass-walled test chamber. The chamber is evacuated and filled with Freon 12, and held at a slightly elevated pressure, 2 to 5 psig. The electrostatic actuator is driven through a Bruel and Kjaer microphone calibration appratus, #4142, and the microphone, a Bruel and Kjaer 1/8 inch, #4138 is powered by a Bruel and Kjaer Power Supply, #2801. Figure 14 shows the response relative to the low frequency (250 Hz) calibration conducted in air using a Bruel and Kjaer pistonphone. Since the frequency range of interest was less than 16 KHz, only a portion of the dynamic range of the microphone was investigated. For the ambient pressure range (0 to 3 psig) used, the effect on microphone sensitivity was negligible, in the frequency range of interest (250 Hz to 50 KHz).

4.4.3.2 Acoustic Data Reduction Methods

The principal method of data reduction employed in this report is to tape record the acoustic signals and then use a spectral analyzer to obtain the amplitude frequency spectrum of the signals. An important feature of the particular system employed is a technique for obtaining the time average of the spectrum. The analog signals are sampled, digitized and stored in a digital computer and then the average computed from these (100 to 200) samples. This average value is then converted back to an analog form to drive the cathode ray tube, CRT, display. For the data obtained on this study the averaging time was varied from 2 to 4 seconds and the results were found to be very time steady. To illustrate, in a run of 40 seconds in duration there would be 10 frequency spectra produced (for a 4 second averaging time) and these spectra would be nearly identical.

The primary advantage of this technique is in reducing the data scatter, particularly for broadband noise, since at any frequency it provides the time averaged value of the signal amplitude. The CRT display is then photographed using a special 35 mm camera. Figure 15 shows the CRT display amplitude versus the relative db level of the signal on the tape. There are three separate runs on this figure and to obtain quantitative measurements from the spectral displays the db difference from the calibration signals must be used. If a calibration signal produces an amplitude of 25/60 inches

at a SPL = 160 and the signal of interest has an amplitude of 20/60 inches then the signal SPL level is 160 - (53.4 - 46.6) or 153.2 db (for data reduction run (1)).

4.4.3.3 Blade Passing Frequency Results - Long Inlet Duct

There are four parameters of interest in this investigation; (1) upstream distance from rotor inlet plane, x, which is normalized by the rotor chord length, C, (2) relative inlet Mach number at the rotor tip, M_r, (3) incidence angle of the flow, α, and (4) compressor speed, N = (rpm), or expressed as blade passing frequency, BPF. Mach number and the incidence angle vary simultaneously as the flow through the compressor is changed by the discharge valve. Figures 16, 17 and 18 show the variation of the SPL (contained in a 10 Hz bandwidth around BPF) with upstream axial distance from the rotor. On each figure three different discharge valve settings are given for each compressor speed. In all the cases except one, the BPF noise exhibits a rapid drop-off with increasing axial distance. This unexpected rise, (see Fig. 16) of the BPF content with axial distance appears to be due to the increased broadband noise at that particular position and conditions, (x/c = 3.01, BPF = 13 kc and the intermediate flow setting) when compared to the other axial positions. Close to the rotor (x/c = 0.61) the BPF noise decay with distance is very rapid ranging from 21 db/chord at high compressor speed to about 33 db/chord at the low compressor speed. When the compressor flow is reduced the BPF noise increases for all the compressor speeds, neglecting the slight dip at the x/c = 3.01 station when running at the highest speed.

The changes in BPF noise with the flow reductions are very large for the low speed (13 - 13.25 kc) runs and the high speed (15.1 kc) runs while for the intermediate speed (14 kc) runs they are much smaller. One would expect the BPF content to be increased due to increase in the incidence angle as this will increase the separation of the unattached shock (at these high angles) and delay the MPT noise generation. These changes, however, are much too large to be totally accounted for by the upstream motion of the bow shock wave due to this increase in incidence angle.

Since both the relative Mach number and the incidence angle are varying together, the two effects are somewhat confounded, to alleviate this situation the same data is redrawn on Figures 19, 20 and 21 as a function of the relative Mach number, with the incidence angle as a parameter, for the three axial transducer locations. Close to the rotor (x/c = 0.61) the BPF content decreases with increasing M_r and increases with increasing α. The variation with Mach number is expected since the higher Mach number would be expected to have a faster decay of the BPF content due to faster development

of the "skewed" wave patterns. The effect of increasing the incidence angle is apparently causing an increase in overall SPL close to the rotor, as well as a shift in shock position as mentioned before.

At x/c = 1.76 raising the incidence angle at a fixed Mach number causes very little change until close to stall, when a rise in the BPF content occurs. This increase in BPF noise does not appear to be due to an increase in the broadband noise level.

At x/c = 3.01, raising the incidence angle at high Mach numbers causes the BPF content to decrease and then rise. For this position raising the Mach number causes the BPF content to decrease. This dropping phenomenon is associated with the decay of the BPF content and the strength at the rotor inlet plane since it did show up at x/c = 0.61. The overall trends observed are that BPF noise decreases with increasing M_r and increases with increasing α.

Oscilloscope photos of the wall static pressure wave forms are shown on Figures 22 and 23. The effect of compressor speed, principally Mach number is shown on Figure 22, the flow conditions are similar to the high flow conditions (wide open discharge valve) as shown on Figure 13. The top trace is from a 40 tooth gear mounted on the compressor drive shaft with a notched tooth positioned such that it passes the magnetic pickup when the blade number 1 is passing the tangential position of the pressure transducers. The position of the major perturbations of the wave form (from a uniform wave at BPF) are closely correlated to the position of the major imperfections of the rotor as described in section 4.4.1. These wave forms would be representative of the (wide open discharge valve) data as shown on Figures 19, 20 and 21. The decrease of the BPF content with distance and Mach number is clearly evident from this figure. Also the signals are seen to be "locked to the rotor" and spiralling up the inlet duct. The effect of throttling the compressor at a fixed speed is shown on Figure 23. Again the conditions are similar to those on Figure 18.

4.4.3.4 Multiple Pure Tone Distribution - Long Inlet Duct

Figures 24 through 32 show the SPL spectrum for the three transducers located in the inlet duct as well as for the plenum microphone. From these figures it can be seen that the spectra are very rich in MPT content. In particular, even close to the rotor (at x/c = 0.61) the MPT content is quite large, and in some cases the predominant MPT's are greater than the BPF noise. On the left side of each spectra are the calibration signal level, the deflection that signal would have and the calibration curve to use on Figure 15 (as

explained in section 4.4.3.2), these values are used to obtain quantitative measurements of the spectra.

The distribution of these tones is fairly uniform, so that by measuring the maximum peak in the frequency range from 3 to 10 KHz a fairly good idea of the MPT content is obtained. Table 4 shows the SPL at the BPF, at the mid-range and at the low frequency end of the spectrum for all the nine runs. On Figures 33 through 35 the SPL of the peak MPT in the mid-band of the spectrum (3 to 10 KHz) is shown. In general the MPT strength decreases in the upstream direction but not as fast as the BPF noise, and the rate of decrease slows with increasing Mach number. Apparently due to the large nonuniformities of the rotor the prominent MPT's are established very quickly and decay slowly in the upstream direction. This decay of the prominent MPT's is predicted by the results of the analysis. The axial decay of the MPT's are in apparent contradiction with previous reported results. The reasons for this difference appear to be due to two effects: (1) the level of the MPT's at the first measuring point (x/c = 0.61) are large in this study indicating that the nonuniformities are larger than used previously. This will cause an early establishment of the predominant MPT's. With smaller nonuniformities a larger axial distance is required before the MPT's develop significantly. (2) The previous results indicate that the level of the MPT's reach a plateau and then travel upstream unchanged. These results, however, are based on measurements taken in an inlet bellmouth, which may alter the MPT evolution process with respect to what occurs in a constant area annulus.

At the lowest speeds, reducing the fan weight flow with the discharge valve reduced the MPT level. This trend changes as compressor speed increases and at the highest speed reducing the through flow causes an increase in the MPT level. Varying the compressor speed at a fixed discharge setting causes the MPT noise to have a maximum near a relative Mach number of 1.15. When compared to the BPF noise, Table 4, the dominance of the mid-range MPT's over the BPF noise is a monotonically increasing function with axial distance for the higher speed runs (BPF $\geq$ 14 KHz), and shows a rising and then a falling dominance for the lowest speed run. This is due to the more rapid decrease of the MPT's with distance for this compressor speed (BPF = 13 KHz).

4.4.3.5 Plenum Measurements

The SPL frequency spectra as measured in the inlet reverberant chamber (plenum) are shown on Figures 24 through 32 for the long inlet duct case. The BPF drops rapidly with relative Mach number as can be seen on Figure 36. The long inlet data has not been corrected for the frequency response of the microphone, this will reduce the SPL at BPF by 6.5 db. The

plenum BPF noise is much less sensitive to the incidence angle when compared to the wall static measurements in the inlet duct. This can be seen by comparing Figure 36 to Figure 21 (for the long inlet case), the plenum measurements can be plotted on a single line. Overall trends are quite comparable, though, having an initial rapid decrease with M_r and then a leveling off.

By removing inlet annulus and keeping everything else the same, the effect of inlet duct length on the sound emission is investigated. On Figure 36 the SPL at BPF with the short inlet is shown, along with the case for the long inlet. The level of the BPF noise for both of the plenum measurements are much lower than the wall statics, as is expected. The short inlet case is about 16 db higher in SPL (remembering to correct the long inlet data) with nearly the same decay with relative Mach number. For this short inlet case, to correlate the near field to the sound emission, a rough comparison can be made between Figure 19 (x/c = 0.61) and Figure 36. Again the effect of incidence angle is much less in the plenum measurements and the trend of the decay of the SPL at BPF is comparable for both cases.

Figures 37, 38 and 39 show the plenum SPL frequency spectra for the short inlet runs. Table 5 shows the plenum SPL of the rotor frequency (RF) noise, the level of the prominent MPT in the mid-range of frequency (3 to 10 KHz) and the blade passing frequency noise. These data are all taken at a fixed microphone position and may not be representative of the overall emitted sound due to the variation of the signal with position, as can be seen by referring to Figure 36. Therefore an error of approximately 4 db is possible in these measurements. Overall the MPT's of the short inlet are more uniformly distributed than for the long inlet case. The largest difference in the comparable spectra of the long and the short inlet occurs at frequencies above the rotor frequency. The long inlet results have much lower level mid-range MPT's (particularly at the lowest compressor speeds) than the short inlet case. The MPT's of the long inlet duct, become concentrated at the low frequency and the high frequency end of the spectrum when the compressor weight flow is reduced at constant speed. This concentration of MPT's at the low frequency end (in the long inlet case), is particularly evident for the highest speed runs (BPF = 15 KHz).

The variation of the plenum RF noise with compressor speed, along a fixed load line, is quite different for the two inlet cases. In the case of the long inlet, at the maximum flow setting, the RF noise increases steadily, but at the intermediate and the near-stall setting it rises, then drops with increases of compressor speed. This rising and dropping also occurred in the predominant MPT's of the wall static

measurements, at x/c = 3.01. With the short inlet, the maximum flow setting produces a rising and falling RF noise variation with increasing compressor speed, while more restrictive settings continually increase, just the reverse of the long inlet case.

The position of the plenum microphone is the same for the SPL spectra appearing on Figures 24 through 32, 37, 38 and 39 and on Table 5. The variation in SPL as the microphone sweeps across the plenum chamber can be seen by referring to Figure 36.

4.4.4 Experimental Summary

4.4.4.1 Long Inlet Duct

The BPF noise, in general, decreases rapidly with upstream axial distance from the rotor, decreases with relative Mach number of the rotor and increases with the flow incidence angle.

The level of the dominant MPT, also decreased in the upstream direction but not as rapidly as the BPF noise and less rapidly as compressor speed is raised. Comparing the MPT noise to the BPF noise yields a monotonically increasing dominance with distance of the MPT noise over the BPF noise for the cases of the higher speed runs (BPF $\geq$ 14.0 KHz). At a fixed discharge setting the MPT noise increases with compressor speed until the relative Mach number is about 1.15 and then it decreases. At a fixed compressor speed the variation of the MPT with flow reductions ranged from decreasing the MPT level (at the lowest speed) to increasing the MPT level at the intermediate and highest speeds.

The angular position of the major disturbances to the pressure wave forms spiralling up the inlet duct are well correlated to the major nonuniformities of the rotor geometry.

4.4.4.2 Short Versus Long Inlet Duct

By changing the long inlet annulus (4.125" in length) and starting the inlet bellmouth nearly at the rotor inlet plane a 16 db increase in BPF noise level is obtained. With either inlet the plenum BPF noise falls off rapidly with relative Mach number, until about M_r = 1.2. The incidence angle variations are seen to have a much smaller effect on the plenum BPF noise than on the inlet duct wall static BPF noise.

The correlation of the measurements made in the inlet duct to the emitted sound are also of interest in this study. By comparing x/c = 3.01 wall static measurements to the plenum (long inlet) results a qualitative measure of this can be

obtained. In all cases the noise at the rotor frequency dominates the plenum measurements, with the BPF noise showing up only at the lowest speed runs. The BPF noise is much lower within the plenum but has about the same rate of decay with M_r as at x/c = 3.01. A reduction of the MPT's above the 20^{th} multiple of the rotor frequency is another major difference in the spectrum between the x/c = 3.01 location and the corresponding plenum measurements.

To compare the short inlet measurements in the plenum to the wall statics, the position, x/c = 0.61, can be used as representing the events close to the rotor. Again the BPF noise is lower in the plenum, but has a comparable rate of decay with Mach number. The rotor frequency noise again dominates the plenum measurements, in contrast to the wall static results at x/c = 0.61. The mid-range MPT's are suppressed but not as much as the case with the long inlet.

The overall effect of having a short inlet appears to be:

(1) a large increase in BPF noise,

(2) an increase in the mid-range MPT's, resulting in a more uniform spectral distribution of the MPT's,

(3) an increase in RF noise, that is almost negligible at the lowest speeds and increases with compressor speed.

4.4.5 Comparison Between Theory and Experiments

Only the effects of stagger angle errors and blade spacing errors are included in the calculations. The limited size of the model fan impeded any precise measurements of the blade contour errors. Thus this effect, which could have potentially significant bearing on MPT, is not included in the computed results.

In the analysis, it was assumed that shocks are attached at the leading edge. However in the model fan, the leading edges of the blades are quite blunt and the shock is probably detached. The detached shocks introduce two modifications. First, the standoff distance displaces the origin of the shock slightly ahead of the leading edges. The displacement effects themselves have no bearing on the MPT but the blade-to-blade variations of standoff distance could modify the MPT evolution. Such standoff distance variations would, however, be effectively the same as the blade spacing variations and this might not have appreciable effects on the MPT generation. Second the appearance of a subsonic region downstream of the detached shock delays the incipience of shock expansion fan interference. Therefore at a given axial distance upstream of rotor, the amount of shock expansion

fan interaction would become less and MPT evolution might be reduced. In any event, since the computer programming was written for the attached shock, the effects of detached shock could not be taken into account. Instead an ad hoc improvision was made in the following way to handle blunt leading edges. The model blade contour on the suction surface is not unlike a wedge, but near the leading edge it is joined into a small circle. In the computation, it is assumed that the attached shocks start at the transition point between the wedge and the circle.

Since this ad hoc assumption breaks down for low Mach number, the computation will be limited to the case of higher Mach number. A relative Mach number of 1.25 is used. As for the angle of attack, the restriction that the shocks should be attached at the transition point put some light on the choice of angle of attack. Here the angle of attack is chosen to be 1.8 degrees, somewhat less than the values at which the experiments were conducted. These input data were tabulated in Table 6. In Fig. 18, where the decay of the sound pressure level centered at the blade passing frequency is shown, the computed value is compared with the experimental results. The agreement is fairly good considering the various assumptions made in the analysis and particularly the fact that blade contour nonuniformity, a possibly important factor, is not used in the computation. The computed evolution of the MPT is plotted in Fig. 40. In this figure, positions K-1, K-2 and K-3 correspond to the positions of the probes located at $x/c = 0.61$, $x/c = 1.76$ and $x/c = 3.01$, respectively. When one compares this with the measured results, Figs. 30, 31 and 32, it is noticed that in the computed results there are virtually no MPT's between tenth harmonic and thirtieth harmonic, whereas in the experimental results there are many MPT's in between. The main reason for this difference is considered to be due to the blade contour nonuniformity, the effect of which, as repeatedly mentioned, is not included in the computed results. However the computed results do predict that the largest MPT is the first harmonic of the shaft frequency, which agrees with the experimental results.

5.0 CONCLUSIONS AND RECOMMENDATIONS

A theoretical and experimental investigation was conducted on multiple pure tone noise. Multiple pure tone sound from aircraft engines is characterized by a noise spectrum containing numerous spikes at integer multiples of the shaft rotational frequency.

In the analysis, it is assumed that the flow is two-dimensional and inviscid and the bow shocks emanating from the blades are attached to the leading edges. The analysis, consisting of the construction of shock expansion wave diagram, predicts the generation and evolution of MPT from the prescribed blade-to-blade nonuniformities in rotor geometry. The results show that even small nonuniformities, within the manufacturing tolerances, can cause a significant amount of multiple pure tone noise. The trend of the computed MPT evolution agrees with a previously observed one. Among different kinds of nonuniformities investigated, errors in blade stagger or blade contours are much stronger generators of MPT noise than errors in blade spacings.

The experimental results concur with the axial decay of BPF noise measured by previous investigators. Other aspects of these experiments have explored the effects of relative Mach number, incidence angle and inlet duct length on the BPF and MPT noise evolution. The results are discussed in section 4.4.4, Experimental Summary.

In order to compare the experimental results with the analysis, the MPT distributions were computed from the measured blade nonuniformities of the model fan. Due to the lack of measurements of the blade contour nonuniformity, an important MPT generator, the comparison between theoretical and experimental results is not exact. However, the computed result correctly predicts the position of the maximum peak of multiple pure tones in the frequency spectrum. The computed decay rate with axial distance of sound at blade passing frequency compares favorably with the measured results, as well as the level of the BPF noise. The angular position of the major disturbances to the pressure waveforms spiralling up the inlet duct are well correlated to the major nonuniformities of the rotor geometry as is predicted by the analysis.

In summary this study has conducted a combined analytical and experimental program that has demonstrated (1) the MPT sound is due to rotor geometry imperfections, and the angular position of the pressure waveform distortions are correlated to the location of these imperfections, (2) the evolution of the MPT sound can be predicted by a two-dimensional, inviscid analysis using the known rotor nonuniformities, (3) rotor relative Mach number and incidence angle are important

parameters to the evolution of the MPT sound in the Mach number range tested, (4) the inlet duct length has an important influence on the MPT sound emission.

As a logical next step for possible future effort in the prediction of MPT sound, the following extensions are recommended;

(1) In the analysis, to include the effects of detached bow shocks.

(2) In the experiments, to measure the blade contour nonuniformities.

(3) Extend the Mach number range.

REFERENCES

1. Kester, J.D., "Generation and Suppression of Combination Tone Noise from Turbof n Engines," Paper No. 19, Proceedings AGARD Fluid Dynamics Panel, Saint-Louis, France, May 1969.

2. Sofrin, T.G., Pickett, G.F., "Multiple Pure Tone Noise Generated by Fans at Supersonic Tip Speeds," International Symposium on the Fluid Mechanics and Design of Turbomachinery, Pennsylvania State University, September 1970.

3. Philpot, M.G., "The Buzz-Saw Noise Generated by a High Duty Transonic Compressor," ASME Paper No. 70-GT-54, May 1970.

4. McCune, J.E., "A Three-Dimensional Theory of Axial Compressor Blade Rows - Application in Subsonic and Supersonic Flows," Journal of Aeronautical Sciences, 25, pp. 545-560, 1958.

5. McCune, J.E., "The Transonic Flow Field of an Axial Compressor Blade Row," Journal of Aeronautical Sciences, 25, pp. 116-616, 1958.

6. Blackstock, D.T., "Connection Between the Fay and Fubini Solutions for Plane Sound Waves of Finite Amplitude," Journal of the Acoustical Society of America, Vol. 39, No. 6, June 1966, pp. 1019-1026.

7. Ferri, A., "Aerodynamic Properties of Supersonic Compressors," in 'Aerodynamics of Turbines and Compressors,' ed. by Hawthorne, W.R., Vol. V. of High Speed Aerodynamics and Jet Propulsion, Princeton University Press, 1964.

8. Hawkings, D.L., "Multiple Tone Generation by Transonic Compressors," Paper No. E. 4, Symposium on Aerodynamic Noise, Loughborough University of Technology, England, September 1970.

9. Ffowcs-Williams, J.E., "Sources of Sound in Fluid Flows," International Symposium on the Fluid Mechanics and Design of Turbomachinery, Pennsylvania State University, September 1970.

10. Wells, R.J., and McGrew, J.M., "The Use of Gases Other Than Air in the Acoustic Testing of Model Compressors," ASME Paper No. 67-GT-22.

11. Schroeder, M.R., "New Method of Measuring Reverberation Time," Journal of the Acoustical Society of America, Vol. 37, March 1965, pp. 409-412

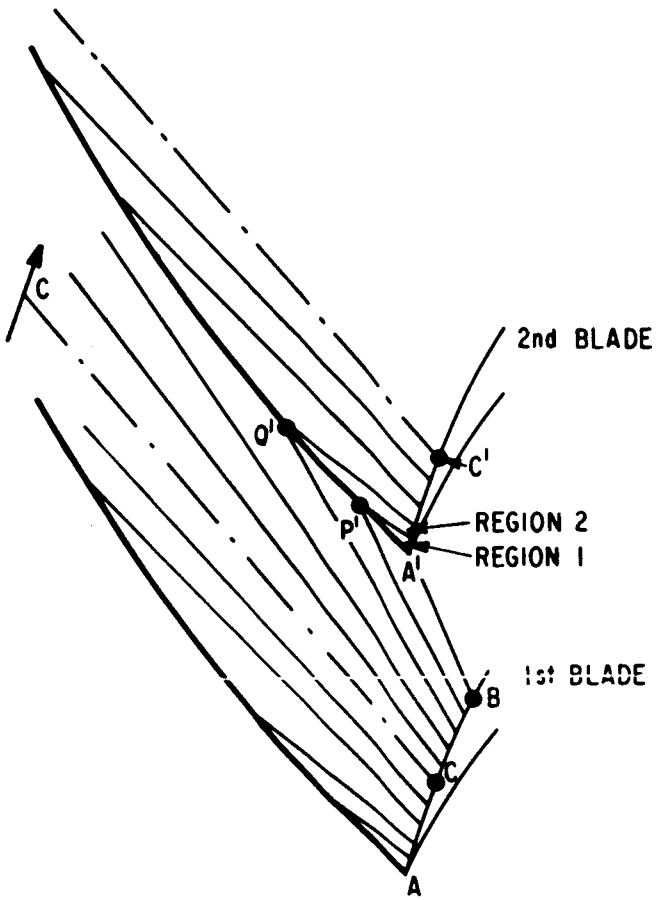

Figure 1. Wave Systems for Idealized Uniform-Bladed Rotor.

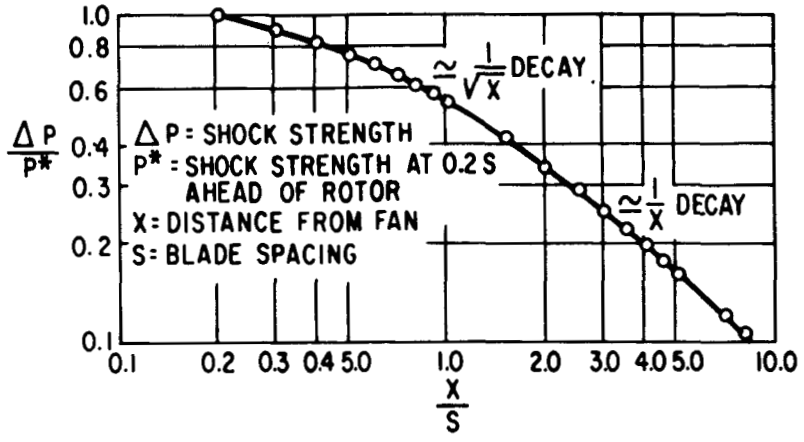

Figure 2. Computed Decay of Shock Strength for an Ideal Uniform Rotor.

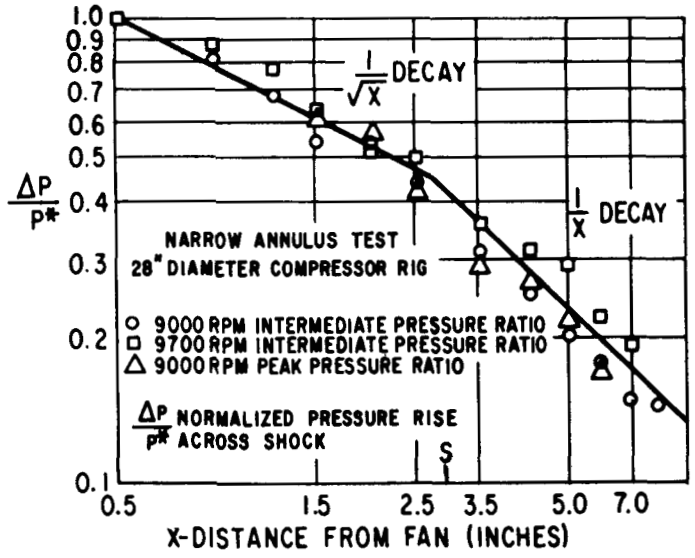

Figure 3. Measured Decay of Shock Strength (Figure 14 of Ref. 2).

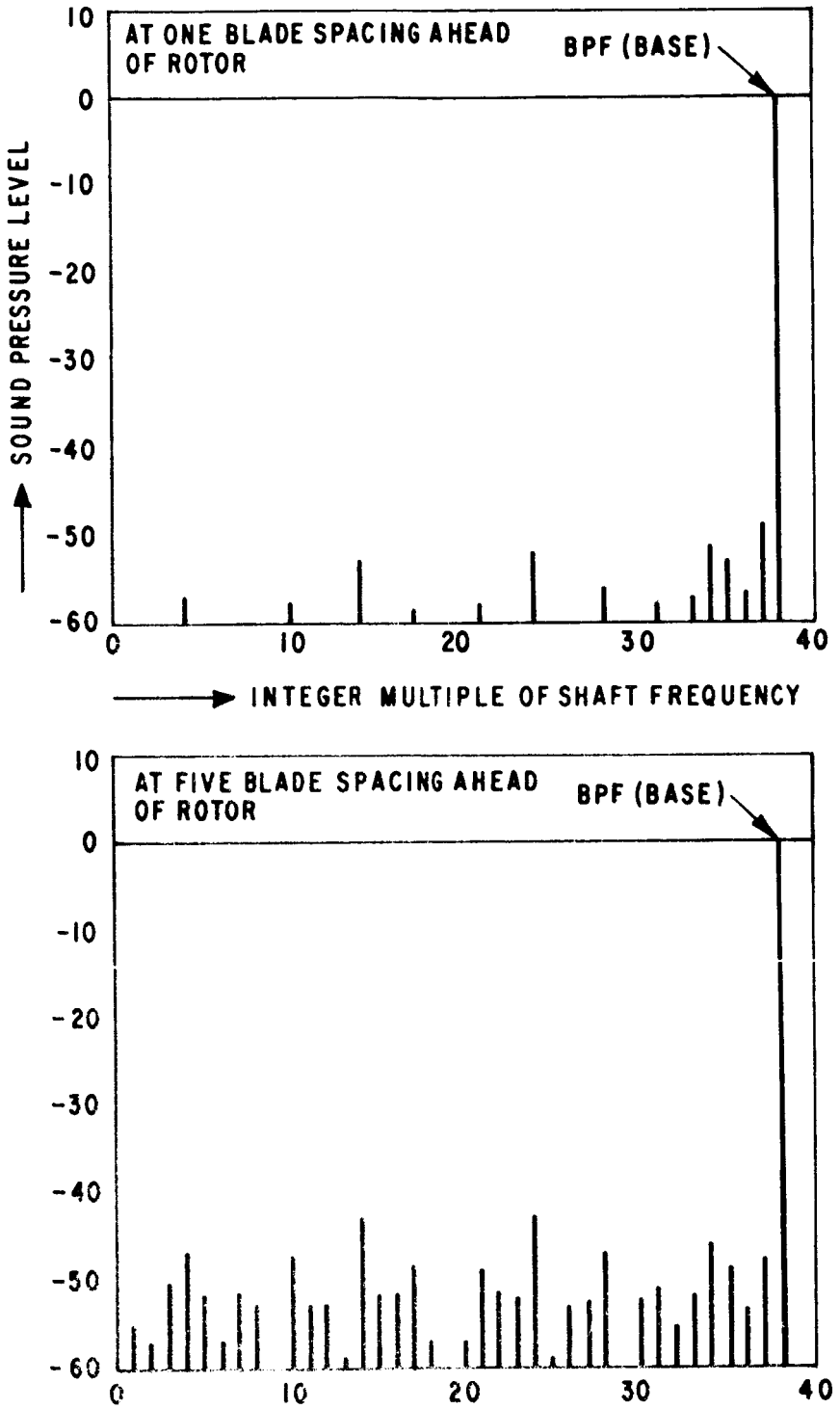

Figure 4(a). Effect of Blade Spacing Errors (Error Distribution, A-1 of Table 2).

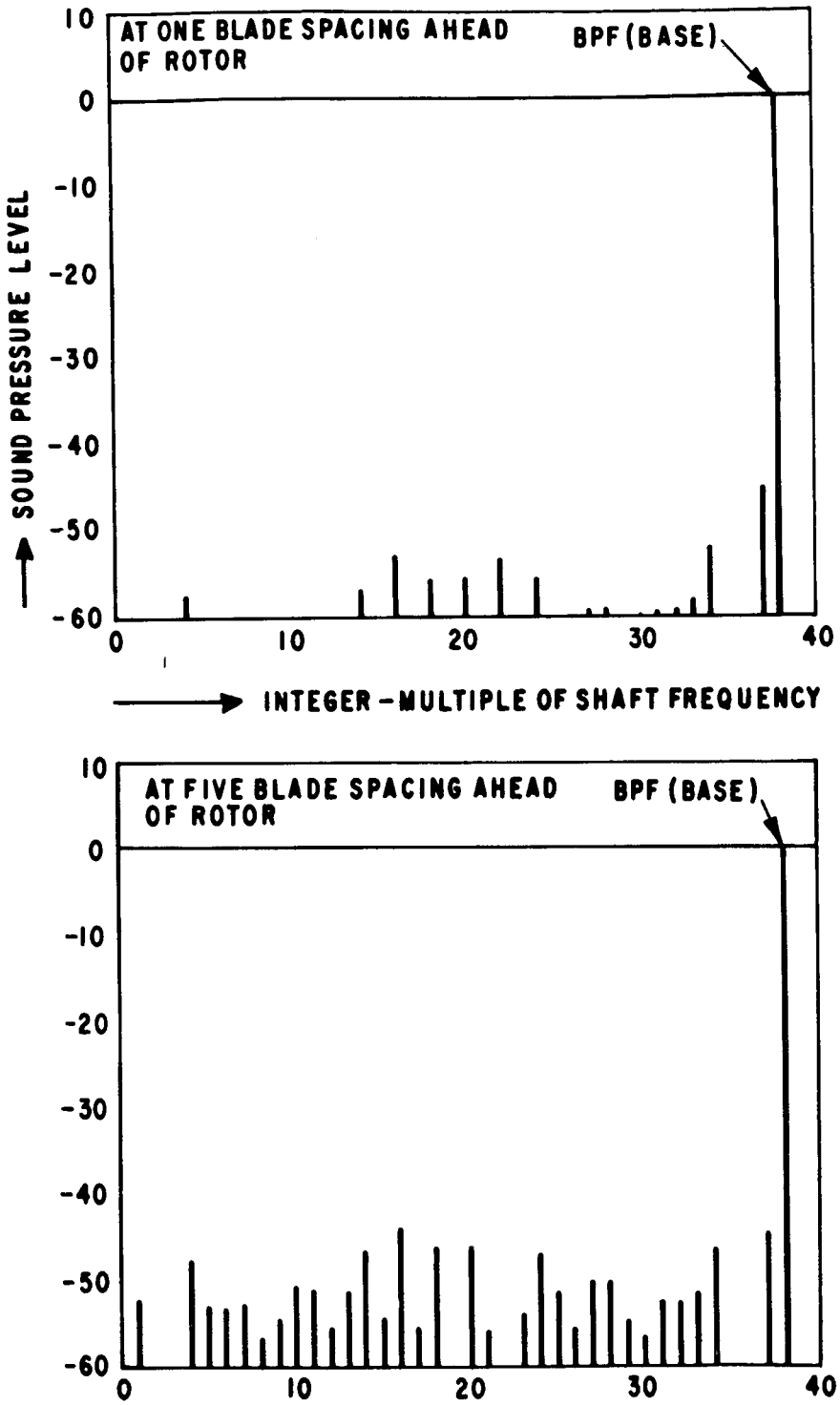

Figure 4(b). Effect of Blade Spacing Errors (Error Distribution, A-2 of Table 2).

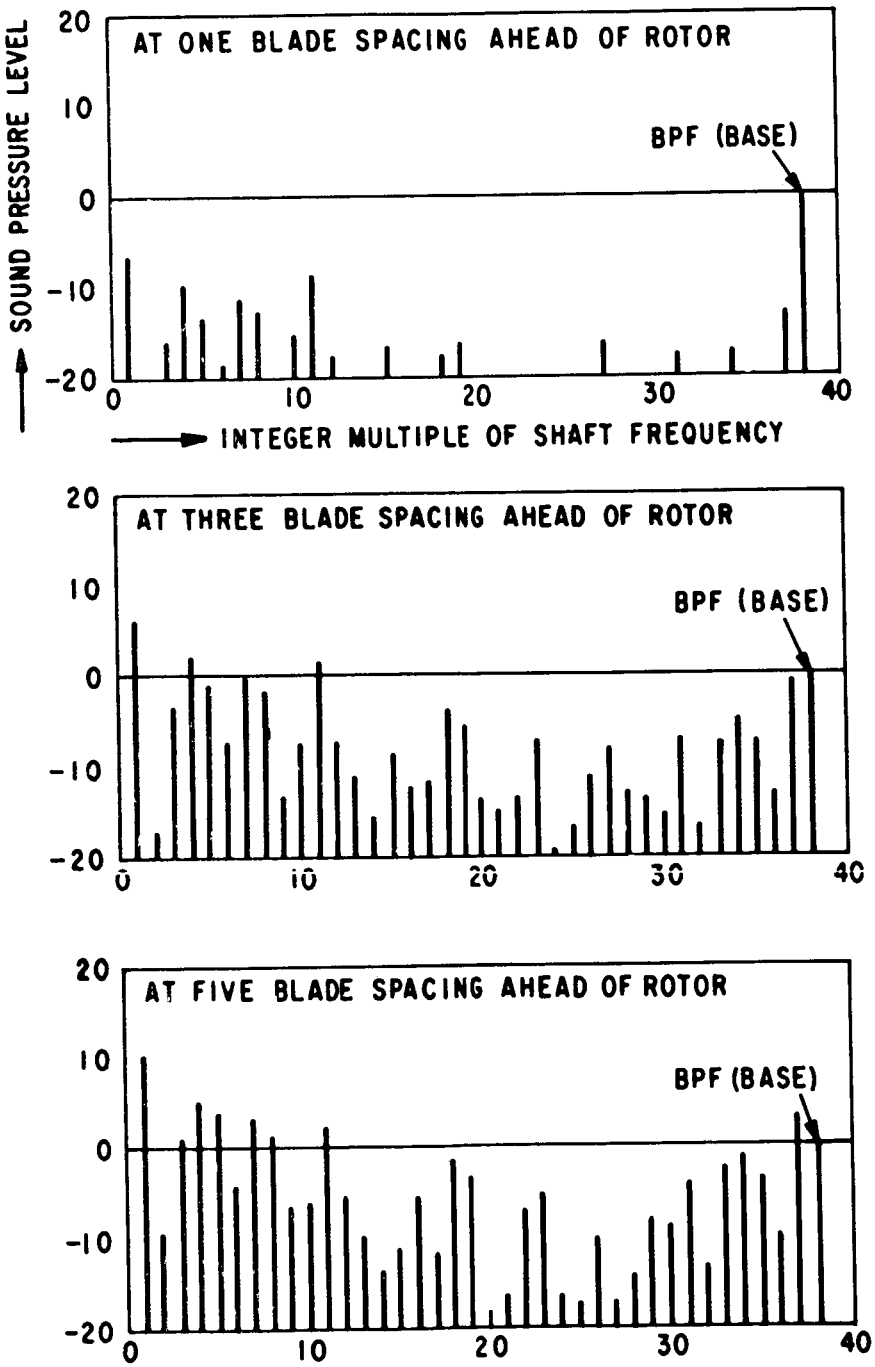

Figure 5(a). Effect of Stagger Errors (Error Distribution, B-1 of Table 3).

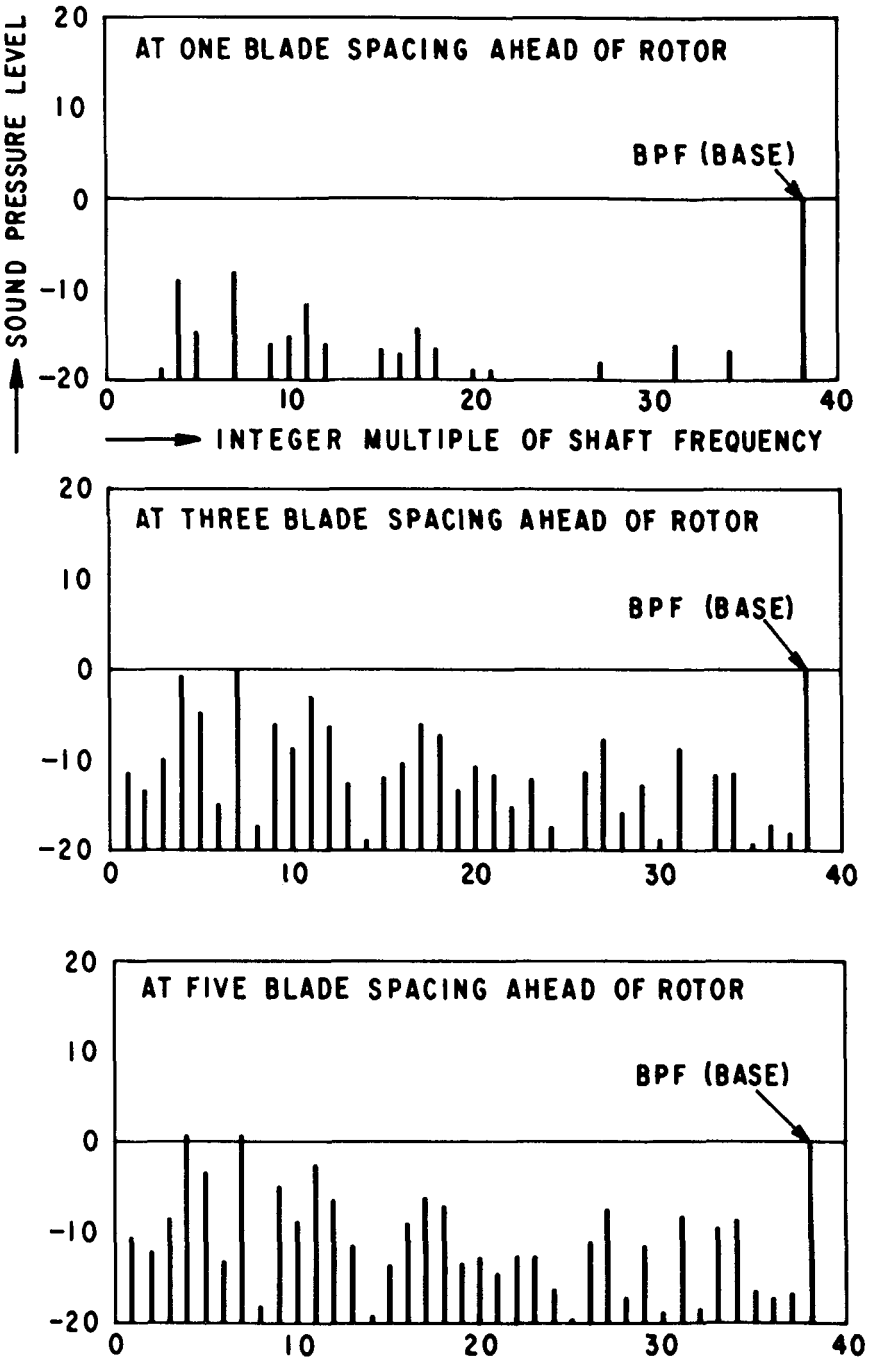

Figure 5(b). Effect of Stagger Errors (Error Distribution, B-2 of Table 3).

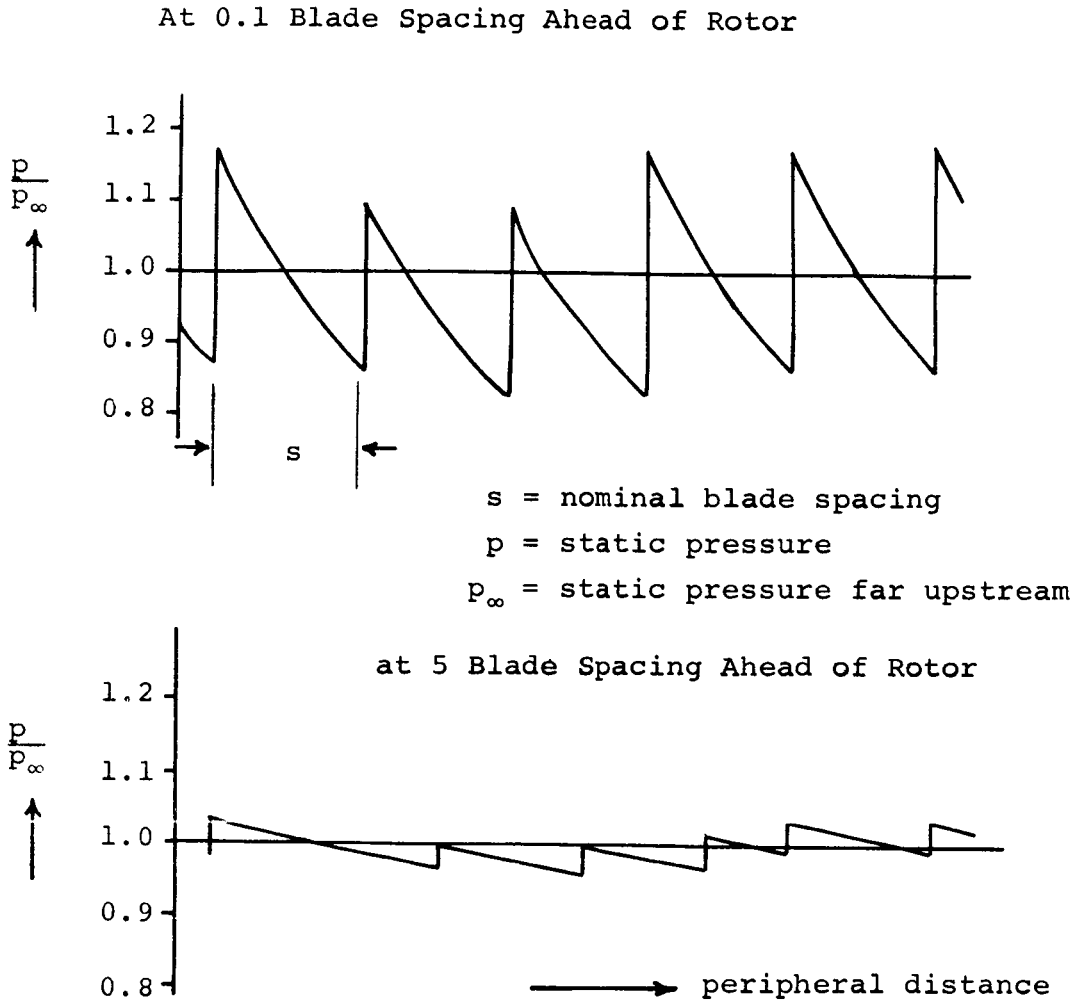

Figure 6. Change of Pressure Profiles.

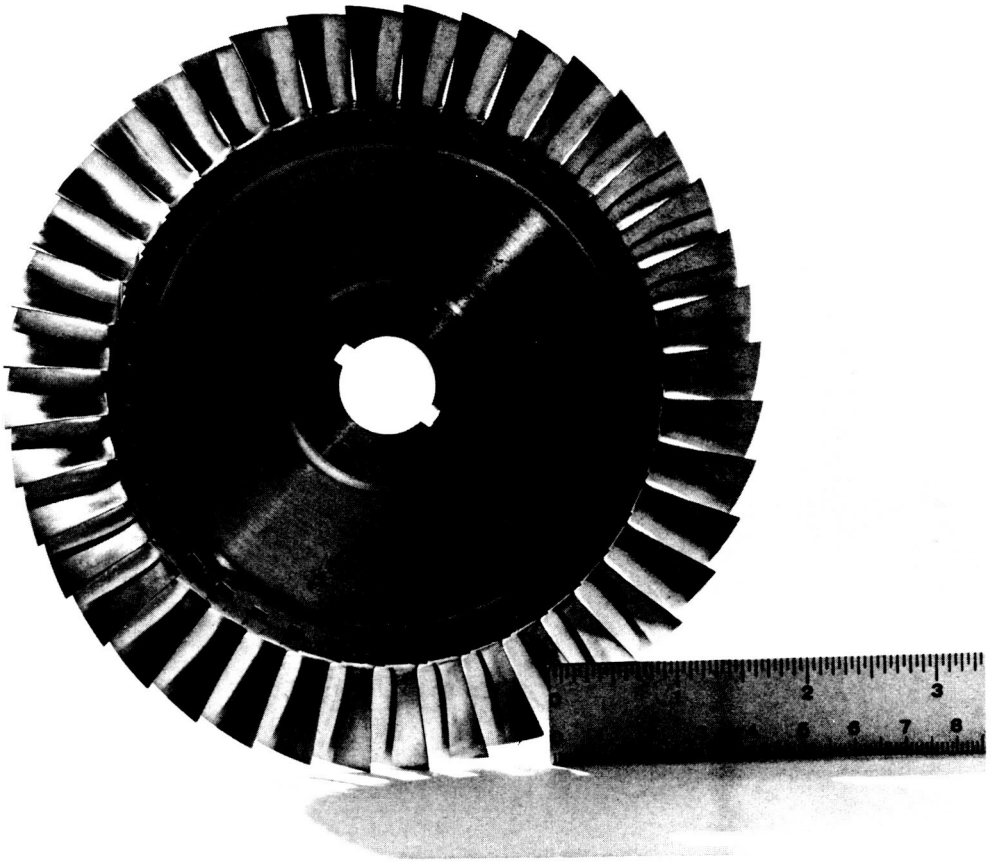

Figure 7. Scale Model Rotor.

MODEL COMPRESSOR ROTOR (40 BLADES)

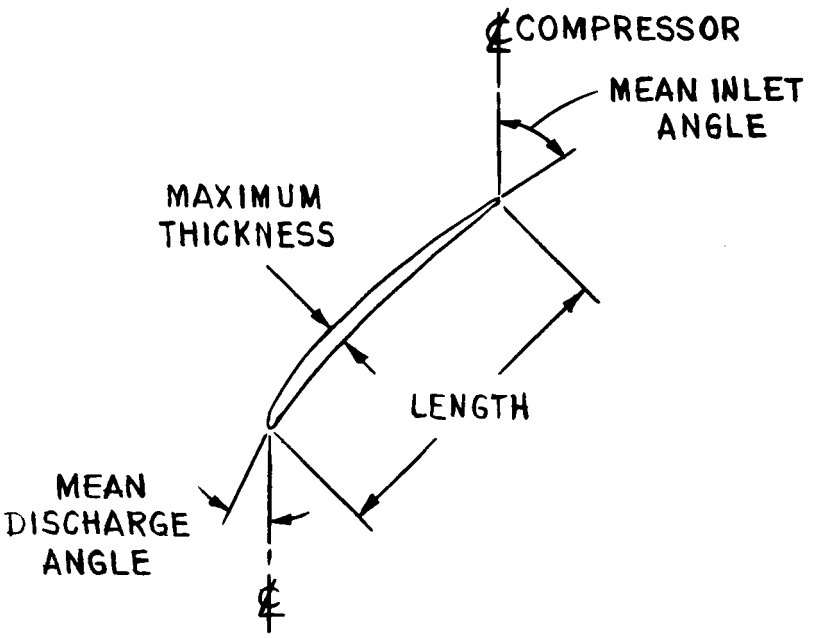

	TIP	PITCH	HUB
RADIUS (IN.)	2.957	2.549	2.196
MAX. THICKNESS (IN.)	0.014	0.020	0.022
LENGTH (IN.)	0.591	0.520	0.445
MEAN INLET ANGLE	63°54'	56°43'	55°56'
MEAN DISCH. ANGLE	57°14'	48°33'	40°26'

Figure 8. Rotor Blade Geometry.

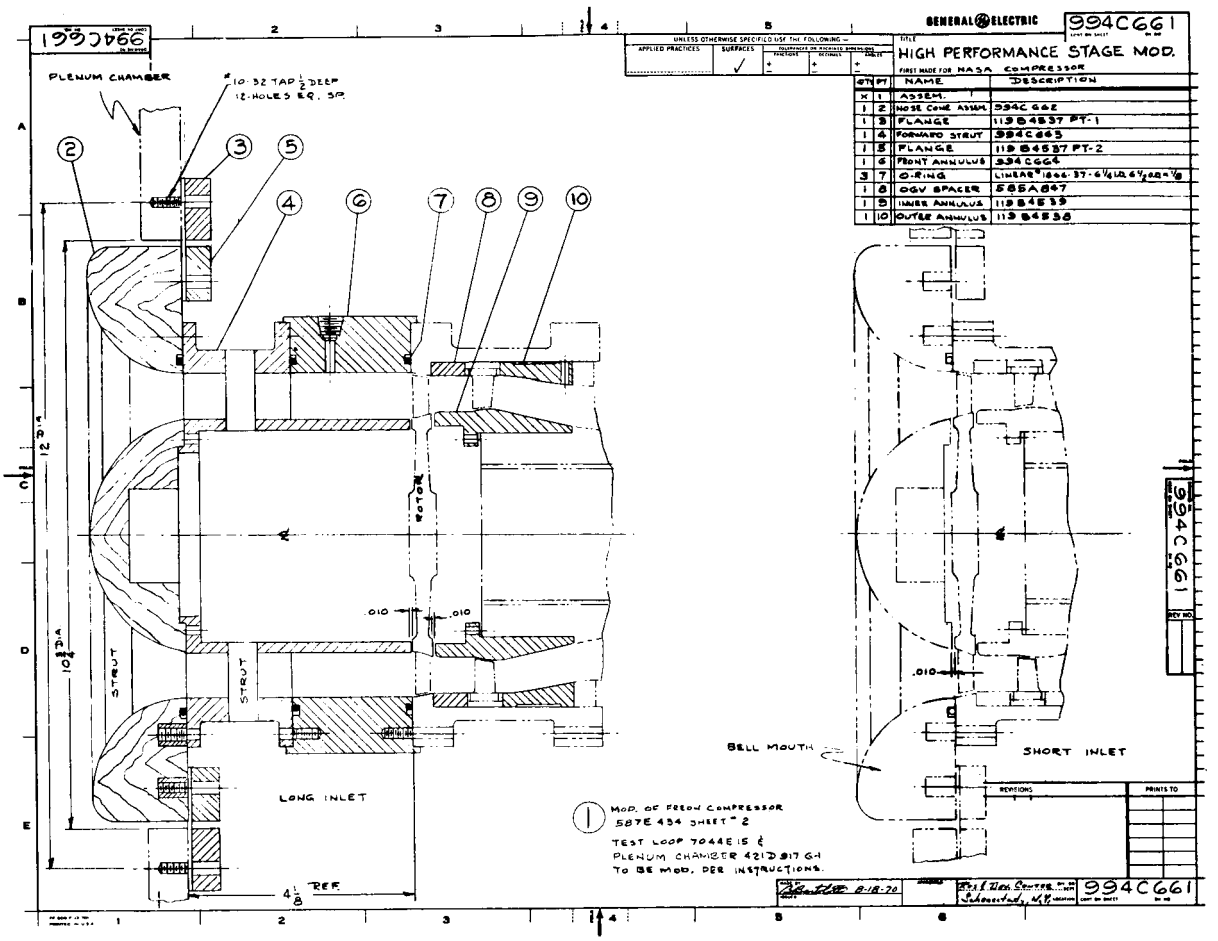

Figure 9. Compressor Layout.

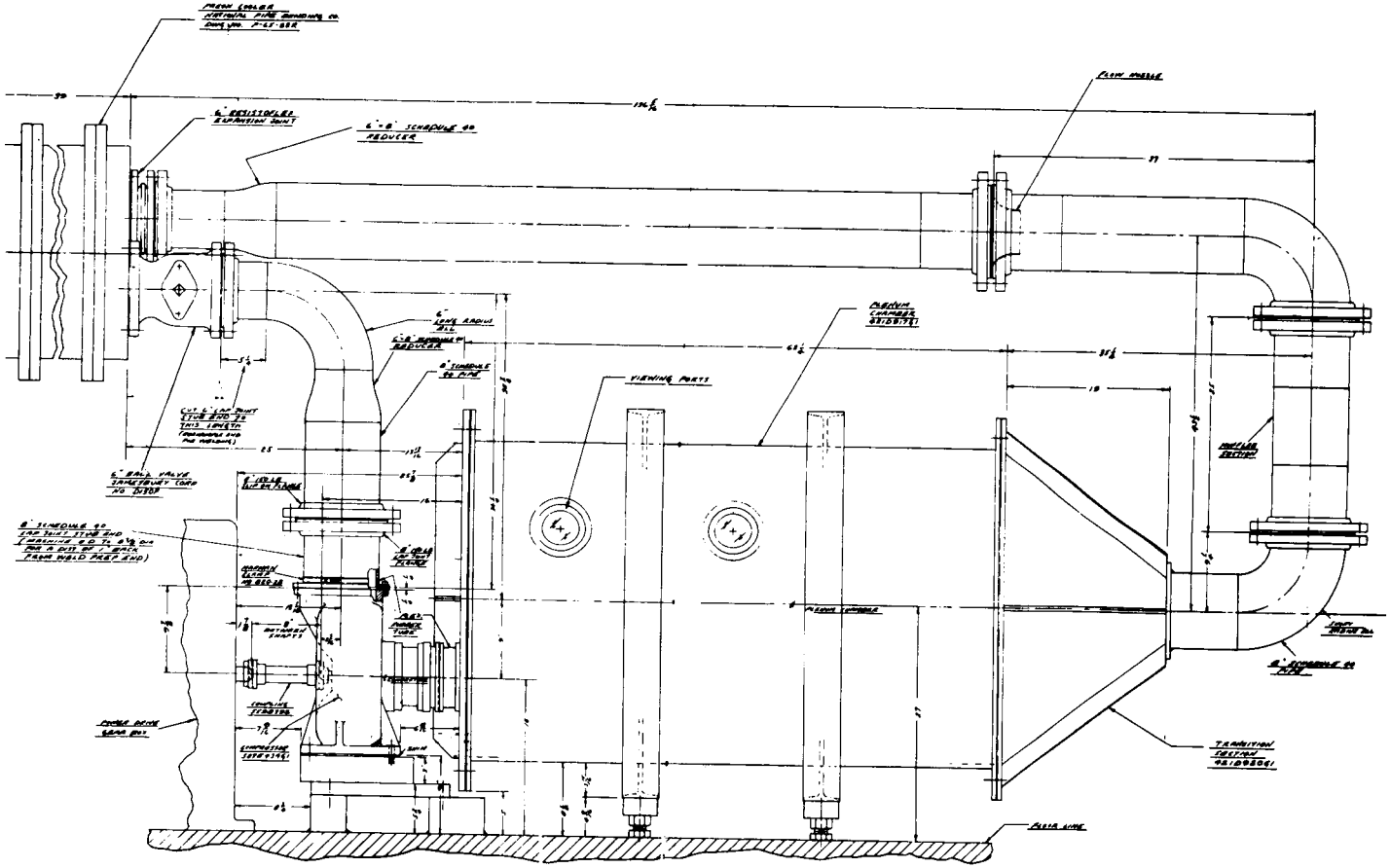

Figure 10. Schematic of Test Loop with Inlet Plenum.

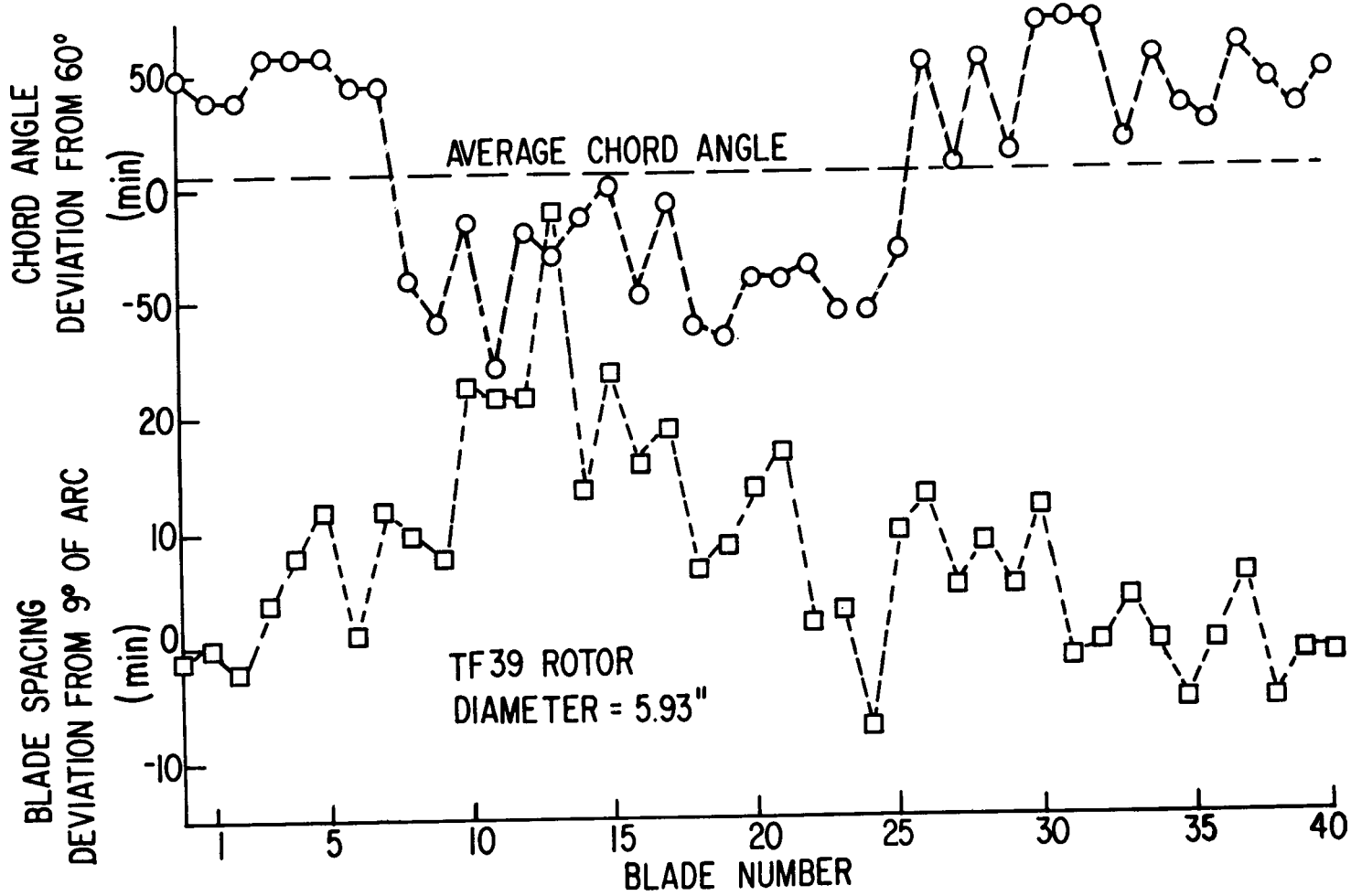

Figure 11. Rotor Nonuniformities.

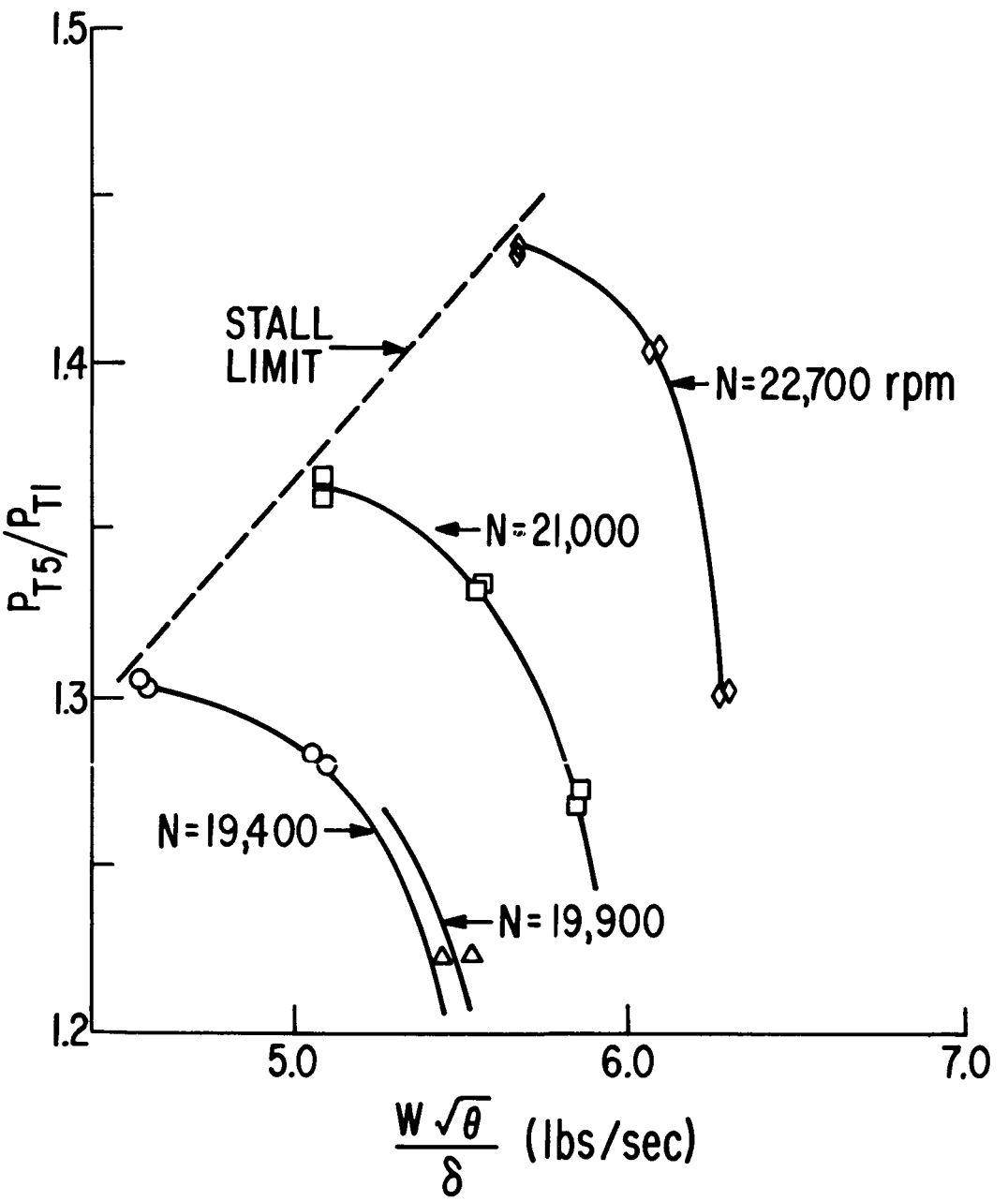

Figure 12. Model Compressor Performance Map.

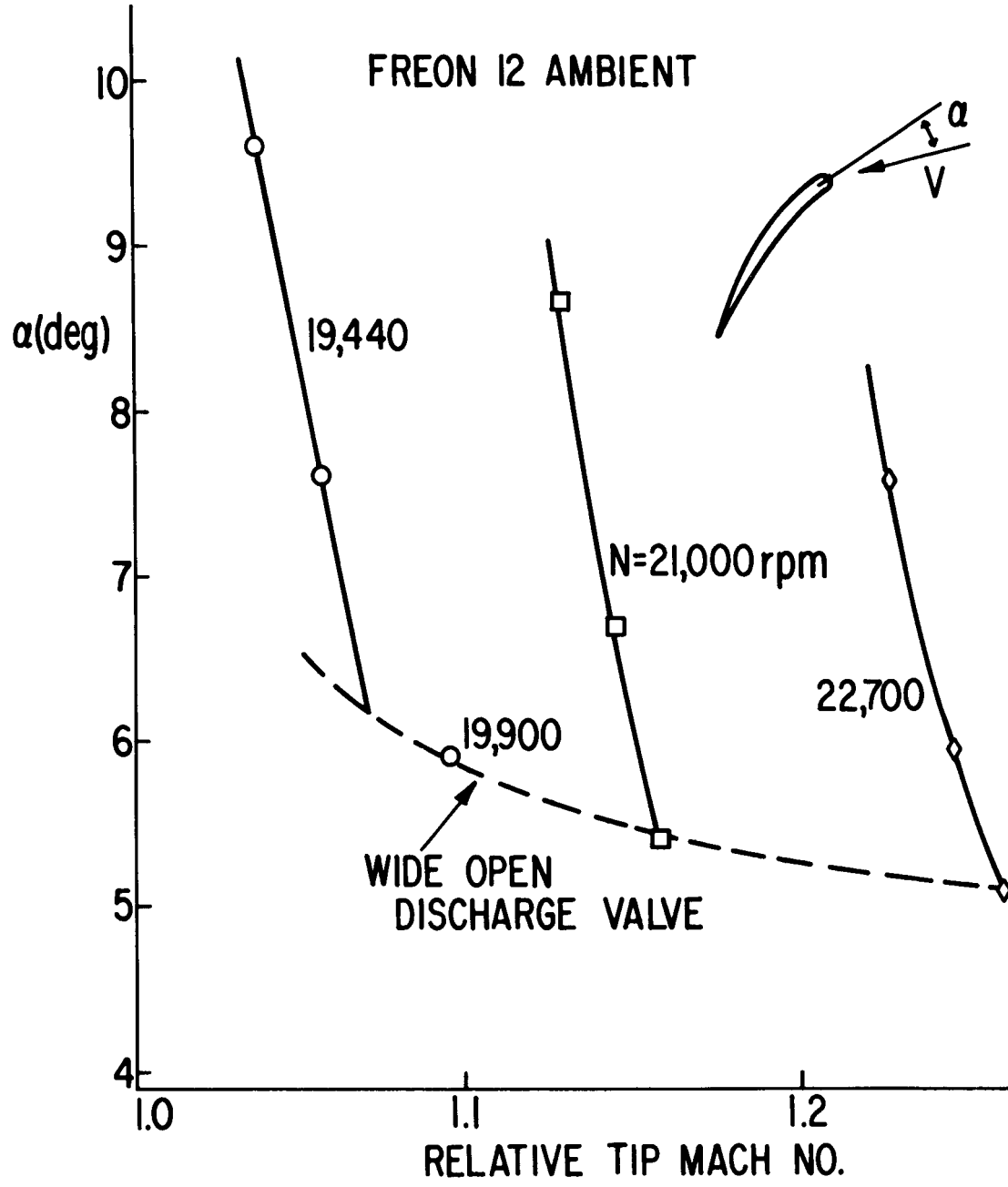

Figure 13. Incidence Angle Versus Mach Number.

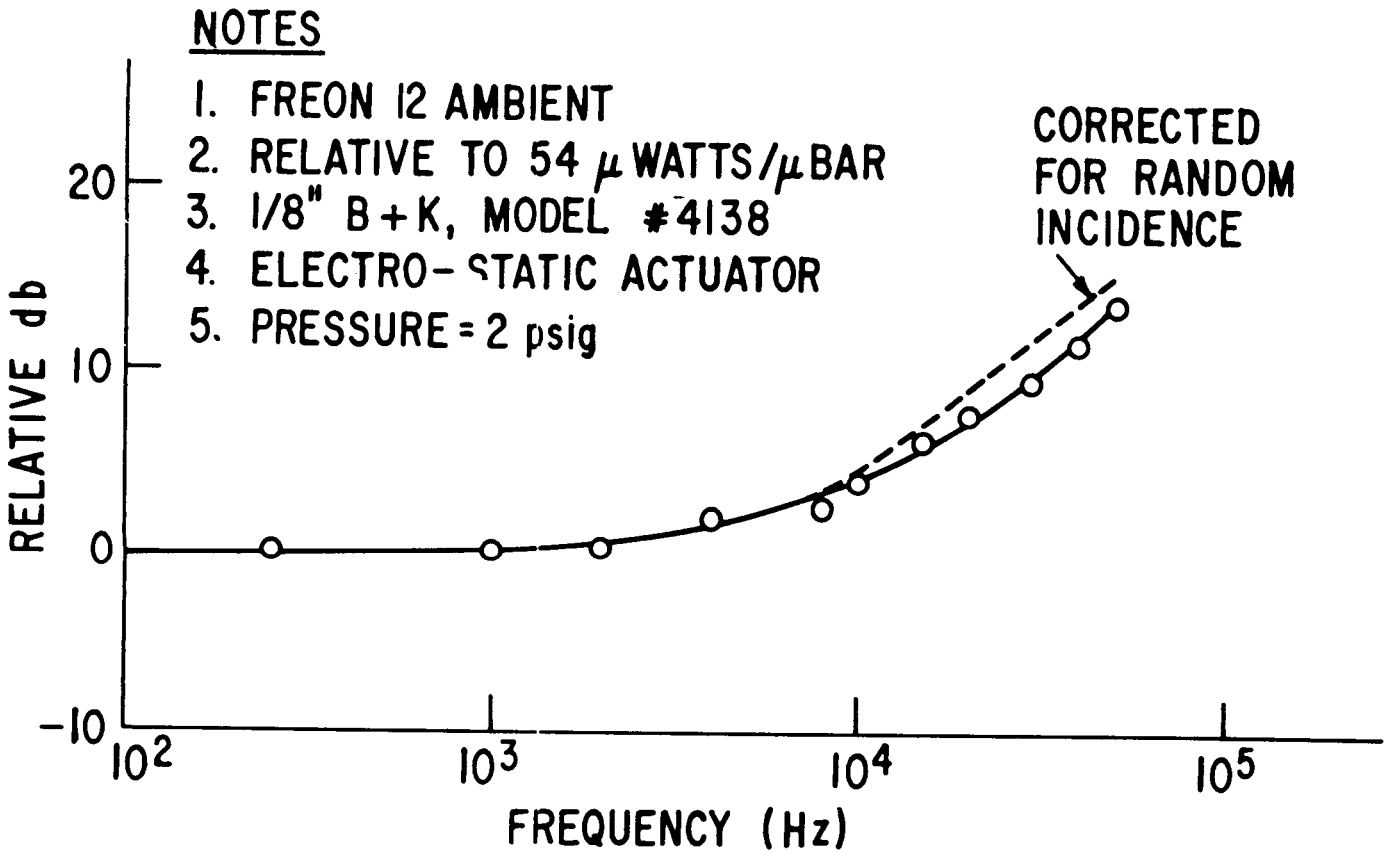

Figure 14. Calibration Curve of the Plenum Microphone.

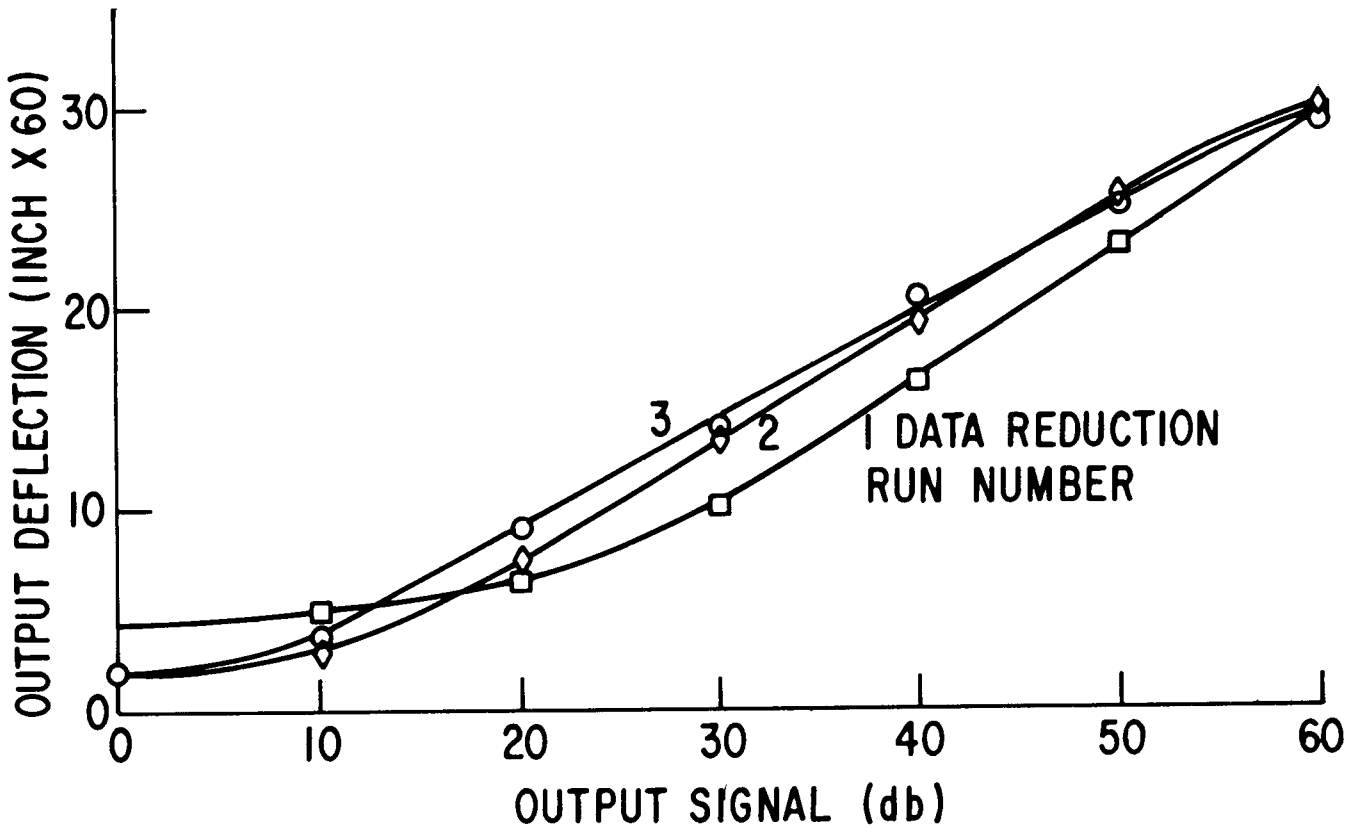

Figure 15. Spectral Analyzer CRT Output Characteristics.

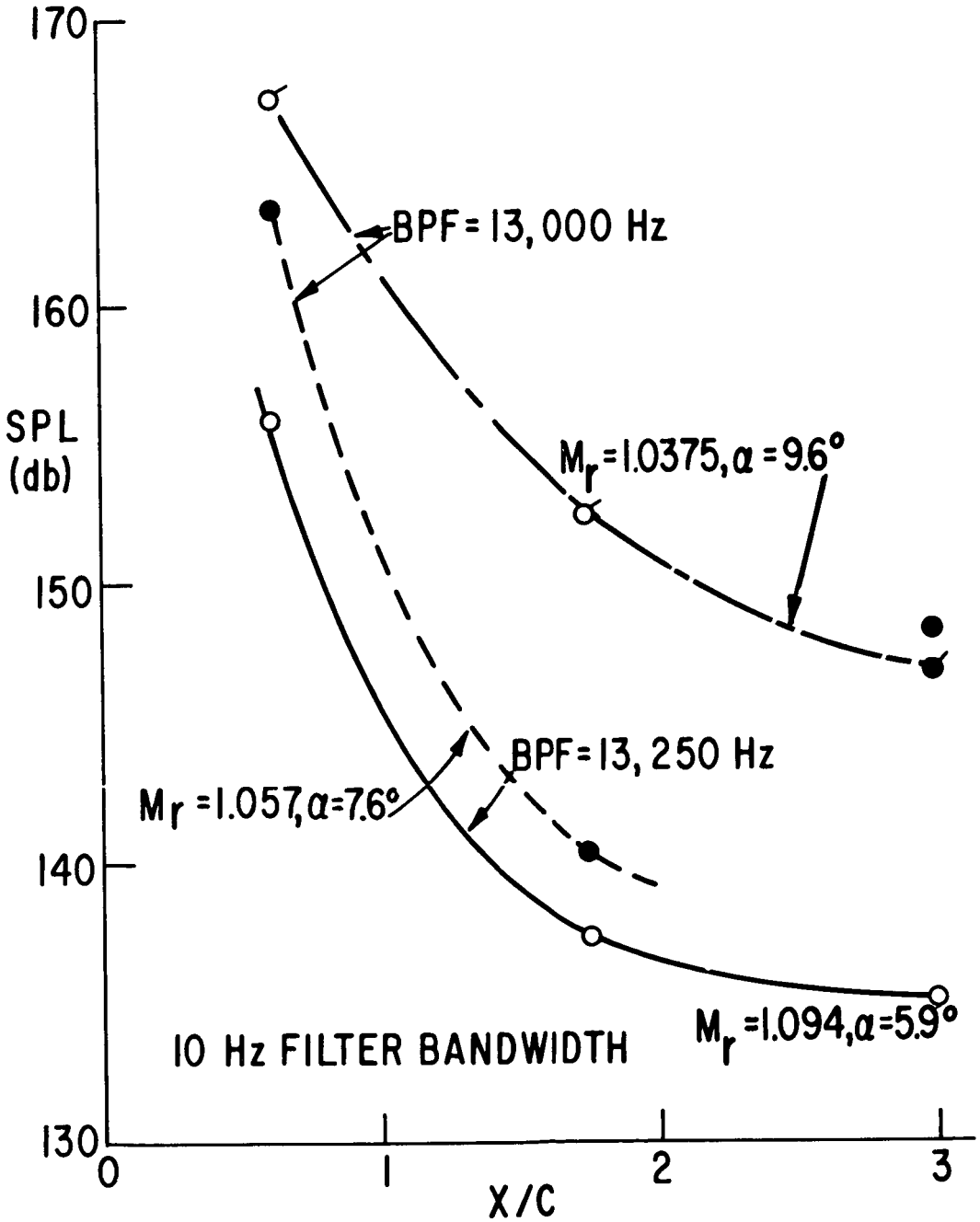

Figure 16. BPF Noise Versus Axial Distance.

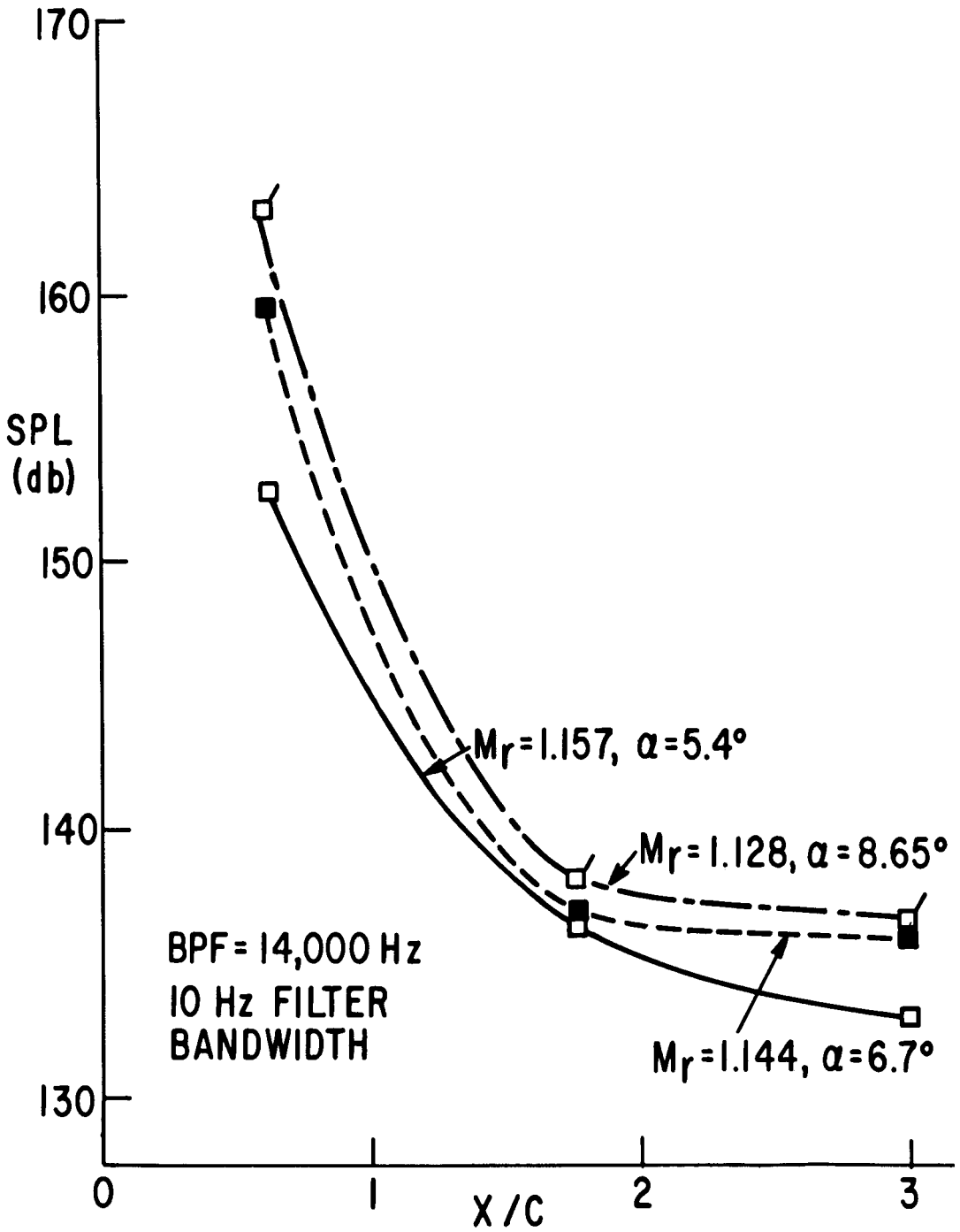

Figure 17. BPF Noise Versus Axial Distance.

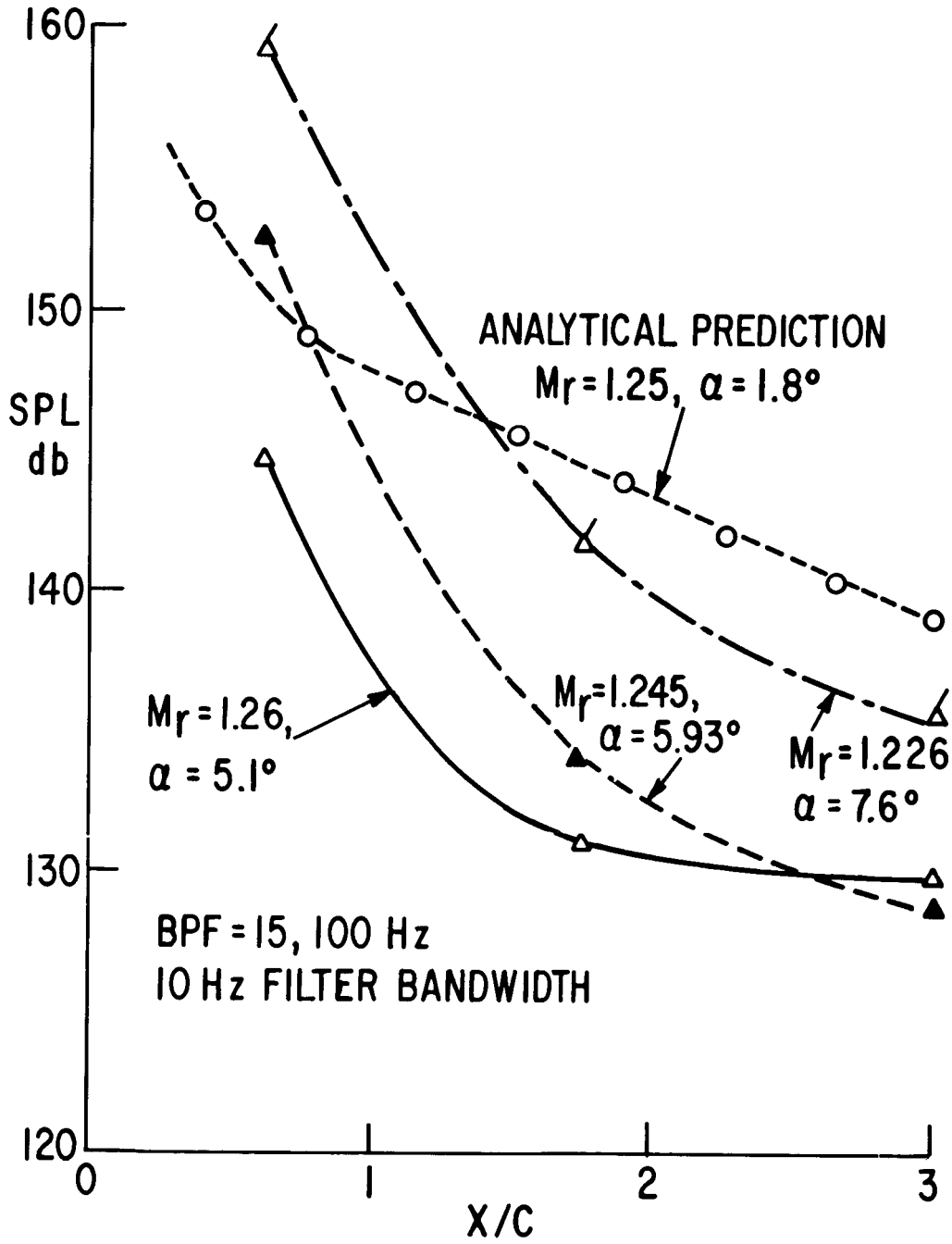

Figure 18. BPF Noise Versus Axial Distance.

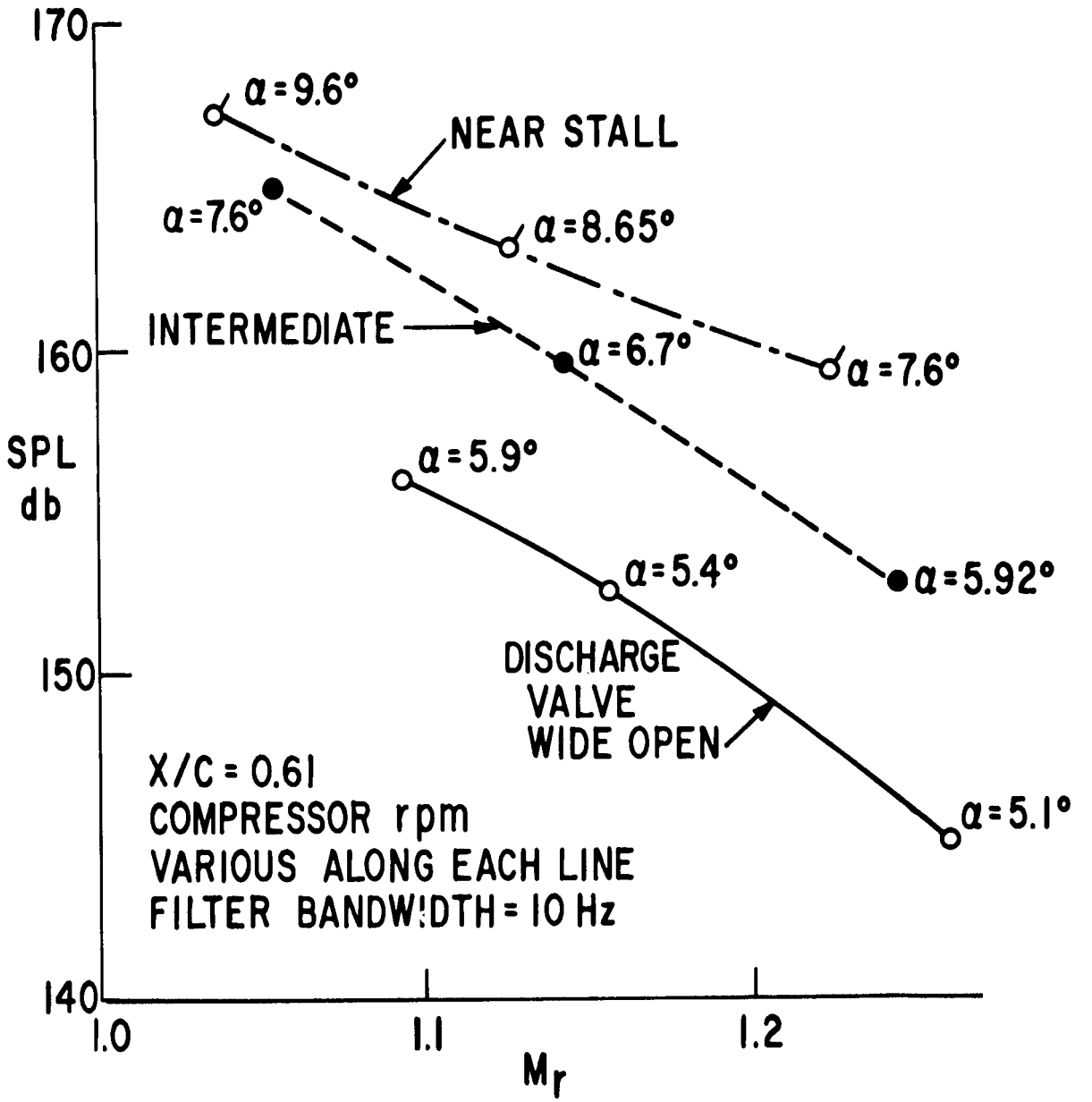

Figure 19. BPF Noise Versus Relative Mach Number.

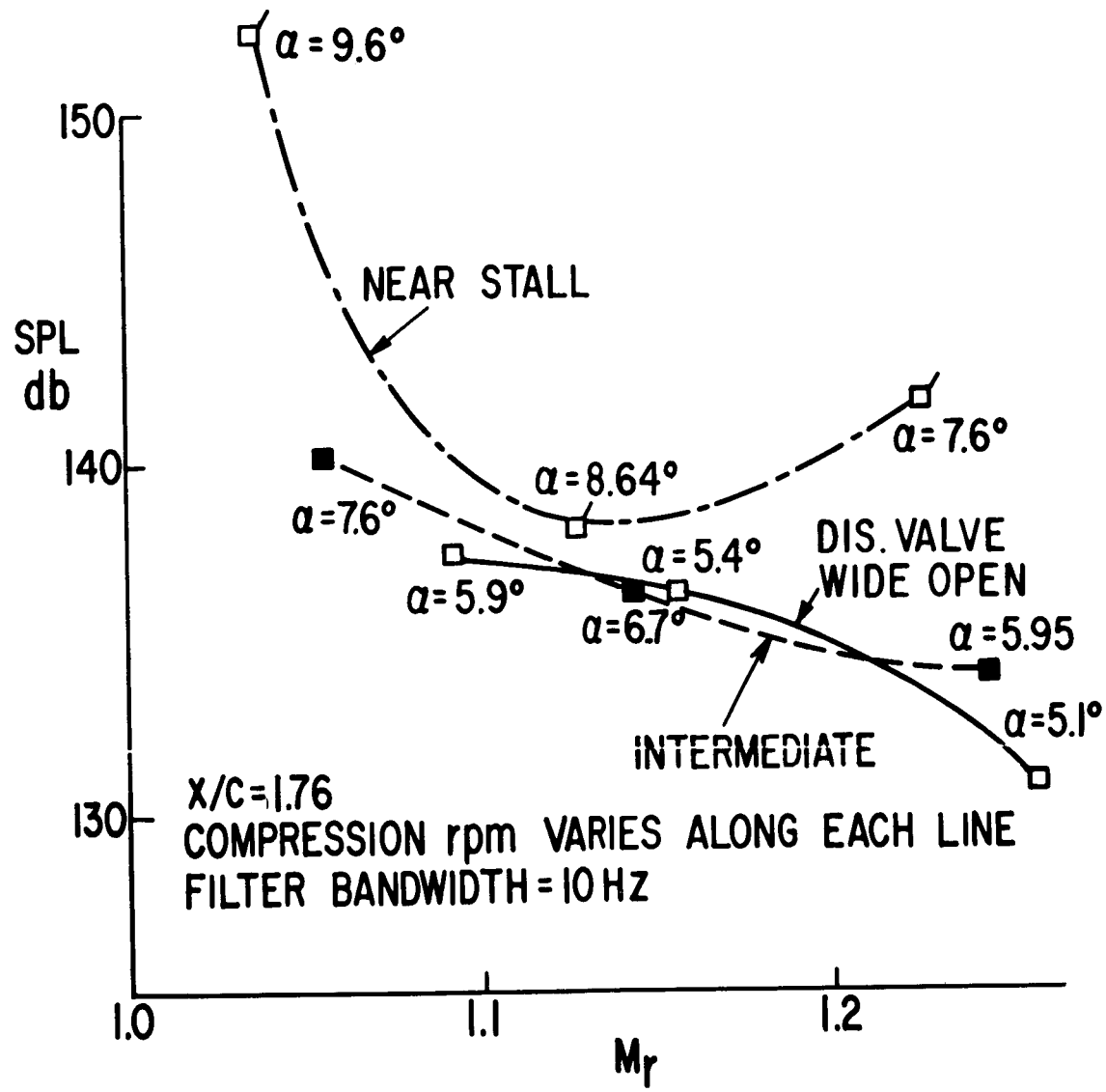

Figure 20. BPF Noise Versus Relative Mach Number.

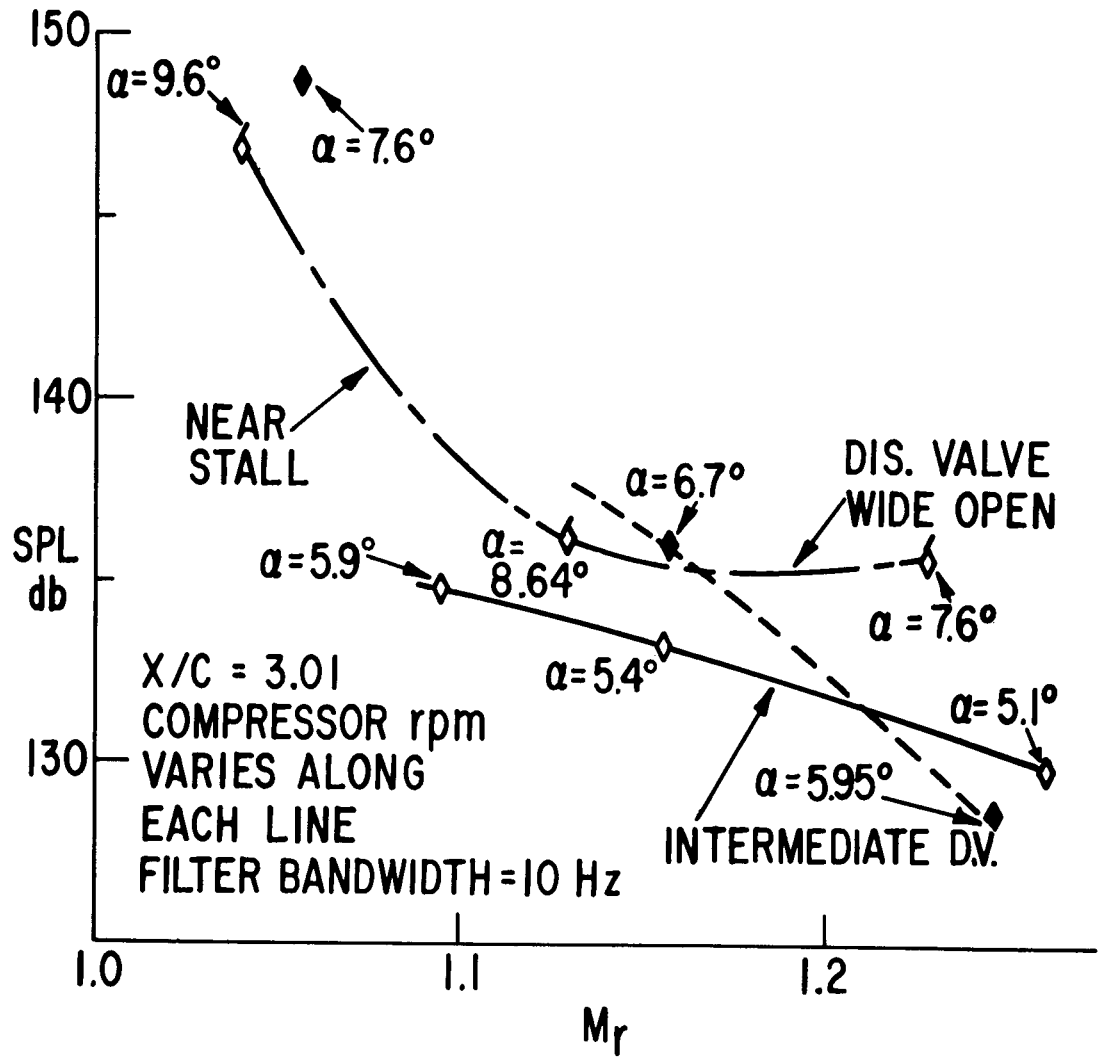

Figure 21. BPF Noise Versus Relative Mach Number.

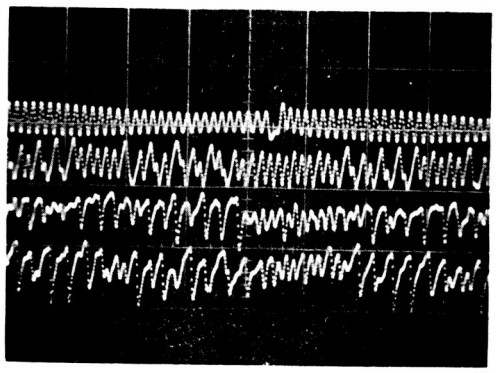

Tach.
x/c = 0.61
x/c = 1.76
x/c = 3.01

BPF = 13.25 KHz
5 psi/cm
2 psi/cm
2 psi/cm

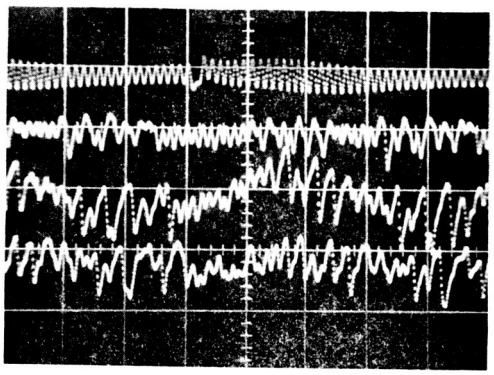

Tach.
x/c = 0.61
x/c = 1.76
x/c = 3.01

BPF = 14 KHZ
5 psi/cm
2 psi/cm
2 psi/cm

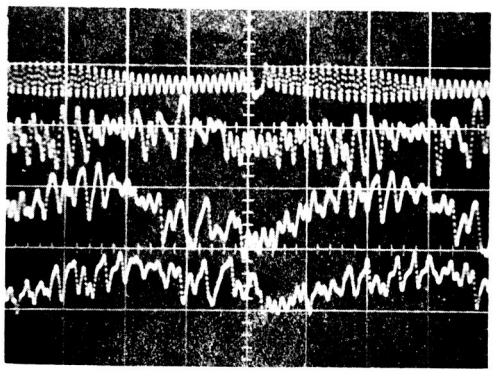

Tach.
x/c = 0.61
x/c = 1.76
x/c = 3.01

BPF = 15.1 KHz
2 psi/cm
2 psi/cm
1.6 psi/cm

Time ——————
0.5 ms/cm

Discharge Valve Wide Open

Figure 22. Wall Static Pressure Traces in the Long Inlet Duct.

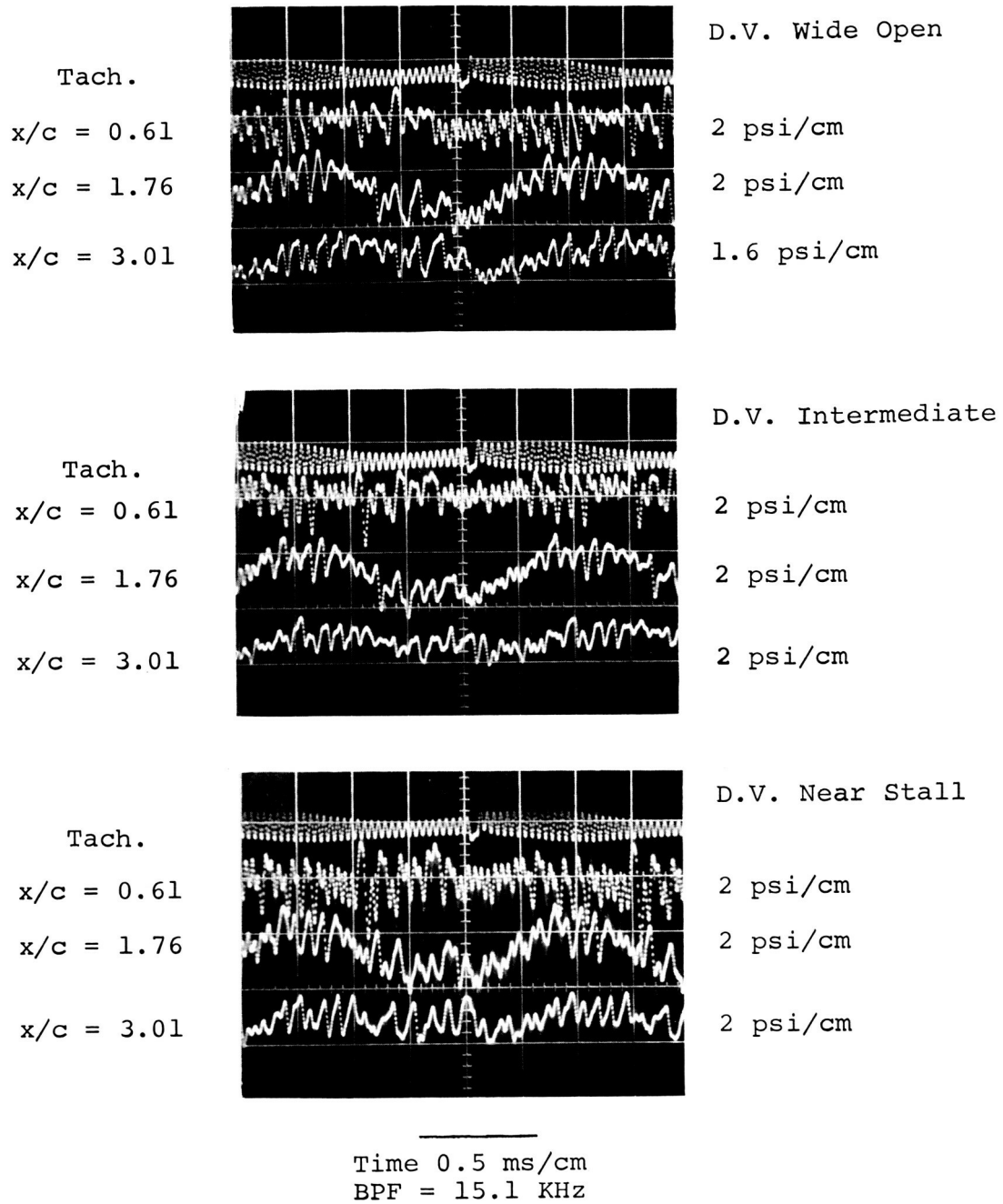

Figure 23. Wall Static Pressure Traces in the Long Inlet Duct.

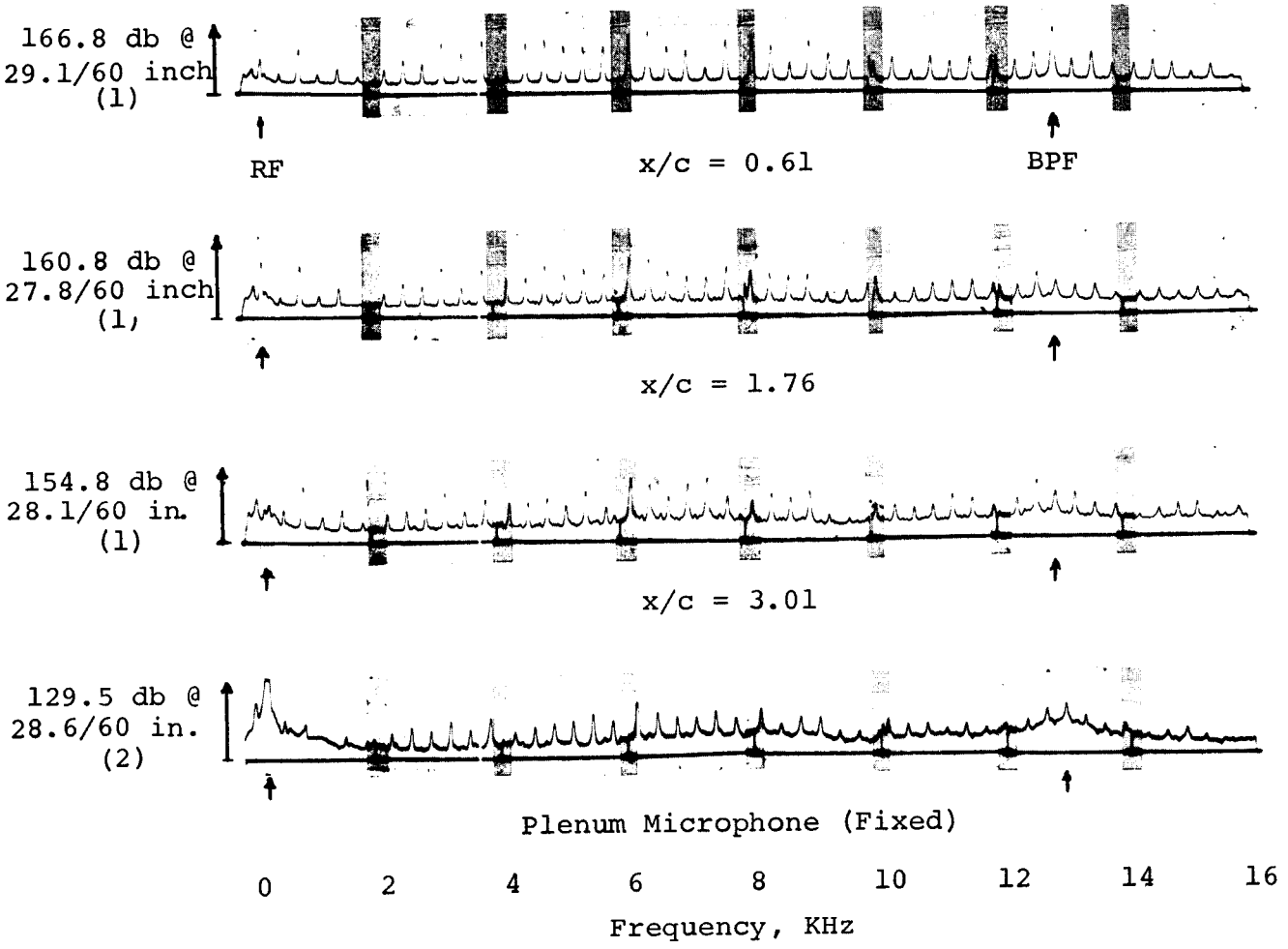

Figure 24. Wall Static SPL Spectrum, BPF = 13.25 KHz, High Flow, Flow Conditions - Mr = 1.094, α = 5.9°.

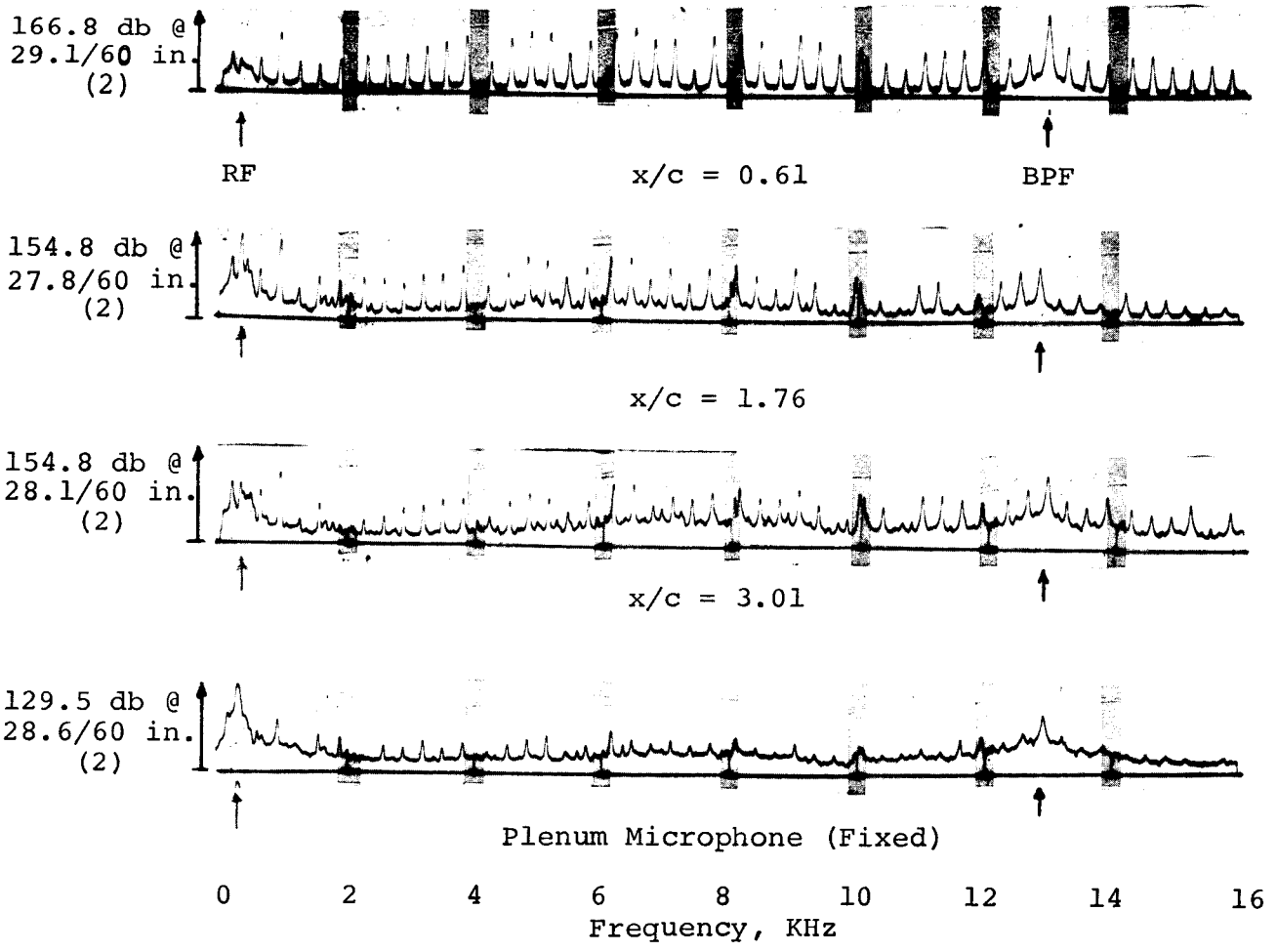

Figure 25. Wall Static SPL Spectrum, BPF = 13 KHz, Intermediate Flow, Flow Conditions - Mr = 1.056, α = 7.6°.

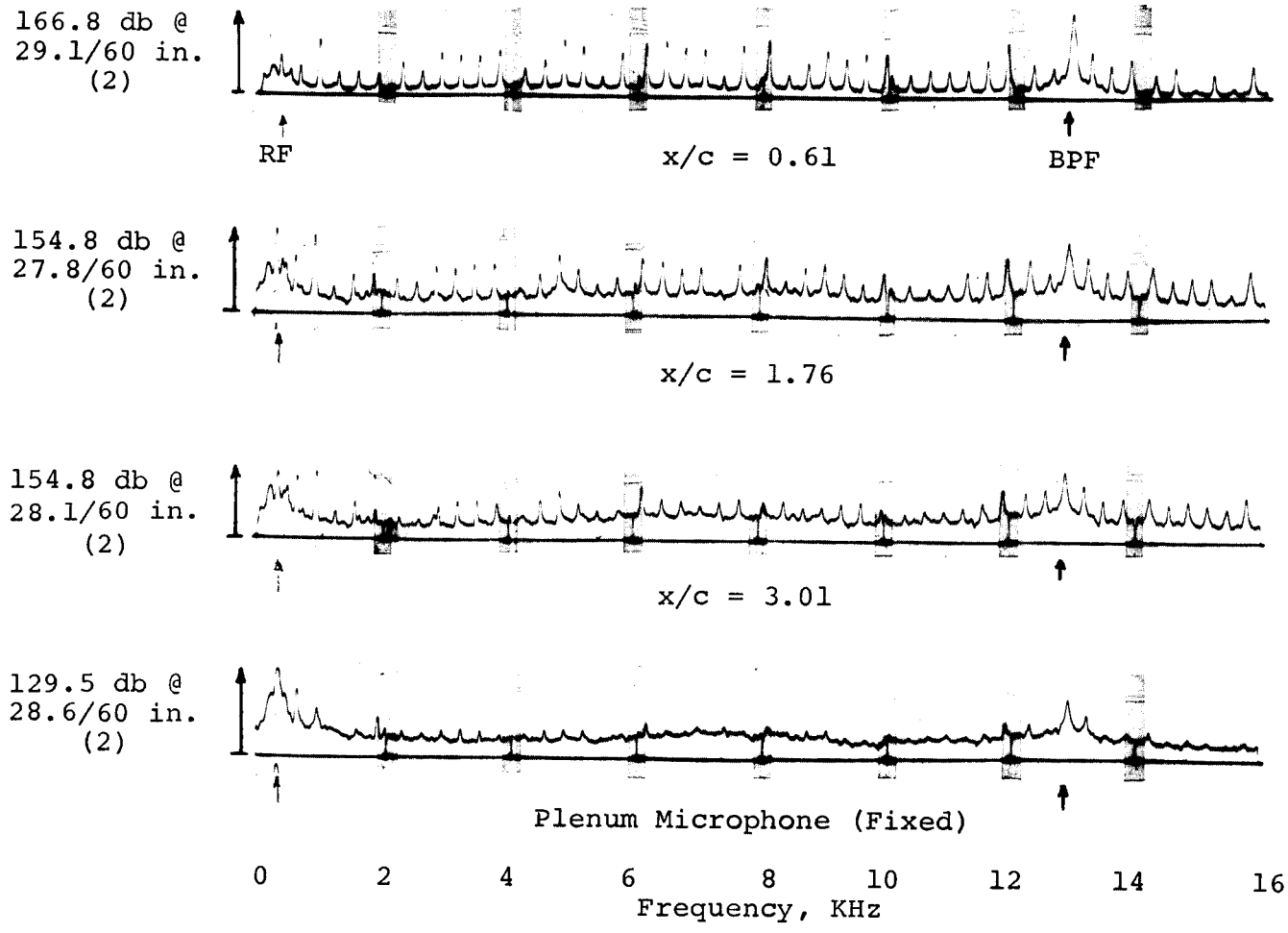

Figure 26. Wall Static SPL Spectrum, BPF = 13 KHz, Near Stall, Flow Conditions - Mr = 1.037, α = 9.6°.

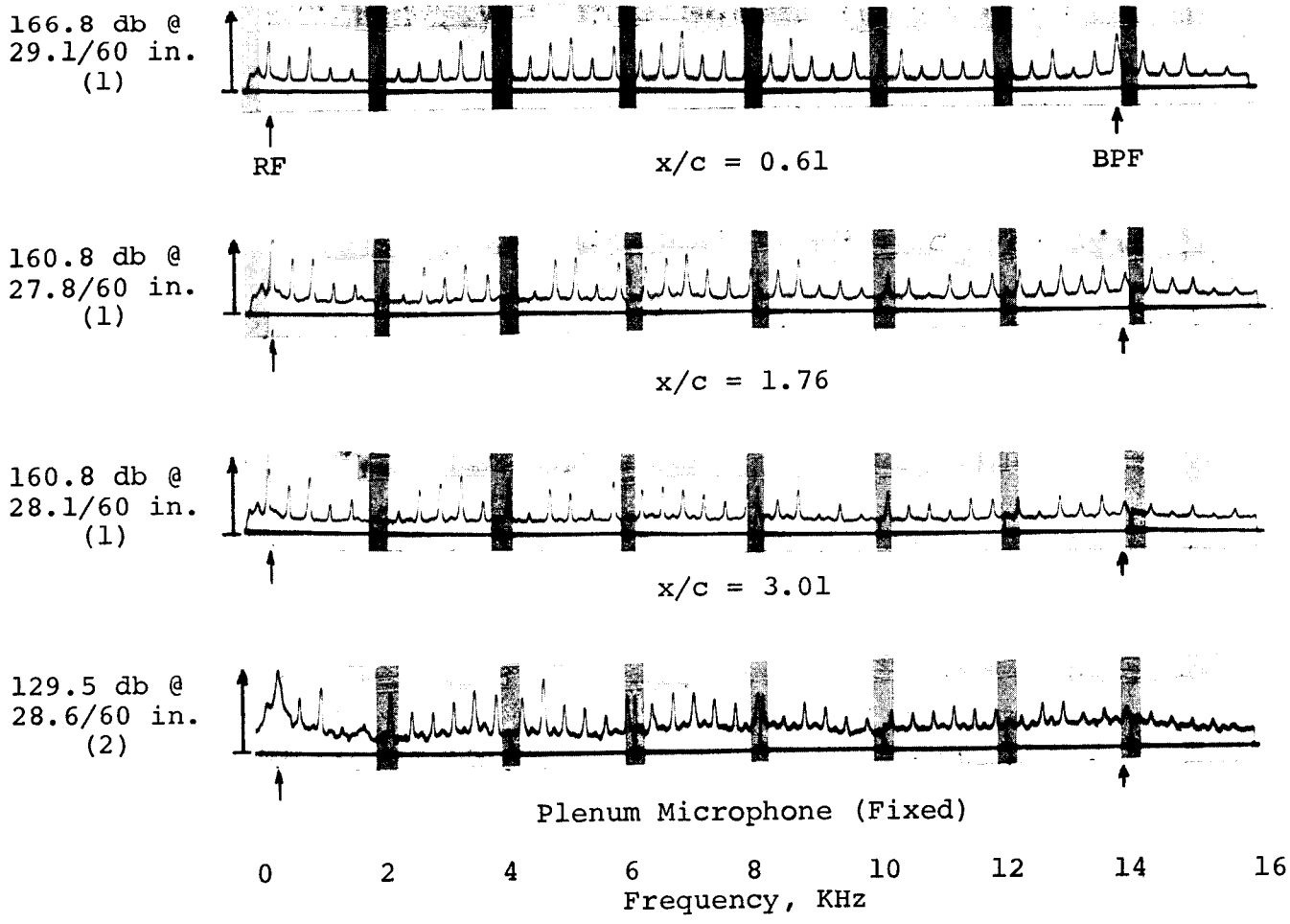

Figure 27. Wall Static SPL Spectrum, BPF = 14 KHz, High Flow, Flow Conditions - Mr = 1.158, α = 5.4°.

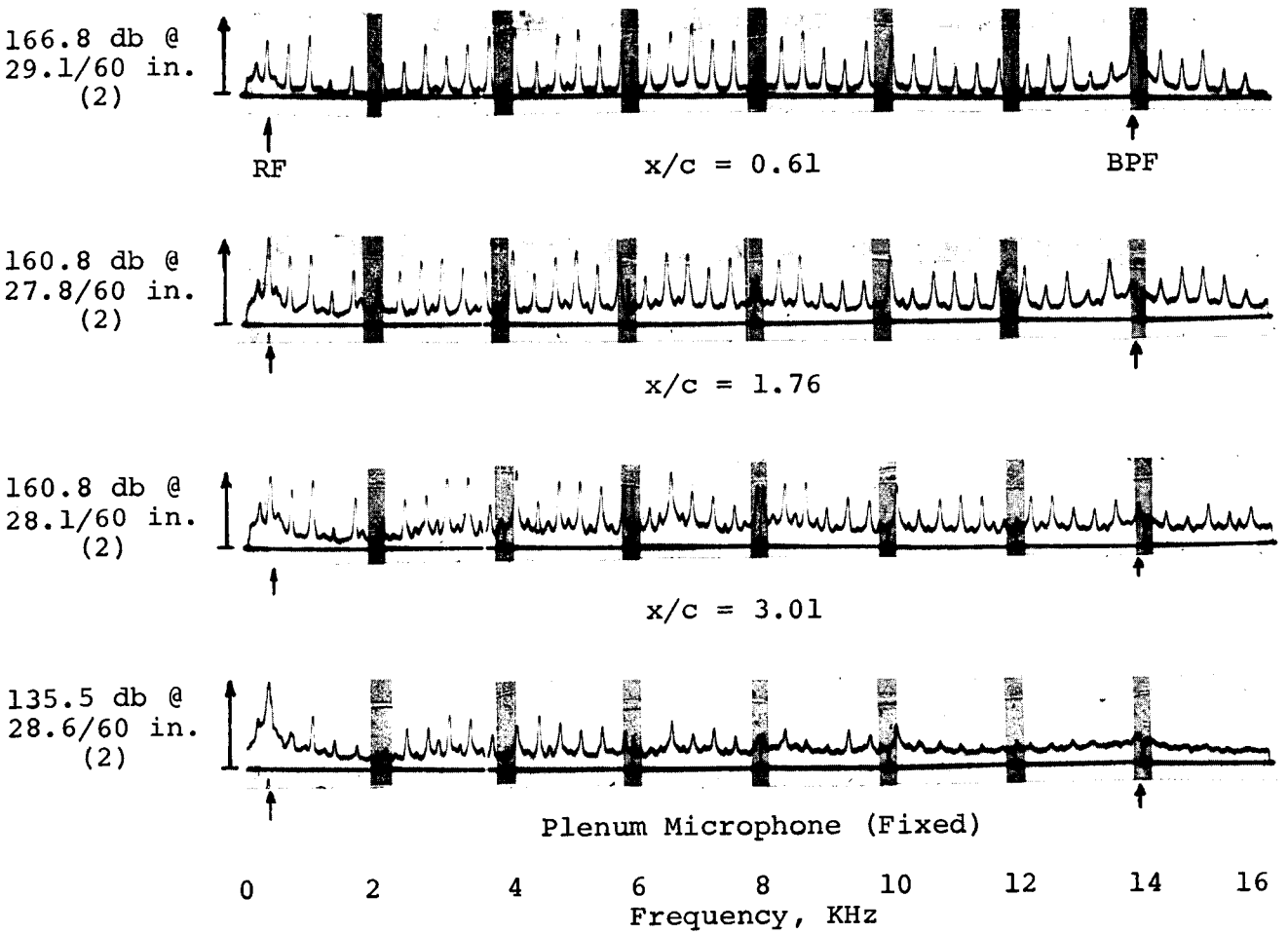

Figure 28. Wall Static SPL Spectrum, BPF = 14 KHz, Intermediate Flow, Flow Conditions - Mr = 1.144, α = 6.7°.

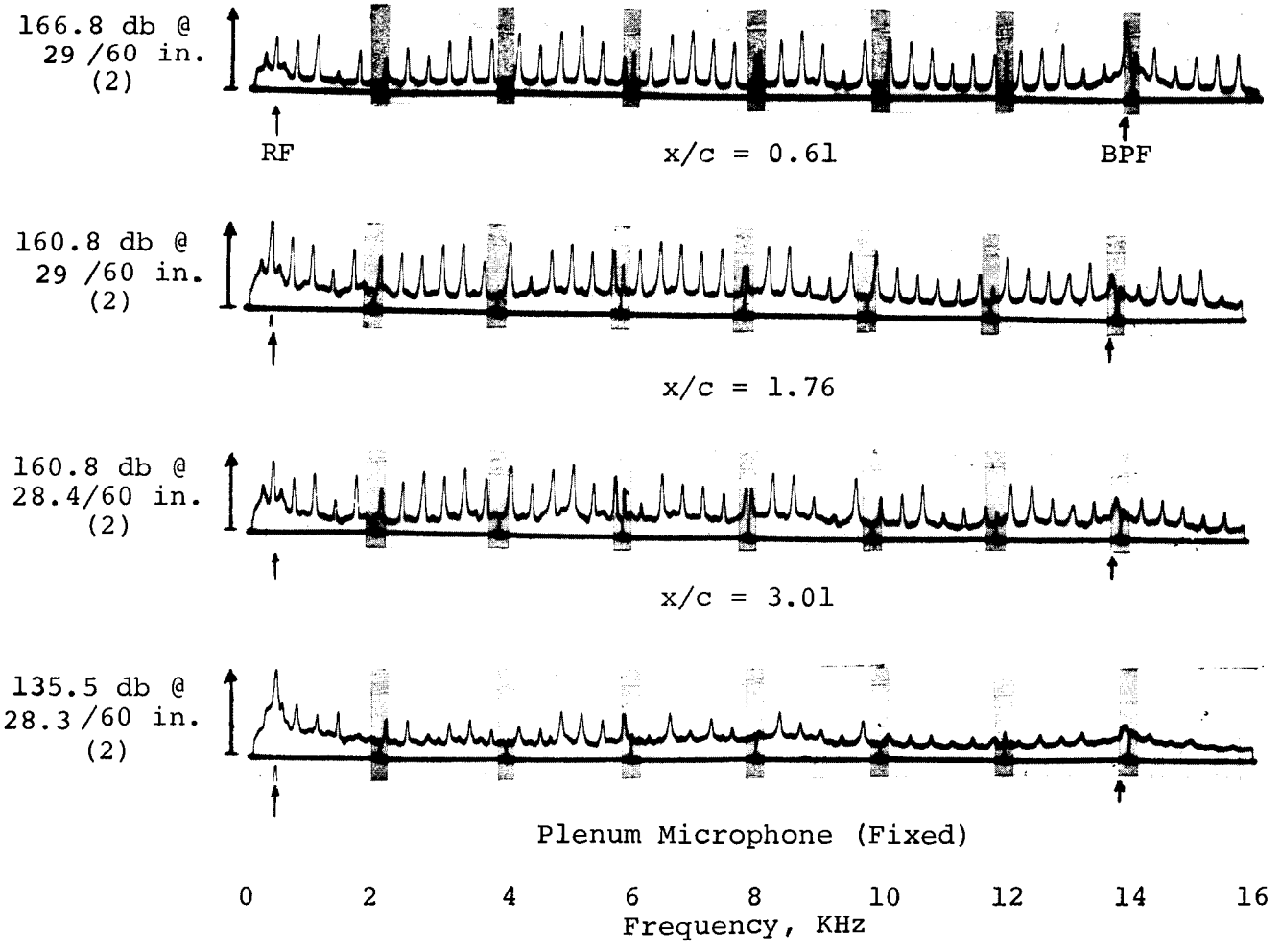

Figure 29. Wall Static SPL Spectrum, BPF = 14 KHz, Near Stall, Flow Conditions - Mr = 1.128, α = 8.65°.

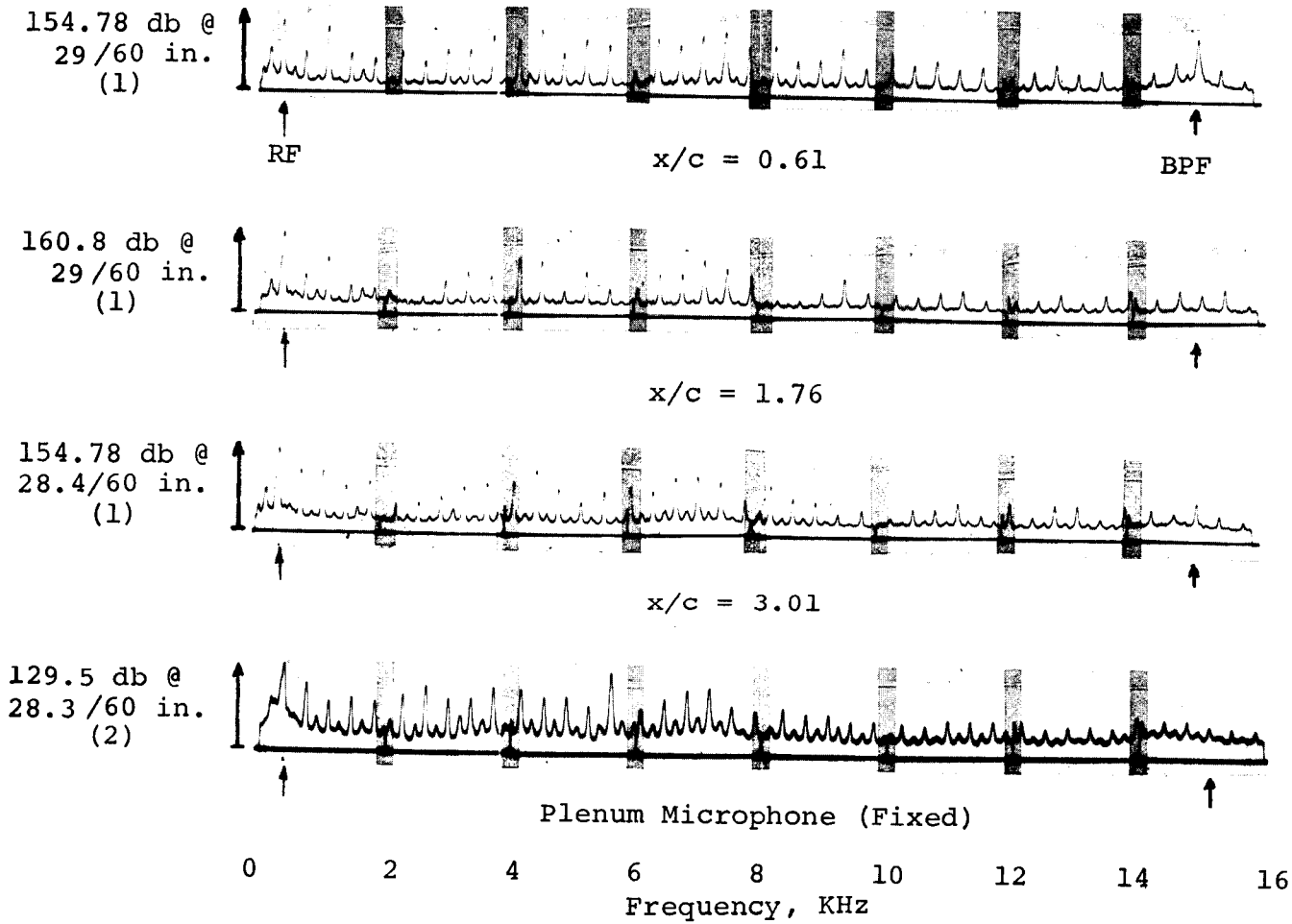

Figure 30. Wall Static SPL Spectrum, BPF = 15.1 KHz, High Flow, Flow Conditions - Mr = 1.26, α = 5.1°.

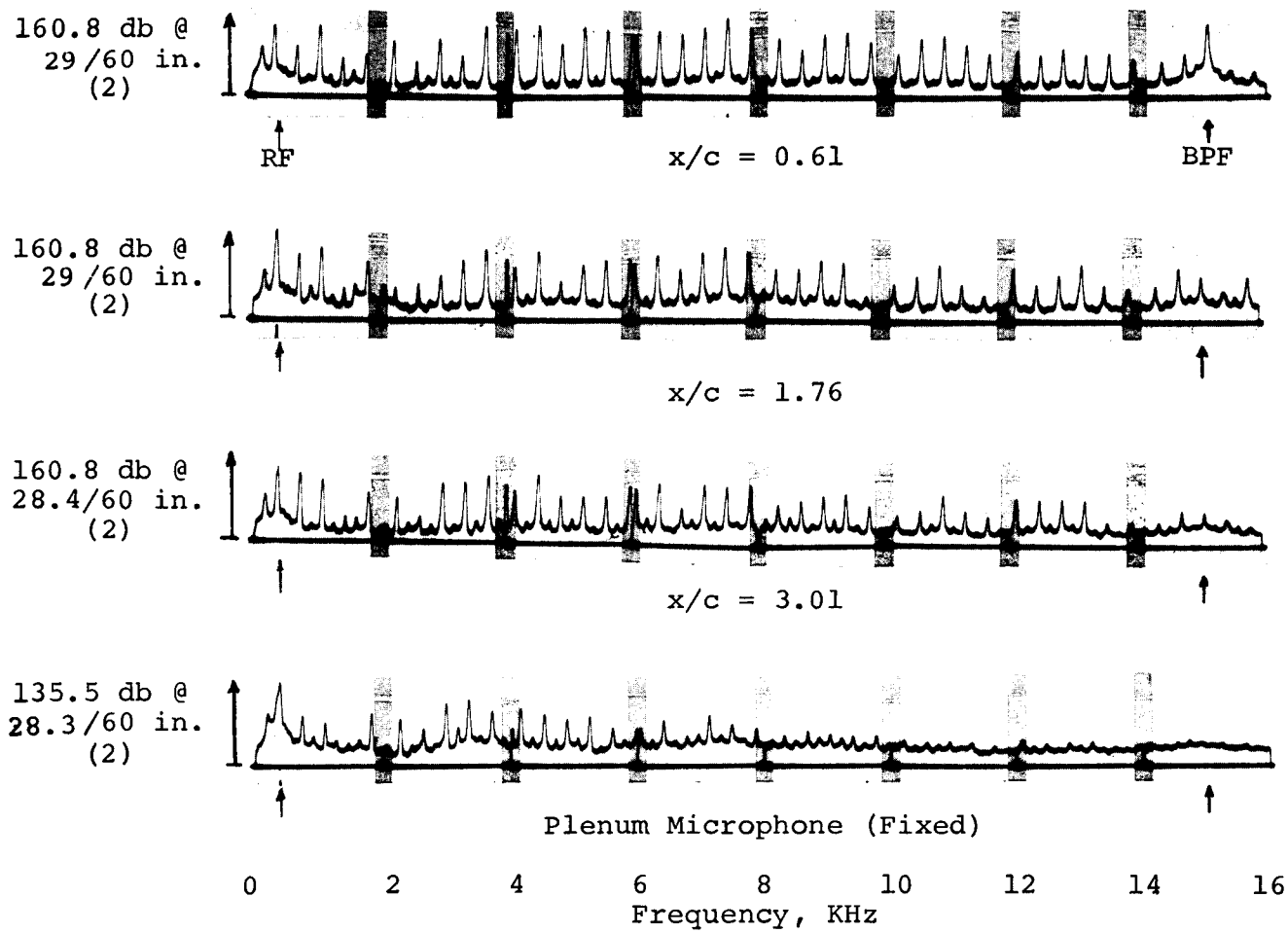

Figure 31. Wall Static SPL Spectrum, BPF = 15.1 KHz, Intermediate Flow, Flow Conditions - Mr = 1.245, α = 5.96°.

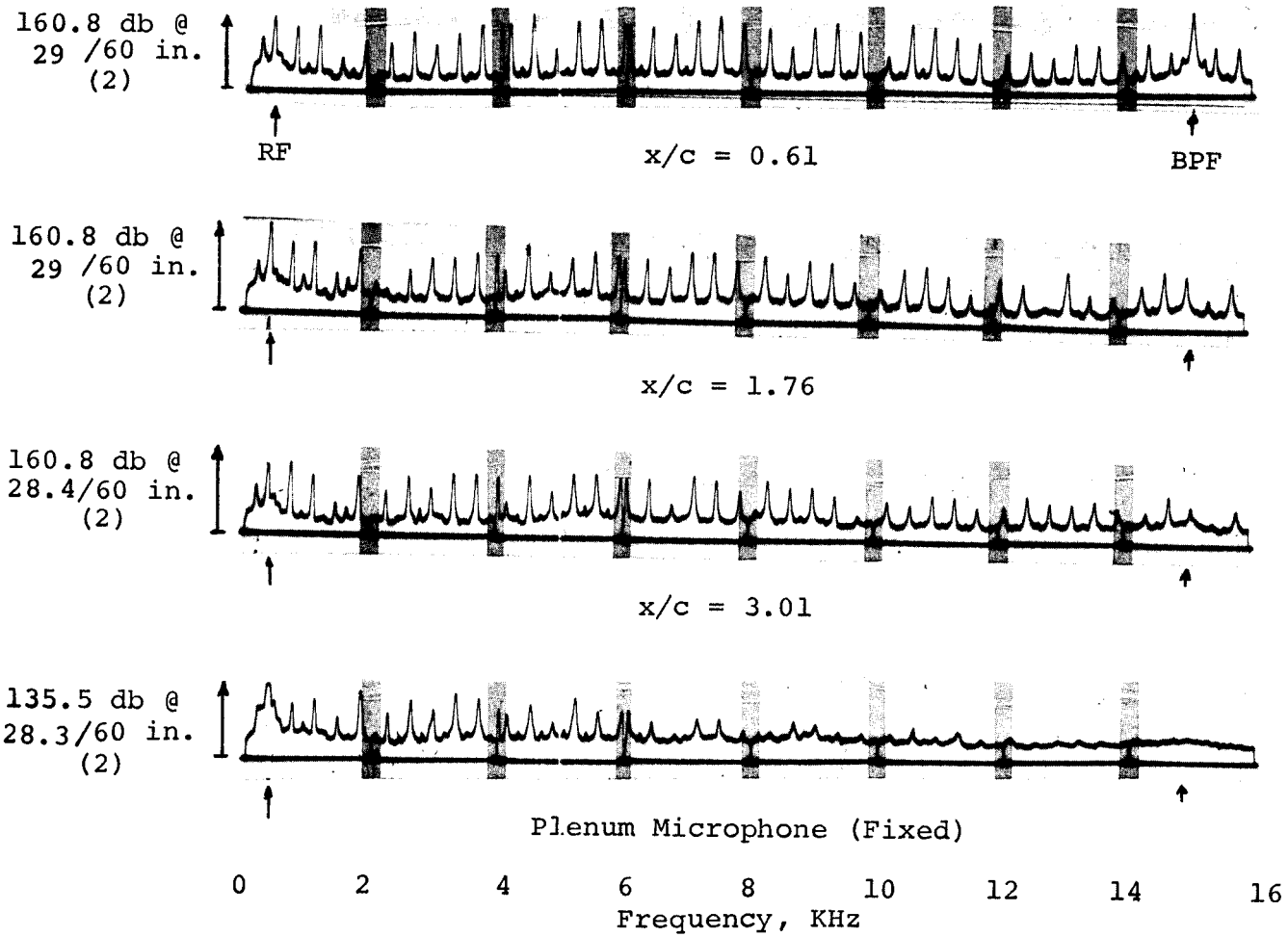

Figure 32. Wall Static SPL Spectrum, BPF = 15.1 KHz, Near Stall, Flow Conditions - Mr = 1.226, α = 7.6°.

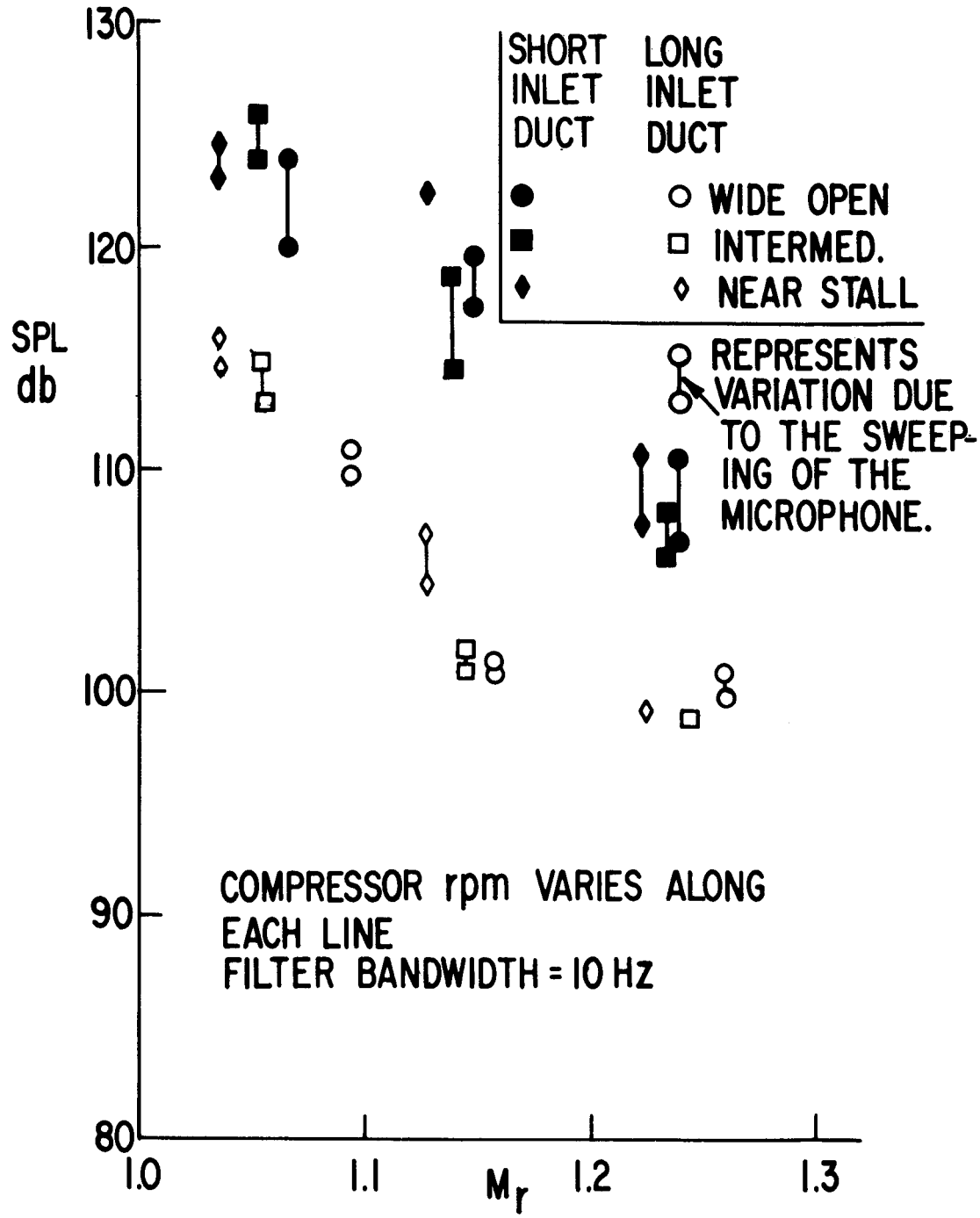

Figure 33. Plenum BPF Noise Versus Mach Number.

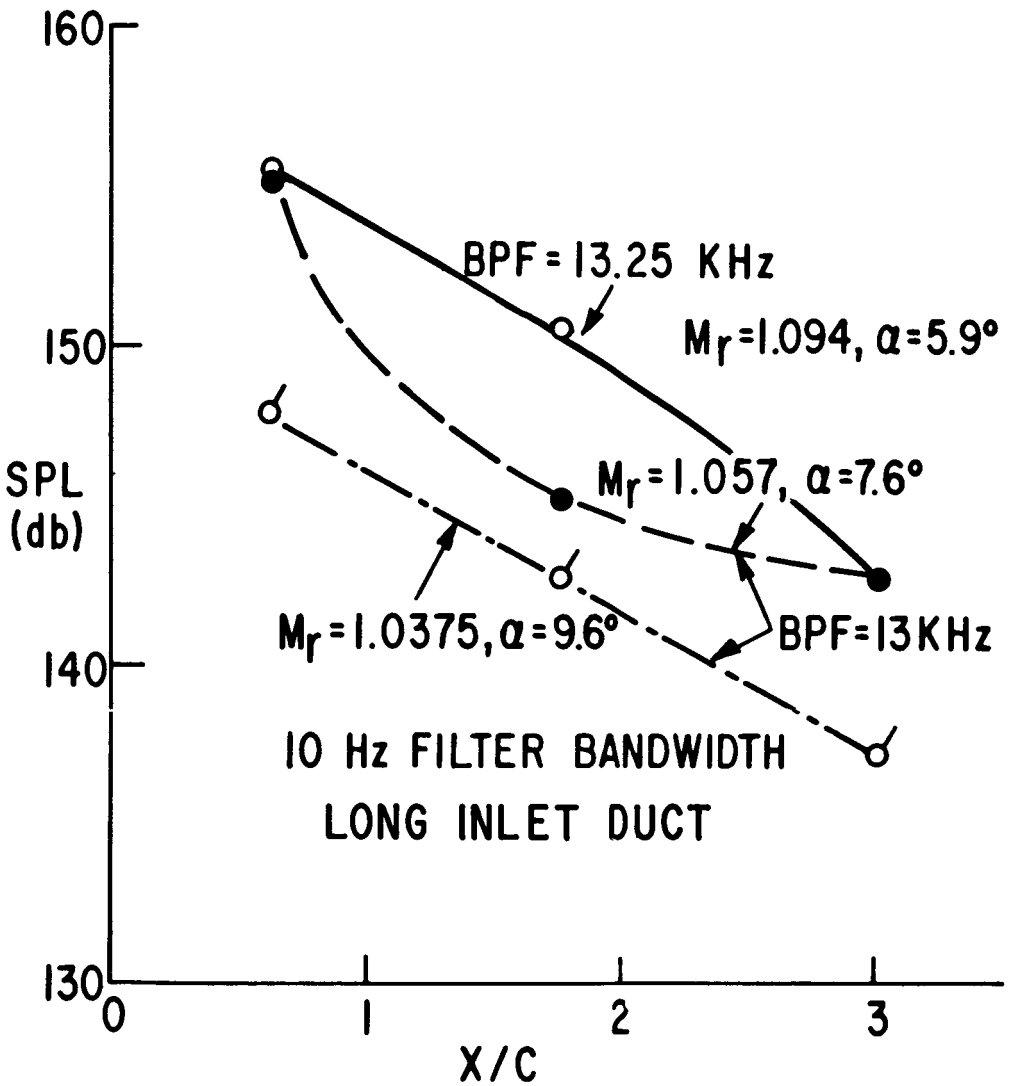

Figure 34. MPT Noise Versus Axial Distance, Low Speed.

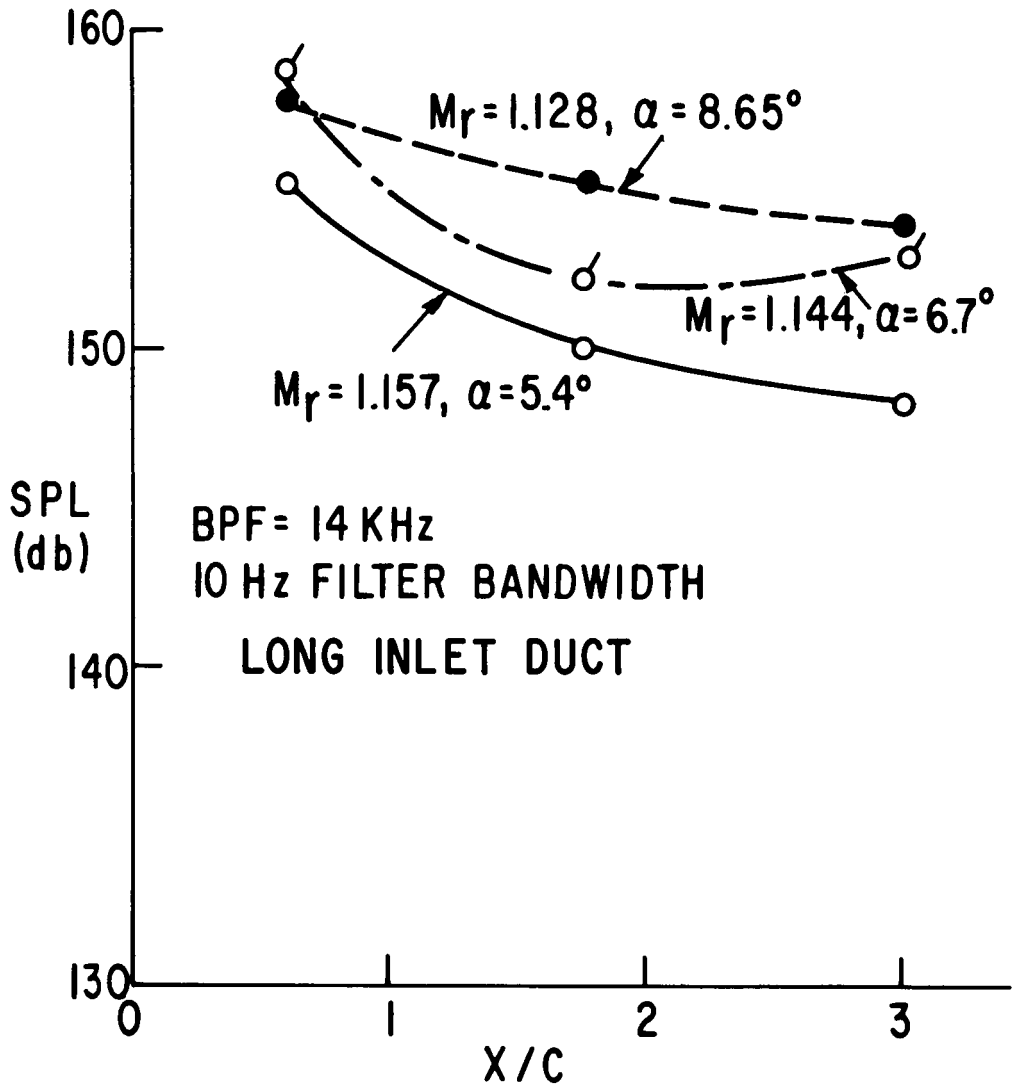

Figure 35. MPT Noise Versus Axial Distance, Intermediate Speed.

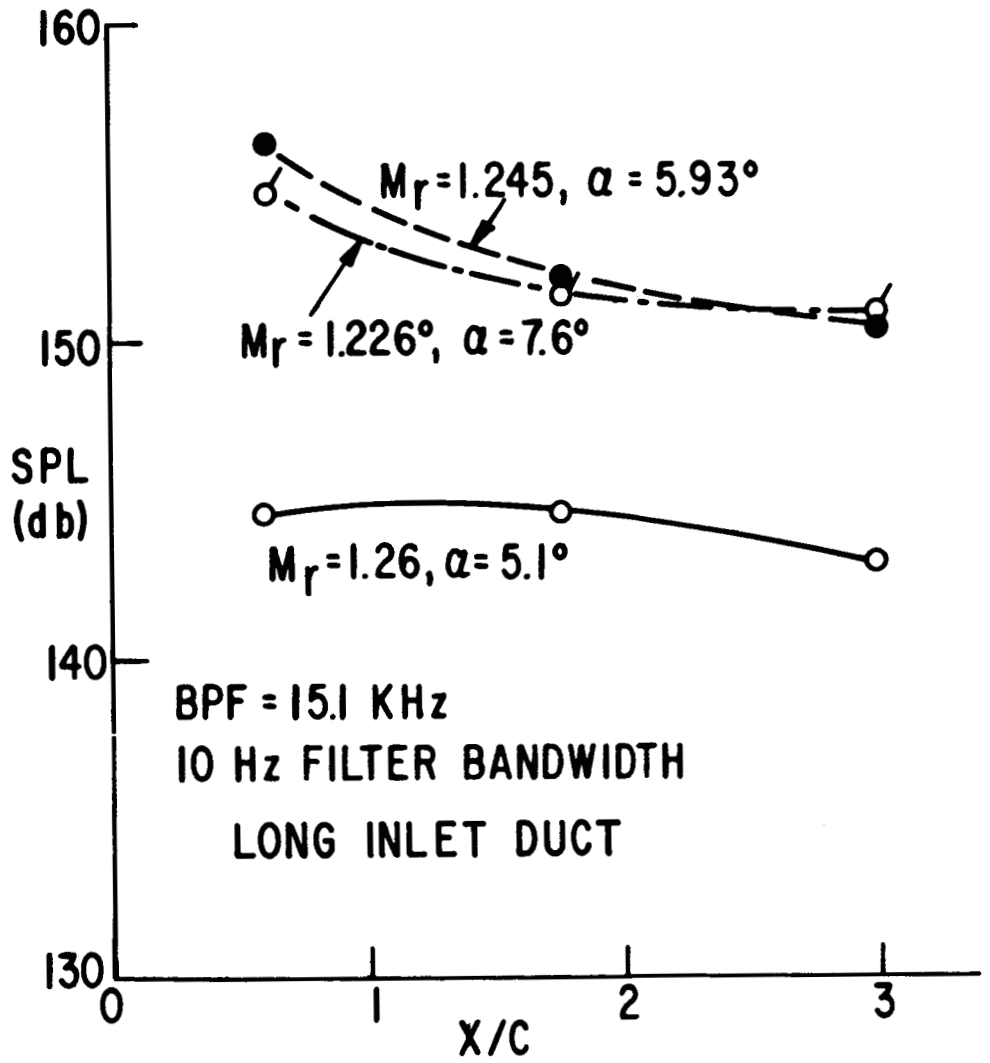

Figure 36. MPT Noise Versus Axial Distance, High Speed.

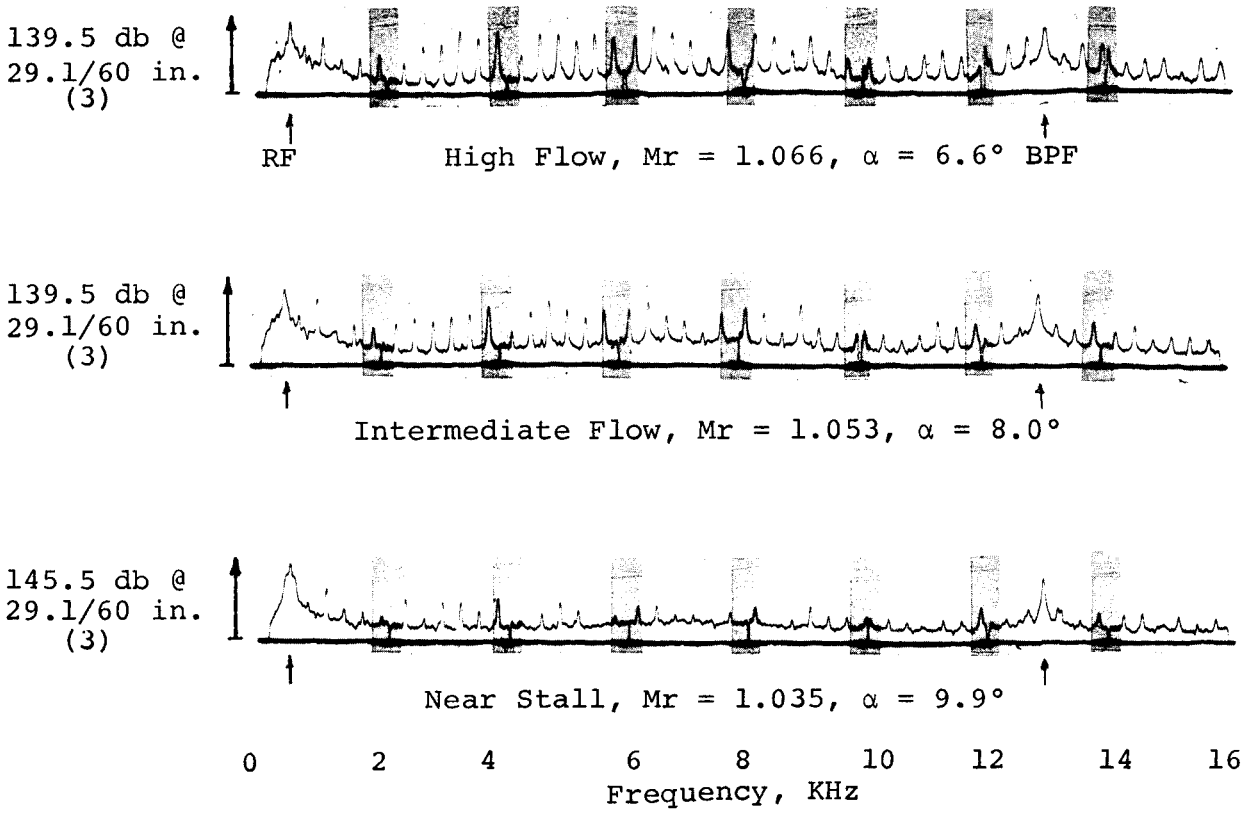

Figure 37. Plenum SPL Spectrum, Short Inlet, BPF = 13 KHz, Microphone Steady.

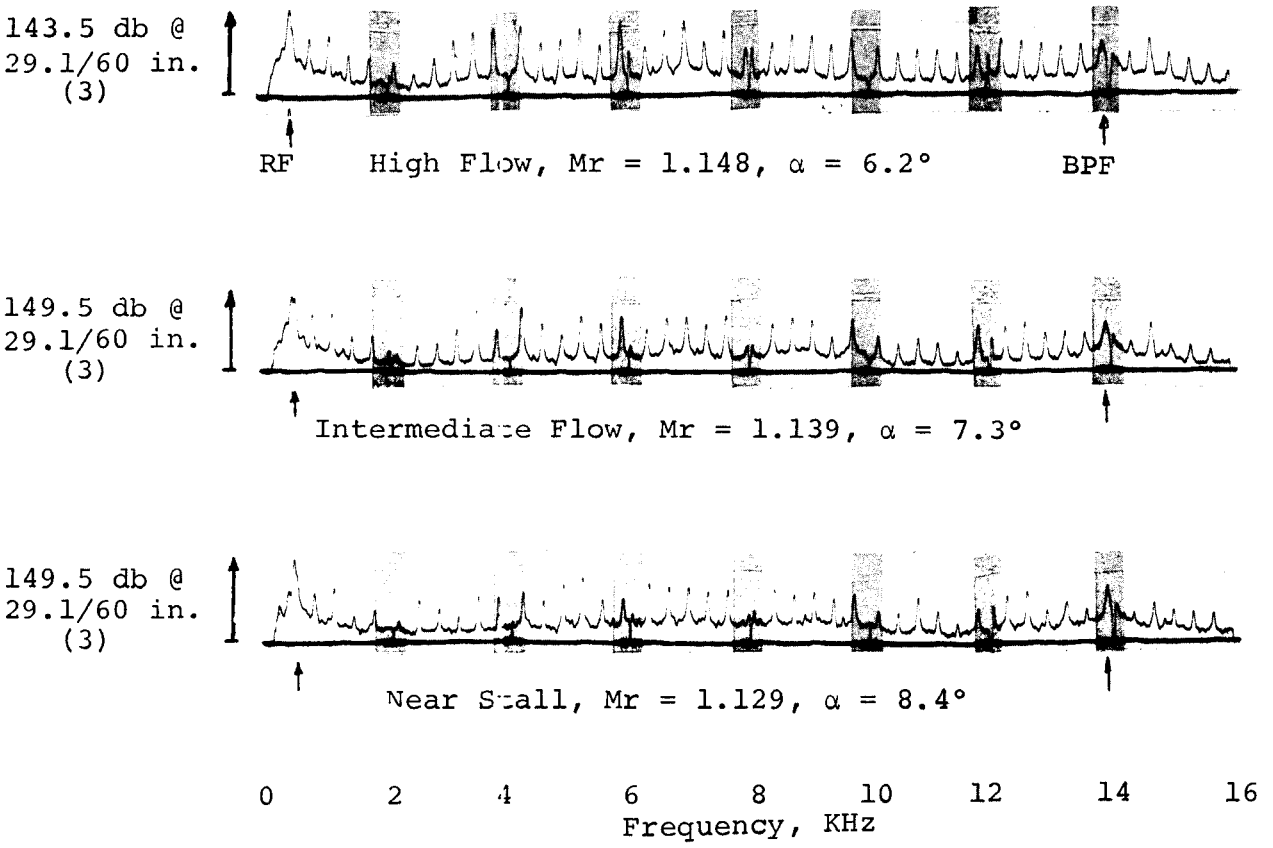

Figure 38. Plenum SPL Spectrum, Short Inlet, BPF = 14 KHz, Microphone Steady.

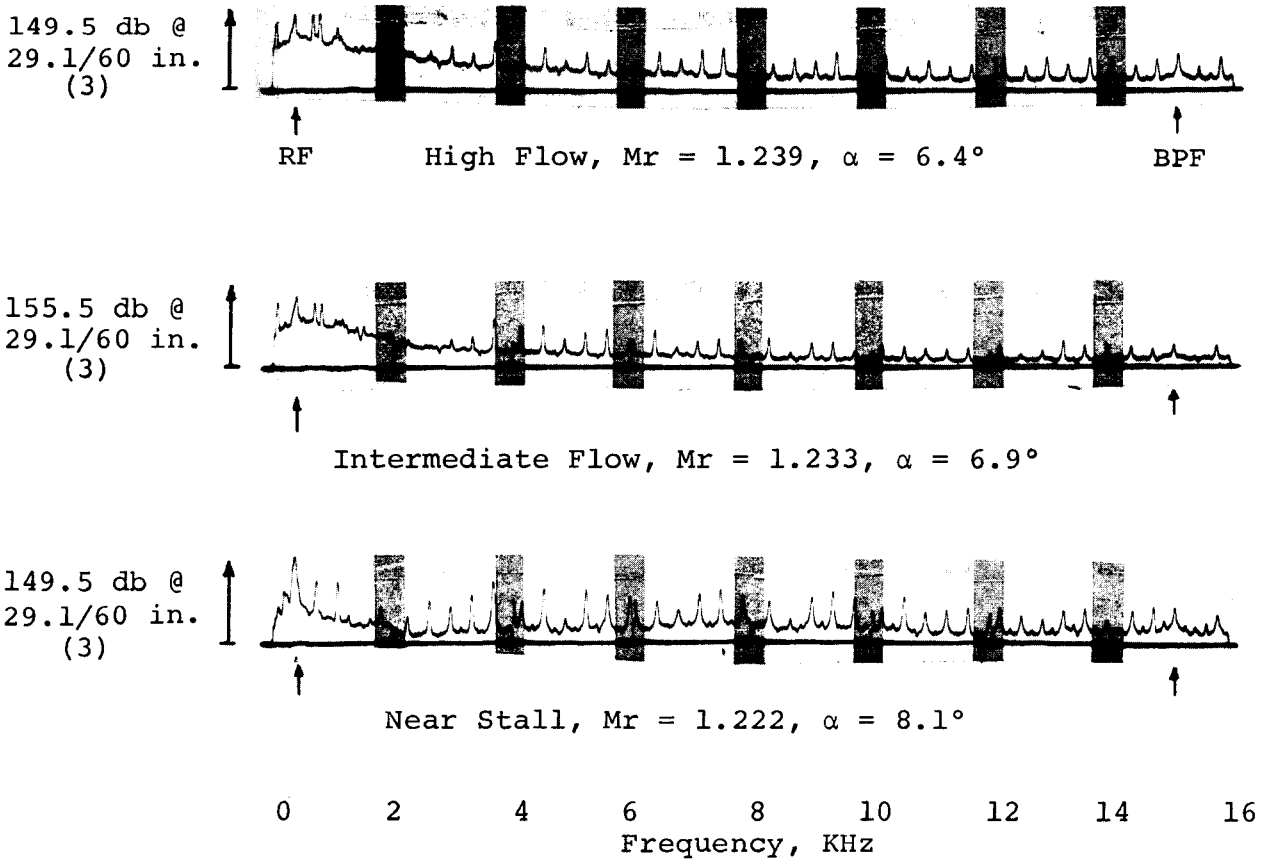

Figure 39. Plenum SPL Spectrum, Short Inlet, BPF = 15.1 KHz, Microphone Steady.

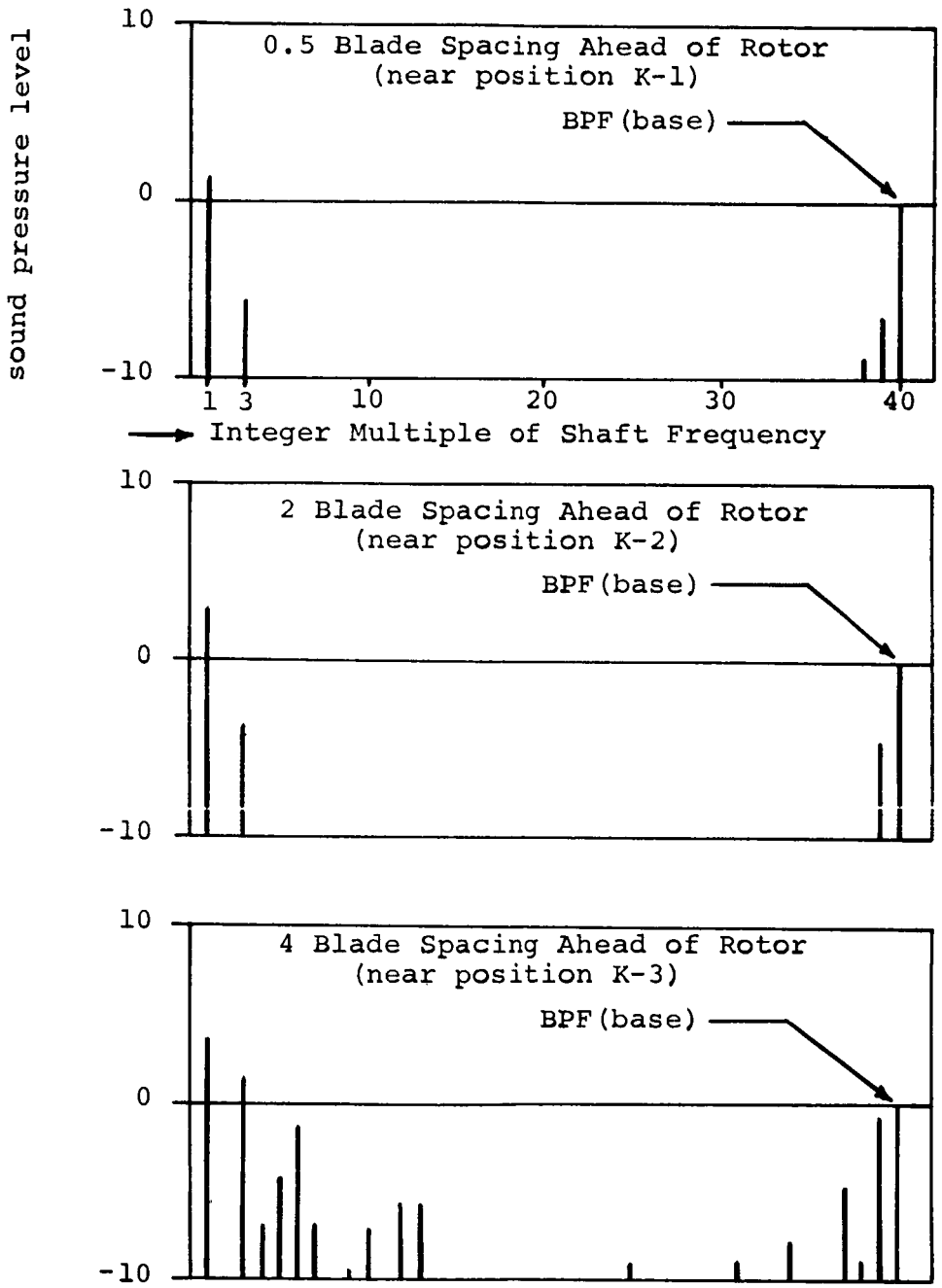

Figure 40. Computed Evolution of MPT for Model Rotor (M_∞ = 1.25, angle of attack = 1.8 degrees)

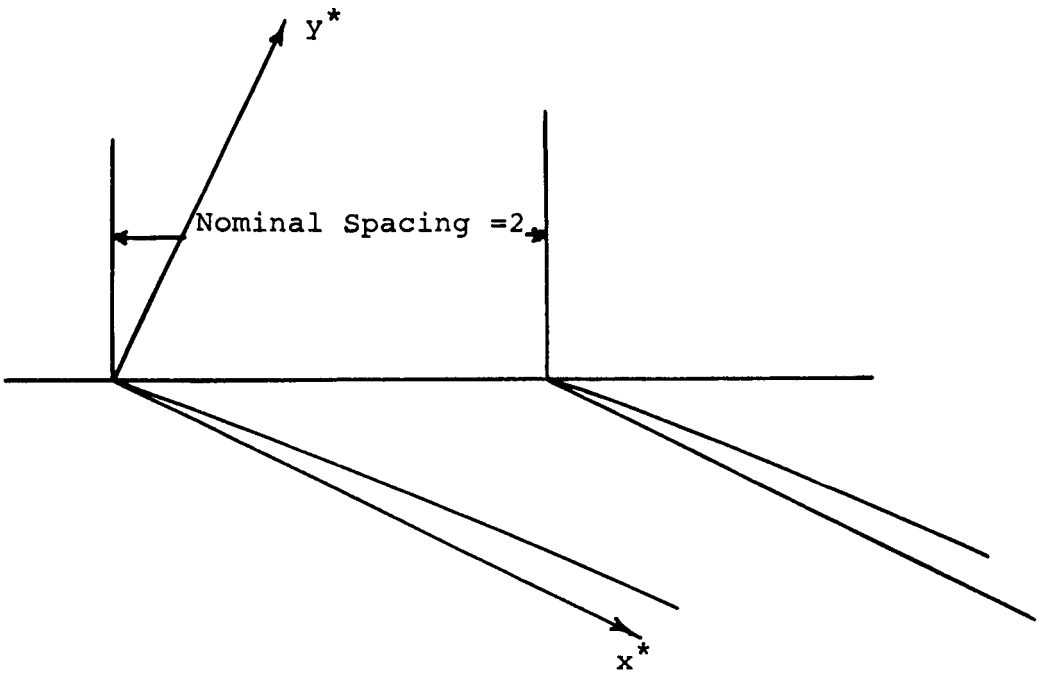

Figure 41. Coordinate System.

Table 1

Cascade Geometry and Tolerances

Mach number far upstream	1.4
incidence angle far upstream	72 degrees (measured from axial direction)
number of blades	38
nominal stagger angle	65 degrees (measured from axial direction)
tolerance in stagger	± 3/4 degrees
tolerance in blade spacing	± 0.1% of nominal spacing
nominal surface contour	*parabolic shape

* $$\frac{2y^*}{s} = -0.555 \left(\frac{2x^*}{s}\right)^2 + 0.17633 \left(\frac{2x^*}{s}\right)$$

where x*: taken along the line the angle of which measured from the axial direction is equal to stagger angle (see Fig. 40)

s: nominal spacing

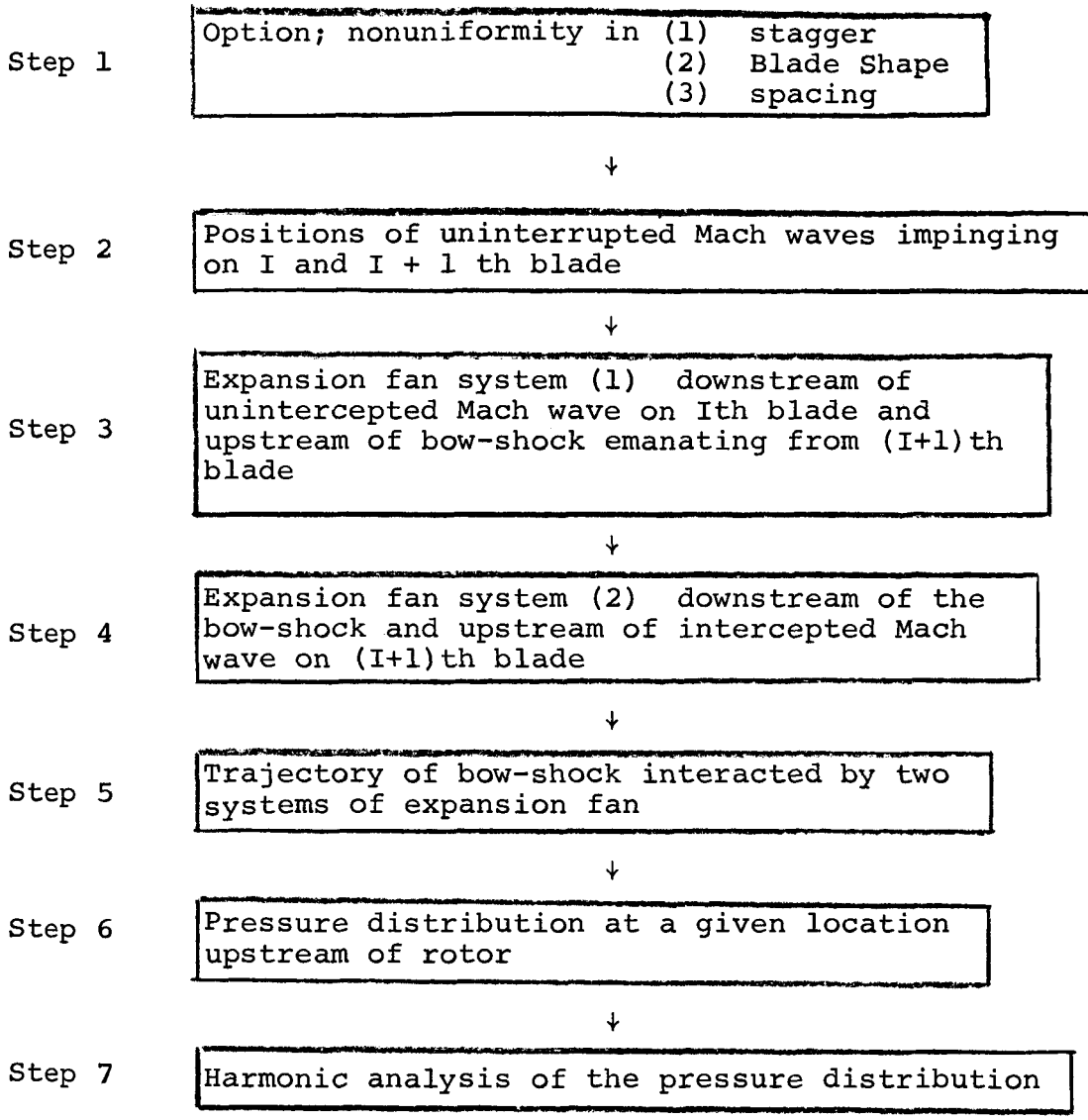

FLOW CHART

Figure 42. Structure of program "MPT".

BLADE SPACING ERRORS DISTRIBUTION

Table 2

Blade No.	A-1	A-2
1	+*	-
2	+	+
3	+	-
4	-	-
5	+	-
6	-	+
7	-	+
8	+	-
9	-	+
10	+	-
11	+	-
12	-	+
13	-	-
14	-	+
15	+	-
16	+	+
17	-	+
18	+	+
19	+	-
20	-	+
21	+	-
22	-	-
23	-	+
24	-	+
25	-	+
26	+	+
27	+	-
28	-	+
29	+	-
30	+	-
31	-	+
32	+	-
33	-	+
34	+	-
35	-	+
36	-	-
37	+	+
38	+	-

*
+ means + 0.1% error
- means - 0.1% error

STAGGER ERRORS DISTRIBUTION

Table 3

Blade No.	B-1	B-2
1	+*	-
2	+	+
3	+	+
4	+	+
5	-	-
6	-	-
7	+	+
8	+	-
9	+	+
10	+	+
11	+	+
12	-	-
13	-	-
14	+	+
15	-	-
16	-	-
17	+	+
18	-	-
19	-	+
20	-	+
21	+	+
22	-	-
23	-	-
24	-	-
25	+	+
26	-	-
27	+	+
28	-	-
29	+	+
30	-	-
31	+	+
32	+	+
33	-	-
34	-	-
35	+	-
36	+	+
37	+	-
38	+	+

*
+ means + 0.75 degrees error
- means - 0.75 degrees error

TABLE 4

ACOUSTIC SUMMARY - LONG INLET

BPF(KHz)	Mr	α(deg)	X/C	SPL/BPF db	ΔSPL*/MRF≠ db	ΔSPL/MRF db	SPL/MRF db
13.25	1.094	5.9	0.61	155.9	-9.8/3	-1.2/20	154.7/20
			1.76	137.5	12.3/1	+13.1/19	150.6/19
			3.01	135.0	5.5/3	9.2/19	144.2/19
13	1.057	7.6	0.61	165.9	-16/1	-11.3/20	154.6/20
			1.76	140.3	17.1/1	4.9/19	145.2/19
			3.01	148.4*	-1.7/3	-7/19	144.4/19
13	1.0375	9.6	0.61	167.2	-18.7/3	-19.4/25	147.8/25
			1.76	152.4	5.4/1	-9.7/25	142.7/25
			3.01	146.9	-3.6/1	-9.7/19	137.2/19
14	1.157	5.4	0.61	152.5	-2.7/1	2.7/20	155.2/20
			1.76	136.4	22.3/1	13.6/20	150/20
			3.01	133.1	18.2/1	15.2/10	148.3/10
14	1.144	6.7	0.61	159.5	-8/3	-1.8/20	157.7/20
			1.76	136.4	29.8/1	18.8/12	155.2/19
			3.01	136.0	16.7/1	17.9/12	153.9/19
14	1.128	8.65	0.61	163.1	-11.6/3	-4.4/15	158.7/15
			1.76	138.2	26.9/1	13.9/19	152.1/19
			3.01	136.0	16.5/1	16.9/15	152.9/15
15.1	1.26	5.1	0.61	144.7	4.1/1	0.4/12	145/12
			1.76	131.0	27.5/1	14.6/11	145.6/11
			3.01	129.9	22.9/1	13.2/12	143.1/12
15.1	1.245	5.93	0.61	152.6	1.3/1	3.6/20	156.2/20
			1.76	134.0	33.1/1	18/20	152/20
			3.01	128.8	26.4/1	21.7/10	150.5/20
15.1	1.226	7.6	0.61	159.2	-6.6/1	-4.6/12	154.6/12
			1.76	141.8	24/1	9.9/12	151.7/12
			3.01	135.5	14.4/2	15.2/20	150.7/20

* Broadband noise high

≠ MRF - Multiples of rotor frequency

\+ ΔSPL - Deviation from SPL at BPF

Table 5

Acoustic Summary - Plenum

BPF (KHz)	M_r	α (deg)	SPL/RF db	SPL/MRF* db	SPL/BPF db	
13.25	1.094	5.9	129.3	109.7/19	103.7	
13.	1.057	7.6	133.9	103.6/19	108.3	
13.	1.0357	9.6	135.7	97.0/19	109.5	
14.	1.157	5.4	131.3	122.9/13	97.5	
14.	1.144	6.7	139.9	117.1/9	97.2	Long Inlet
14.	1.128	8.65	141.1	113.9/14	101.6	
15.1	1.26	5.1	135.7	128.0/16	95.9	
15.1	1.245	5.93	136.0	123.8/10	95.5	
15.1	1.226	7.6	131.5	124.3/10	95.8	
13.	1.066	6.6	129.5	123.2/20	119.1	
13.	1.053	8.0	130.8	121.5/15	121.8	
13.	1.035	9.9	139.6	116.4/12	125.2	
14.	1.148	6.2	143.8	133.2/20	113.9	
14.	1.139	7.3	139.5	132.0/12	116.5	Short Inlet
14.	1.129	8.4	146.9	131.3/15	123.3	
15.1	1.239	6.4	141.6	119.9/21	108.7	
15.1	1.233	6.9	144.3	127.8/10	106.7	
15.1	1.222	8.1	148.1	129.3/10	109.6	

*MRF - Multiples of rotor frequency.

Table 6

Input Data for MPT Computation of Experimental Rotor

Mach Number far upstream	1.25
incidence angle far upstream	63.8 degrees (measured from axial direction)
number of blades	40
nominal stagger angle	62 degrees (measured from axial direction)
errors in stagger	see Fig. 11
errors in blade spacing	see Fig. 11
nominal surface contour near the leading edge	* parabolic shape

* $\frac{2y^*}{s} = -0.04279 \left(\frac{2\pi^*}{s}\right)^2 + 0.06993 \left(\frac{2x^*}{s}\right)$

Appendix 1. Description of Computer Program "MPT"

The main structure of this program is shown in Fig. 42 and a brief description is given below. In step 1, various options are provided so that examinations can be carried out on the effects of manufacturing errors in:

(1) stagger angle,

(2) blade shape near the leading edge, and

(3) spacing.

The effects of each error can be investigated independently of other errors or can be examined along with others. As explained in the section 2.0, it is necessary for the subsequent computation to identify the positions of the uninterrupted Mach wave that are attached to the blades. This is done in step 2. In step 3 and 4, two expansion fan systems upstream and downstream of the bow shock are obtained. The trajectory of the bow shock interacted by the two expansion-fan systems is obtained in step 5. Pressure distribution at a given axial location as a function of peripheral distance is obtained in step 6. In the final step 7, the Fourier analysis of the pressure distribution is performed to determine the harmonic components.

Throughout the program, the unit length is taken to be half of nominal spacing. In addition to the main program, the following subroutines are needed to execute the program.

Subroutine	ISPRESS
"	INSLOP
"	SHOCK
"	PRAND
"	INPRAND
"	FOUCU
"	TANGEN
"	COORD
"	DMACH

The functions of these subroutines are as follows:

ISPRESS compute isentropic pressure ratio between two given Mach numbers.

INSLOP	given the tangent to the airfoil contour, compute the position.
SHOCK	given the upstream Mach number and wedge angle, compute the shock angle and downstream flow condition.
PRAND	given Mach number, compute Prandtl-Meyer function ν.
INPRAN	given Prandtl-Meyer function, compute Mach number.
FOUCU	harmonic analyzer.
TANGEN	given the position on the airfoil, compute the tangent to the surface.
COORD	given the x coordinate of airfoil, compute y coordinate.
DMACH	given a point in expansion fan, compute Mach wave passing through it.

The following input data are necessary to execute the computation.

	INPUT	FORTRAN SYMBOL
(1)	Mach number far upstream	EMACH
(2)	Far upstream flow angle, measured from axial direction, in degrees	THETA
(3)	Number of blades	NB
(4)	Number of Mach wave behind the unintercepted Mach wave (usually 90)	NS
(5)	Maximum axial distance ahead of rotor as ratio to half of the nominal spacing	YMAX
(6)	Number of segment from rotor to maximum axial distance	NSEG
(7)	Number of coefficients of polynomial representing suction surface contour (see 15)	NPRO
(8)	Number of coefficients of polynomial representing suction surface tangent versus coordinate (see 16)	NSLO

(9)	Number of points between shock and unintercepted Mach wave to obtain pressure profile (usually 10)	MMM
(10)	Spacing option If 1, different spacing between blades If 2, identical spacing	ISOP
(11)	Spacing between blades as ratio to half of the nominal spacing; in case of identical spacing, only first spacing is needed	SPACG(I)
(12)	Stagger option If 1, different stagger angle If 2, identical stagger angle	ISTAGR
(13)	Stagger angle, measured from axial direction, in degrees; in case of identical stagger, only first stagger angle is needed	STAGR(I)
(14)	Suction surface option If 1, different suction surface shape If 2, identical suction surface shape	IBSURF
(15)	Jth coefficients of polynomial representing blade shape of Ith blade, C(I,J); $y^* = C(I,1) + C(I,2) X^{*} + \cdots + C(I,J) X^{*(J-1)}$ (for X^*, Y^*, see Fig. 41) In ca e of identical surface shape, only C(1,J) is needed	COEFF(I,J)
(16)	Jth coefficients of polynomial representing tangent-coordinate relationship of Ith blade, A(I,J); $X^* = A(I,1) + A(I,2)\frac{dy^*}{dx^*} + \cdots + A(I,J)(dy^*/dx^*)^{(j-1)}$ In case of identical surface shape, only A(1,J) is needed	SCOEF(I,J)

Throughout the program, the value of specific heat ratio, γ, is taken to be 1.4. In the case of problem involving a gas other than air, the value of γ, designated as GAMMA in the program, has to be changed accordingly.

Appendix 2 Listing of Program "MPT"

```
      **  EMACH=INLET RELATIVE MACH NUMBER
      **  THETA=INLET VELOCITY ANGLE MEASURED FROM AXIS IN DEGREES
      **  NB=NUMBER OF BLADES
      **  NS=NUMBER OF POINTS ON BLADE DOWNSTREAM OF THE UNINTERCEPTED
      **       MACH WAVE
      **  ISOP=SPACING OPTION
      **         IF 1, DIFFERENT SPACING
      **         IF 2, IDENTICAL SPACING
      **    IF IDENTICAL, ONLY FIRST SPACING, SPACING(1), IS NEEDED.
      **  SPACG(I)=SPACING BETWEEN THE BLADES,GIVEN AS RATIO TO CHORD
      **  ISTAGR=STAGGER OPTION
      **         IF 1, DIFFERENT STAGGER
      **         IF 2, IDENTICAL STAGGER
      **     IF IDENTICAL,ONLY FIRST STAGGER,STAGR(1), IS NEEDED
      **  STAGR(I)=STAGGER ANGLE,ANGLE BETWEEN MEAN CHORD + AXIAL
      **       DIRECTION,IN DEGREES
      **  IBSURF=BLADE SURFACE SHAPE OPTION
      **          IF 1,DIFFERENT SHAPE
      **          IF 2, IDENTICAL SHAPE
      **     IF IDENTICAL, ONLY THE COEFFICIENTS OF FIRST BLADE,COEFF(1,J)
      **       ARE NEEDED.
      **  NPRO=NUMBER OF COEFFICIENTS OF POLYNOMIAL REPRESENTING BLADE
      **       SHAPE
      **  WARNING- LARGER BY 1 THEN THE ORDER OF POLYNOMIAL
      **  COEFF(I,J)=J-TH POLYNOMIAL COEFFICIENTS OF I-TH BLADE,
      **              I=1,------,NPRO
      **  WARNING- START WITH COEFF(I,1) INSTEAD OF COEFF(I,0)
      **  NSLO=NUMBER OF COEFFICIENTS OF POLYNOMIAL REPRESENTING XCHORD
      **    (DEPENDENT)-DY/DX(INDEPENDENT) RELATION
      ** WARNING-LARGER BY 1 THAN THE ORDER OF POLYNOMIAL
      **  SCOEF(I,J)=J-TH POLYNOMIAL COEFFICIENTS OF ABOVE RELATION,
      **      J=1,------, NSLO
      **  WARNING- START WITH SCOEFF(I,1) INSTEAD IF SCOEFF(I,0)
      **  YMAX=MAXIMUM DISTANCE AHEAD OF ROTOR IN AXIAL DIRECTION,
      **       GIVE AS RATIO OF CHORD
      **  NSEG=NUMBER OF DIVISION OF YMAX
      **  MMM=NUMBER OF POINTS BEHIND A SHOCK TO OBTAIN PRESSURE PROFILE
```

```
      COMMON SCOEF(62,10),COEFF(62,10),TP(62,62),TX(62,62),ABSC(62),
     AX,Y,XNU,SLOP,XM,PR,BETA,USLOPE,PRS,N,NPRO,NSLO,NB,
     BM(62),STAGR(62),SPACE(62)
      DIMENSION SPACG(62),SLOPE(202),XMU(202),XMACH(202),PRD(62,102),
     AAD(62,102),BD(62,102),MD(62),DSLOPE(202),SO(62),DELTA(62),
     BBTA(202),SA(202),SB(202),SX(202),SY(202),XT(62),YT(62),
     CUSLP(202),DDELTA(202),TXC(62,10),XTP(62),YTP(62),
     DTXUN(62),TXS(62),YC(202),YC(202),XP(202),YP(202),XXNU(202)
**    READ-IN PROCEDURE
      PAI=3.14159265
      CALL FLGFOF(5,IND)
   10 READ (5,1) EMACH,THETA,NB,NS,YMAX,NSEG
      IF (IND .EQ.1) STOP
      PRINT 473,EMACH,THETA,NB
  473 FORMAT (1H1,10X,16H REL. MACH NO. =,F4.1,16X,23H INLET VELOCITY AN
     1GLE =F4.0,16X,16H NO. OF BLADES =I3)
      THETA=THETA*2./360.*PAI
      NNB=NB-1
      PRINT 478,NS
  478 FORMAT (60H0      NO. OF POINTS DOWNSTREAM OF UNINTERCEPTED MACH W
     1AVE =I4)
    1 FORMAT (2F10.2,2I10,F10.3,I10)
      PRINT 483,YMAX,NSEG
  483 FORMAT (1H0,10X,25H MAXIMUN AXIAL DISTANCE =,F7.3,25X,37H NO. OF S
     1EGMENTS IN AXIAL DIRECTION =I3)
      READ (5,2) NPRO,NSLO,MMM
    2 FORMAT (3I10)
      READ (5,2) ISOP
      PRINT 503,NPRO
  503 FORMAT (67H0      NO. OF COEFFICIENTS OF POLYNOMIAL REPRESENTING B
     1LADE SHAPE =I3)
      GO TO (70,110),ISOP
   70 READ (5,4) (SPACG(I),I=1,NB)
      GO TO 160
  110 READ (5,3) SPACG(1)
    3 FORMAT (F10.3)
      DO 150 I=1,NNB
      SPACG(I+1)=SPACG(1)
  150 CONTINUE
```

```
      160 READ (5,2) ISTAGR
          PRINT 612
  612   FORMAT (1H0,37X,43H J-TH COEFFICIENTS OF I-TH BLADE POLYNOMIAL)
          PRINT 615
  615   FORMAT (120H  COEFF(I,1)  COEFF(I,2)  COEFF(I,3)  COEFF(I,4)  COEF
     1F(I,5)  COEFF(I,6)  COEFF(I,7)  COEFF(I,8)  COEFF(I,9) COEFF(I,10)
     2)
          GO TO (180,230),ISTAGR
      180 READ (5,4) (STAGR(I),I=1,NB)
          DO 210 I=1,NB
  200     STAGR(I)=STAGR(I)*2.*PAI/360.
  210     CONTINUE
          GO TO 280
      230 READ (5,3) STAGR(1)
          STAGR(1)=STAGR(1)*2.*PAI/360.
          DO 270 I=1,NNB
          STAGR(I+1)=STAGR(I)
  270     CONTINUE
      280 READ (5,2) IBSURF
          GO TO (300,410),IBSURF
  300     DO 340 I=1,NB
          READ (5,5) (COEFF(I,J),J=1,NPRO)
  340     CONTINUE
          DO 390 I=1,NB
          READ (5,5) (SCOEF(I,J),J=1,NSLO)
  390     CONTINUE
          GO TO 540
      410 READ (5,5) (COEFF(1,J),J=1,NPRO)
          DO 460 J=1,NPRO
          DO 450 I=1,NNB
          COEFF(I+1,J)=COEFF(I,J)
  450     CONTINUE
  460     CONTINUE
        4 FORMAT (8E10.4)
        5 FORMAT (8E10.4)
          READ (5,5) (SCOEF(1,J),J=1,NSLO)
          DO 520 J=1,NSLO
          DO 510 I=1,NNB
          SCOEF(I+1,J)=SCOEF(I,J)
```

```
      510   CONTINUE
      520   CONTINUE
      540   DO 976 I=1,NB
            PRINT 973,I
      973   FORMAT (14H0           I =,I3)
            PRINT 975,(COEFF(I,J),J=1,NPRO)
      975   FORMAT (1P10E12.4)
      976   CONTINUE
            PRINT 978,NSLO
      978   FORMAT (78H0      NO. OF COEFFICIENTS OF POLYNOMIAL REPRESENTING O
     1HORD - DY/DX RELATION =I3)
            PRINT 981
      981   FORMAT (1H0,47X,51H J-TH COEFFICIENTS OF I-TH INVERSE - DY/DX REL A
     1TION)
            PRINT 984
      984   FORMAT (120H  SCOEF(I,1)  SCOEF(I,2)  SCOEF(I,3)  SCOEF(I,4)  SCOE
     1F(I,5)  SCOEF(I,6)  SCOEF(I,7)  SCOEF(I,8)  SCOEF(I,9) SCOEF(I,10)
     2)
            DO 989 I=1,NB
            PRINT 973,I
            PRINT 975,(SCOEF(I,J),J=1,NSLO)
      989   CONTINUE
            PRINT 992,MMM
      992   FORMAT (66H0      NO. OF POINTS BETWEEN A SHOCK AND UNINTERCEPTED
     1MACH WAVE =I3)
            PRINT 995
      995   FORMAT (1H0,19X,2H I,20X,27H SPACING BETWEEN THE BLADES,13X,14H ST
     1AGGER ANGLE)
            DO 1003 I=1,NB
            DEG=STAGR(I)*180./PAI
            PRINT 1002,I,SPACG(I),DEG
     1002   FORMAT (I22,1P1E36.4,F36.4)
     1003   CONTINUE
      ***   END OF READ-IN PROCEDURE
            PRINT 1006
     1006   FORMAT (2X,///////)
            DO 1370 I=1,NB
      ***   UNINTERCEPTED MACH WAVE POSITION OF I-TH BLADE
            SLOPE(1)=THETA-STAGR(I)
```

```
      SSS=TAN(SLOPE(1))
      CALL INSLOP(1,SSS)
      XC(1)=X
      CALL COORD(1,XC(1))
      YC(1)=Y
      XMU(1)=ARSIN(1./EMACH)
      SPACE(1)=0.
      XMACH(1)=EMACH
      PRD(1,1)=1.
      CALL PRAND(XMACH(1))
      XXNU(1)=YNU
**    MACH WAVE SYSTEMS BEHIND UNINTERCEPTED MACH WAVE
      DO 910 J=1,NS
      AD(1,J)=TAN(XMU(J)+SLOPE(J)+STAGR(1)-PAI/2.)
      XP(J)=XC(J)*SIN(STAGR(1))+YC(J)*COS(STAGR(1))+SPACE(1)
      YP(J)=-XC(J)*COS(STAGR(1))+YC(J)*SIN(STAGR(1))
      BD(1,J)=YP(J)-XP(J)*AD(1,J)
      SPACE(I+1)=SPACE(I)+SPACG(I)
      XOO=-BD(1,J)/AD(1,J)
      IF (SPACE(I+1).GT.XOO) GO TO 790
770   MD(1)=J-1
      MAD=MD(1)
      GO TO 920
790   XC(J+1)=XC(J)+(SPACG(1)-XC(1))/FLOAT(NS)
      CALL COORD(1,XC(J+1))
      YC(J+1)=Y
      CALL TANGEN(1,XC(J+1))
      SLOPE(J+1)=SLOP
      DSLOPE(J)=-SLOPE(J+1)+SLOPE(J)
      XXNU(J+1)=XXNU(J)+DSLOPE(J)
      CALL INPRAN(XXNU(J+1))
      XMACH(J+1)=XM
      XMU(J+1)=ARSIN(1./XMACH(J+1))
      CALL ISPRES(XMACH(J+1),XMACH(1))
      PRD(1,J+1)=PR
910   CONTINUE
920   K=1
      STAGR(NR+1)=STAGR(1)
      DO 1393 JAM=1,NPRO
```

```
      COEFF(NR+1,JAM)=COEFF(1,JAM)
1393  CONTINUE
      DO 1396 JAX=1,NSLO
      SCOEF(NR+1,JAX)=SCOEF(1,JAX)
1396  CONTINUE
**  INITIAL SHOCK ROUTINE
      IPK=I+K
960   CALL TANGEN(IPK,0)
      SO(IPK)=SLOP
      DELTA(IPK)=SO(IPK)+STAGR(IPK)-(SLOPE(MAD)+STAGR(I))
      CALL SHOCK(XMACH(MAD),DELTA(IPK))
      BTA(1)=BETA
      IF(BTA(1).LT.0.) GO TO 1850
1030  SA(1)=TAN(SLOPE(MAD)+STAGR(I)+BTA(1)-PAI/2.)
      SB(1)=-SA(1)*SPACE(I+1)
      SX(1)=(BD(I,MAD)-SB(1))/(SA(1)-AD(I,MAD))
      SY(1)=SX(1)*SA(1)+SB(1)
** UNINTERCEPTED MACH WAVE BEHIND SHOCK ON I+1-TH BLADE
      USLOP=THETA-STAGR(IPK)
      SSS=TAN(USLOP)
      CALL INSLOP(IPK,SSS)
      XT(IPK)=X
      CALL COORD(IPK,XT(IPK))
      YT(IPK)=Y
** SHOCK-EXPANSION WAVE INTERACTION
      II=1
      J=1
1245  CALL DMACH(IPK,EMACH,THETA,XT(IPK),SX(J),SY(J))
      USLP(J)=USLOPE
      MDJJ=MD(I)-J
      DDELTA(J)=SLOPE(MDJJ)+STAGR(I)-(STAGR(IPK)+USLP(J))
      DDELTA(J)=-DDELTA(J)
      CALL SHOCK(XMACH(MDJJ),DDELTA(J))
      BTA(J+1)=BETA
      SA(J+1)=TAN(SLOPE(MDJJ)+STAGR(I)+BTA(J+1)-PAI/2.)
      SB(J+1)=SY(J)-SX(J)*SA(J+1)
      SX(J+1)=(SB(J+1)-BD(I,MDJJ))/(AD(I,MDJJ)-SA(J+1))
      SY(J+1)=SB(J+1)+SA(J+1)*SX(J+1)
      GO TO 1250
```

```
      1240  J=J+1
            GO TO 1245
      1250  YLIM=0.
            YLIM=YLIM+YMAX/FLOAT(NSEG)*FLOAT(II)
            IF (SY(J+1) .LE. YLIM) GO TO 1240
            IF (SY(J+1) .GT. YLIM) GO TO 1290
      1290  TXO(IPK,II)=(SX(J+1)-SX(J))/(SY(J+1)-SY(J))*(YLIM-SY(J))+SX(J)
            IF (II.GE. NSEG) GO TO 1370
      1350  II=II+1
            GO TO 1250
      1370  CONTINUE
      **  CROSS SECTIONAL PRESSURE ROUTINE
            XT(NB+2)=XT(2)
            YT(NB+2)=YT(2)
            STAGR(NB+2)=STAGR(2)
            SPACE(NB+2)=SPACE(NB+1)+SPACG(1)
            MD11=MD(1)
            DO 1431 JJ=1,MD11
            AD(NB+1,JJ)=AD(1,JJ)
            BD(NB+1,JJ)=BD(1,JJ)-AD(1,JJ)*SPACE(NB+1)
            PRD(NB+1,JJ)=PRD(1,JJ)
      1431  CONTINUE
            DO 1470 MJ=1,NSEG
            TXO(NB+2,MJ)=TXO(2,MJ)+SPACE(NB+1)
      1470  CONTINUE
            DO 1840 J=1,NSEG
            PRINT 1993
      1993  FORMAT (1H0,52X,15H SEGMENT NUMBER)
            PRINT 2022,J
      2022  FORMAT (I59)
            PRINT 2024
      2024  FORMAT (1H0,25X,15H PROFILE NUMBER,10X,20H PERIPHERAL DISTANCE,10X
           1,15H PRESSURE RATIO)
            YLIM=0.
            YLIM=YLIM+YMAX/FLOAT(NSEG)*FLOAT(J)
            CALL DMACH(2,EMACH,THETA,XT(2),TXO(2,J),YLIM)
            TP(1,1)=PRS
            TX(1,1)=0.
            JAS=1
```

```
      NASA=NB+1
      DO 1803 I=1,NASA
      XTP(I+1)=XT(I+1)*SIN(STAGR(I+1))+YT(I+1)*COS(STAGR(I+1))
     A+SPACE(I+1)
      YTP(I+1)=-XT(I+1)*COS(STAGR(I+1))+YT(I+1)*SIN(STAGR(I+1))
      ATP=TAN(YMU(1)+THETA-PAI/2.)
      TXUN(I+1)=(YLIM-YTP(I+1))/ATP+XTP(I+1)
 1803 CONTINUE
      HOW=TXO(2,J)+SPACE(NB+1)
      IF (HOW .LT. TXUN(NB+2)) GO TO 2089
      TP(1,1)=1.
 2089 PRINT 2187,JAS,TX(1,1),TP(1,1)
      DO 1800 I=1,NB
      IF (TXUN(I+1) .GT. TXO(I+1,J)) GO TO 2093
      TXO(I+1,J)=TXUN(I+1)
 2093 IF (TXUN(I+2) .GT. TXO(I+2,J)) GO TO 2140
      TXO(I+2,J)=TXUN(I+2)
 2100 FORMAT (I7,F30.5,2F37.5)
 2140 DO 1660 JM=1,MMM
      KK=I+1
 2150 TX(I,JM+1)=TX(I,1)+(TXUN(I+1)-TXO(I+1,J))*FLOAT(JM)/FLOAT(MMM)
 2160 TXS(I+1)=TXO(2,J)+TX(I,JM+1)
      CALL DMACH(I+1,EMACH,THETA,XT(I+1),TXS(I+1),YLIM)
      TP(I,JM+1)=PRS
      PRINT 2187,I,TX(I,JM+1),TP(I,JM+1)
 2187 FORMAT (I35,2F29.5)
 1660 CONTINUE
      DO 1730 JAK=2,NS
      XL=(YLIM-BD(I+1,JAK))/AD(I+1,JAK)
      IF(XL .GT. TXO(I+2,J)) GO TO 1740
      MJAK=MMM+JAK
      TX(I,MJAK)=(YLIM-BD(I+1,JAK))/AD(I+1,JAK)-TXO(2,J)
      TP(I,MJAK)=PRD(I+1,JAK)
      PRINT 2187,I,TX(I,MJAK),TP(I,MJAK)
 1730 CONTINUE
 1740 JAL=JAK-2
      M(I)=MMM+JAL+2
      M1=M(I)
      TX(I,M1)=TXO(I+2,J)-TXO(2,J)
```

```
311             TP(I,M1)=TP(I,M1-2)+(TX(I,M1)-TX(I,M1-2))*(TP(I,M1-1)-TP(I,M1-2))
312            1/(TX(I,M1-1)-TX(I,M1-2))
313             TX(I+1,1)=TX(I,M1)
314             CALL DMACH(I+2,EMACH,THETA,XT(I+2),TXO(I+2,J),YLIM)
315             TP(I+1,1)=PRS
316             PRINT 2187,I,TX(I,M1),TP(I,M1)
317             PRINT 2385,I,M(I)
318             PRINT 2387
319             PRINT 2100,KK,TXO(I+1,J),TXUN(I+1),YLIM
320             IF (I .GE. NB) GO TO 2321
321             PRINT 2024
322             PRINT 2187,KK,TX(I+1,1),TP(I+1,1)
323       1800  CONTINUE
324       2321  SUM=0.
325             DO 2324 JIM=1,NB
326             SUM=SUM+SPACG(JIM)/FLOAT(NB)
327       2324  CONTINUE
328             DO 2330 JIS=1,NB
329             MILK=M(JIS)
330             DO 2329 JIN=1,MILK
331             TX(JIS,JIN)=TX(JIS,JIN)/SUM
332       2329  CONTINUE
333       2330  CONTINUE
334             PRINT 2389
335             DO 1831 N=1,NB
336             CALL FOUCU
337       1830  FORMAT (I22,F40.8,F35.8)
338       1831  CONTINUE
339             DO 2359 N=1,NB
340             DDECIB=4.342945*ALOG(ABSC(N)/ABSC(NB))
341             PRINT 1830,N,ABSC(N),DDECIB
342       2359  CONTINUE
343       1840  CONTINUE
344             GO TO 2390
345       1850  PRINT 1860
346       1860  FORMAT (19H0 SHOCK IS DETACHED)
347       2385  FORMAT (1H0,10X,18H PROFILE NUMBER IS,I3,15X,24H NUMBER OF DIVISIO
348            1NS ARE,I4)
349       2387  FORMAT (11H0 BLADE NO.,15X,15H SHOCK POSITION,15X,28H UNINTERCEPTE
```

```
350             1D WAVE POSITION,15X,15H AXIAL DISTANCE)
351       2389   FORMAT (1H0,15X,10H HARMONICS,15X,31H SQUARE OF FOURIER COEFFICIEN
352             1TS,15X,9H DIFF. DB)
353       2390   GO TO 10
354             END

   23493 WORDS OF MEMORY USED BY THIS COMPILATION
```

```
  1             SUBROUTINE INPRAN(XNX)
  2             COMMON SCORE(62,10),COEFF(62,10),TP(62,62),TX(62,62),ABSC(62),
  3            AX,Y,XNU,SLOP,XM,PR,BETA,USLOPE,PRS,N,NPRO,NSLO,NB,
  4            BM(62),STAGR(62),SPACE(62)
  5             A0=1.00064
  6             A1=6.82919
  7             A2=-178.313
  8             A3=4146.15
  9             A4=-59440.7
 10             A5=538928
 11             A6=-3.14714E+6
 12             A7=1.17935E+7
 13             A8=-2.737E+7
 14             A9=3.57792E+7
 15             A10=-20127598
 16             XM=A0+A1*XNX+A2*XNX**2+A3*XNX**3+A4*XNX**4
 17            A+A5*XNX**5+A6*XNX**6+A7*XNX**7+A8*XNX**8
 18            B+A9*XNX**9+A10*XNX**10
 19             RETURN
 20             END
```

```
      SUBROUTINE SHOCK(XM1,DELT)
      COMMON SCOEF(62,10),COEFF(62,10),TP(62,62),TX(62,62),ADSC(62),
     AX,Y,XNU,SLOP,XM,PR,BETA,USLOPE,PRS,N,NPRO,NSLO,NS,
     AM(62),STAGR(62),SPACE(62)
      DIMENSION DIFF(10),BE(10)
      GAM=1.4
      PAI=3.141592655
      BETA=ARSIN(1./XM1)
 1730 DIF=2.*1./TAN(BETA)*(XM1**2*SIN(BETA)**2-1.)/(XM1**2*(GAM+
     ACOS(2.*BETA))+2.)-TAN(DELT)
      IF (DIF .GE. 0.) GO TO 1810
 1770 BETA=BETA+1.0*PAI/180.
      C=85.*PAI/180.
      IF (BETA .GT. C) GO TO 2080
      IF (BETA .LE. C) GO TO 1730
 1810 BE(1)=BETA-1.*PAI/180.
      BE(2)=BETA
      DO 1860 I=1,2
      DIFF(I)=2.*1./TAN(BE(I))*(XM1**2*SIN(BE(I))**2-1.)/(XM1**2*
     A(GAM+COS(2.*BE(I)))+2.)-TAN(DELT)
 1860 CONTINUE
      BE(3)=BE(1)-(BE(2)-BE(1))/(DIFF(2)-DIFF(1))*DIFF(1)
      DIFF(3)=2.*1./TAN(BE(3))*(XM1**2*SIN(BE(3))**2-1.)/(XM1**2*(GAM+
     ACOS(2.*BE(3)))+2.)-TAN(DELT)
      IF (DIFF(3) .LE. 0.) GO TO 1990
 1920 BE(4)=BE(1)-(BE(3)-BE(1))/(DIFF(3)-DIFF(1))*DIFF(1)
      DIFF(4)=2.*1./TAN(BE(4))*(XM1**2*SIN(BE(4))**2-1.)/(XM1**2*(GAM+
     ACOS(2.*BE(4)))+2.)-TAN(DELT)
      IF (DIFF(4) .GT. 0.) GO TO 1970
      IF (DIFF(4) .LE. 0.) GO TO 1980
 1970 BE(5)=BE(1)-(BE(4)-BE(1))/(DIFF(4)-DIFF(1))*DIFF(1.
```

```
                GO TO 2990
      1980      BE(5)=BE(4)-(BE(3)-BE(4))/(DIFF(3)-DIFF(4))*DIFF(4)
                GO TO 2990
      1990      BE(4)=BE(3)-(BE(2)-BE(3))/(DIFF(2)-DIFF(3))*DIFF(3)
                DIFF(4)=2.*1./TAN(BE(4))*(XM1**2*SIN(BE(4))**2-1.)/(XM1**2*(GAM+
               ACOS(2.*BE(4)))+2.)-TAN(DELT)
                IF (DIFF(4) .GT. 0.) GO TO 2040
                IF (DIFF(4) .LE. 0.) GO TO 2050
      2040      BE(5)=BE(3)-(BE(4)-BE(3))/(DIFF(4)-DIFF(3))*DIFF(3)
                GO TO 2990
      2050      BE(5)=BE(4)-(BE(2)-BE(4))/(DIFF(2)-DIFF(4))*DIFF(4)
      2990      BETA=BE(5)
                GO TO 4090
      2060      BETA=-10.
      2090      XM2=1./SIN(BETA-DELT)*SQRT((1.+(GAM-1.)/2.*XM1**2*SIN(BETA)
               A**2)/(GAM*XM1**2*SIN(BETA)**2-(GAM-1.)/2.))
                RETURN
                END

  22975 WORDS OF MEMORY USED BY THIS COMPILATION
```

```
1              SUBROUTINE PRAND(XMX)
2              COMMON SCOEF(62,10),COEFF(62,10),TP(62,62),TX(62,62),ABSC(62),
3             AX,Y,XNU,SLOP,XM,PR,BETA,USLOPE,PRS,N,NPRO,NSLO,NB,
4             BM(62),STAGR(62),SPACE(62)
5              GAM=1.4
6              XR=(GAM+1.)/(GAM-1.)
7              XNU=SQRT(XR)*ATAN(SQRT(1./XR*(XMX**2-1.)))-ATAN(SQRT(XMX**2-1.))
8              RETURN
9              END
```

22955 WORDS OF MEMORY USED BY THIS COMPILATION

```
1              SUBROUTINE INSLOP(I,TANG)
2              COMMON SCOEF(62,10),COEFF(62,10),TP(62,62),TX(62,62),ABSC(62),
3             AX,Y,XNU,SLOP,XM,PR,BETA,USLOPE,PRS,N,NPRO,NSLO,NB,
4             BM(62),STAGR(62),SPACE(62)
5              X=SCOEF(I,1)
6              DO 5150 J=2,NSLO
7              X=X+SCOEF(I,J)*TANG**(J-1)
8       5150   CONTINUE
9              RETURN
10             END
```

23073 WORDS OF MEMORY USED BY THIS COMPILATION

```
      SUBROUTINE FOUCU
      DIMENSION CR(100),CI(100),XR(100),XI(100),
     AMM(62)
      COMMON SCOEF(62,10),COEFF(62,10),TP(62,62),TX(62,62),ABSC(62),
     AX,Y,XNU,SLOP,XM,PR,BETA,USLOPE,PRS,N,NPRO,NSLO,NB,
     BM(62),STAGR(62),SPACE(62)
      PAI=3.141592653
      DO 70 I=1,NB
      MM(I)=M(I)-1
   70 CONTINUE
      XX=0.
      CCR=0.
      CCI=0.
      DO 260 I=1,NB
      CR(I)=0.
      CI(I)=0.
      MMII=MM(I)
      DO 230 J=1,MMII
      FNB=NB
      FN=N
      IF (TX(I,J+1) .LE. TX(I,J)) GO TO 3695
      AIJ=(TP(I,J+1)-TP(I,J))/(TX(I,J+1)-TX(I,J))
      BIJ=TP(I,J+1)-AIJ*TX(I,J+1)
      CR(I)=CR(I)+1./FN*(AIJ*(TX(I,J+1)*SIN(FN*2.*PAI/FNB
     A*TX(I,J+1))+FNB/(FN*2.*PAI)*COS(FN*2.*PAI/FNB*TX(I,J+1)))
     B+BIJ*SIN(FN*2.*PAI/FNB*TX(I,J+1)))
     C-1./FN*(AIJ*(TX(I,J)*SIN(FN*2.*PAI/FNB
     D*TX(I,J))+FNB/(FN*2.*PAI)*COS(FN*2.*PAI/FNB*TX(I,J)))
     E+BIJ*SIN(FN*2.*PAI/FNB*TX(I,J)))
      CI(I)=CI(I)+1./FN*(AIJ*(-TX(I,J+1)*COS(FN*2.*PAI/FNB
     A*TX(I,J+1))+FNB/(FN*2.*PAI)*SIN(FN*2.*PAI/FNB*
```

```
32              BTX(I,J+1)))
33              C=BIJ*COS(FN*2.*PAI/FNB*TX(I,J+1)))
34              D=1./FN*(AIJ*(-TX(I,J)*COS(FN*2.*PAI/FNB
35              E*TX(I,J))+FNB/(FN*2.*PAI)*SIN(FN*2.*PAI/FNB*TX(I,J)))
36              F=BIJ*COS(FN*2.*PAI/FNB*TX(I,J)))
37               GO TO 230
38         3695 CR(I)=CR(I)
39              CI(I)=CI(I)
40         230  CONTINUE
41              CCR=CR(I)+CCR
42              CCI=CI(I)+CCI
43         260  CONTINUE
44              XR(N)=CCR
45              XI(N)=CCI
46              ABSC(N)=XR(N)**2+XI(N)**2
47              RETURN
48              END

  22920 WORDS OF MEMORY USED BY THIS COMPILATION
```

```
      SUBROUTINE ISPRES(XM2,XXM1)
      COMMON SCOEF(62,10),COEFF(62,10),TP(62,62),TX(62,62),ABSC(62),
     AX,Y,XNU,SLOP,XM,PR,BETA,USLOPE,PRS,N,NPRO,NSLO,NB,
     BM(62),STAGR(62),SPACE(62)
      GAM=1.4
      PR=((1.+(GAM-1.)/2.*XM2**2)/(1.+(GAM-1.)/2.*XXM1**2))**(GAM/(GAM-
     A1.))
      PR=1./PR
      RETURN
      END
```

22951 WORDS OF MEMORY USED BY THIS COMPILATION

```
      SUBROUTINE TANGEN(I,XXX)
      COMMON SCOEF(62,10),COEFF(62,10),TP(62,62),TX(62,62),ABSC(62),
     AX,Y,XNU,SLOP,XM,PR,BETA,USLOPE,PRS,N,NPRO,NSLO,NB,
     BM(62),STAGR(62),SPACE(62)
      NPROO=NPRO-1
      R=COEFF(I,2)
      DO 5600 J=2,NPROO
      R=R+FLOAT(J)*COEFF(I,J+1)*XXX**(J-1)
 5600 CONTINUE
      SLOP=ATAN(R)
      RETURN
      END
```

23020 WORDS OF MEMORY USED BY THIS COMPILATION

```
      SUBROUTINE DMACH(I,EMACH,THETA,XTHET,XQ,YQ)
      COMMON SCOEF(62,10),COEFF(62,10),TP(62,62),TX(62,62),ABSC(62),
     AX,Y,XNU,SLOP,XM,PR,BETA,USLOPE,PRS,N,NPRO,NSLO,NB,
     BM(62),STAGR(62),SPACE(62)
      DIMENSION XC(12),YC(12),XP(12),YP(12),SL(12),
     AXXNU(12),XM1(12),EP(12),PROD(12),
     BTHET1(12),ANGLMA(12)
      PAI=3.14159265
** I SPECIFIES I-TH BLADE
** EMACH IS MACH NUMBER AT INFINITY
** THETA IS INLET VELOCITY ANGLE MEASURED FROM AXIS, IN DEGRESS
** XTHET IS THE POSITION ON AIRFOIL UPON WHICH UNINTERCEPTED MACH
**  WAVE IMPINGES,MEASURED IN AIRFOIL COORDINATE SYSTEM.
** (XQ,YQ) IS THE POSITION OF THE POINT Q, MEASURED FROM THE ORIGIN.
**  THE MACH WAVE PASSING Q IS TO BE COMPUTED.
      CALL PRAND(EMACH)
      XNUO=XNU
      XC(1)=0.
      DO 540 J=1,10
      CALL COORD(I,XC(J))
      YC(J)=Y
      XP(J)=XC(J)*SIN(STAGR(I))+YC(J)*COS(STAGR(I))+SPACE(I)
      YP(J)=-XC(J)*COS(STAGR(I))+YC(J)*SIN(STAGR(I))
      CALL TANGEN(I,XC(J))
      SL(J)=SLOP
      THET1(J)=SL(J)+STAGR(I)
      XXNU(J)=XNUO+THETA-THET1(J)
      CALL INPRAN(XXNU(J))
      XM1(J)=XM
      ANGLMA(J)=ARSIN(1./XM1(J))
      EP(J)=YQ-YP(J)-TAN(ANGLMA(J)+THET1(J)-PAI/2.)*(XQ-XP(J))
      XC(J+1)=XC(J)+XTHET/10.*FLOAT(J)
      CALL COORD(I,XC(J+1))
      YC(J+1)=Y
      XP(J+1)=XC(J+1)*SIN(STAGR(I))+YC(J+1)*COS(STAGR(I))+SPACE(I)
      YP(J+1)=-XC(J+1)*COS(STAGR(I))+YC(J+1)*SIN(STAGR(I))
      CALL TANGEN(I,XC(J+1))
```

```
      SL(J+1)=SLOP
      THET1(J+1)=SL(J+1)+STAGR(I)
      XXNU(J+1)=XNUO+THETA-THET1(J+1)
      CALL INPRAN(XXNU(J+1))
      XM1(J+1)=XM
      ANGLMA(J+1)=ARSIN(1./XM1(J+1))
      EP(J+1)=YO-YP(J+1)-TAN(ANGLMA(J+1)+THET1(J+1)-PAI/2.)*(XO-XP(J+1))
      PROD(J)=EP(J)*EP(J+1)
      IF (PROD(J) .GT. 0.) GO TO 540
  510 K1=J
      GO TO 550
  540 CONTINUE
  550 XC(1)=XC(K1)
      K2=K1+1
      XC(2)=XC(K2)
      EP(1)=EP(K1)
      EP(2)=EP(K2)
      XC(3)=XC(1)-EP(1)*(XC(2)-XC(1))/(EP(2)-EP(1))
      CALL COORD(I,XC(3))
      YC(3)=Y
      XP(3)=XC(3)*SIN(STAGR(I))+YC(3)*COS(STAGR(I))+SPACE(I)
      YP(3)=-XC(3)*COS(STAGR(I))+YC(3)*SIN(STAGR(I))
      CALL TANGEN(I,XC(3))
      SL(3)=SLOP
      THET1(3)=SL(3)+STAGR(I)
      XXNU(3)=XNUO+THETA-THET1(3)
      CALL INPRAN(XXNU(3))
      XM1(3)=XM
      ANGLMA(3)=ARSIN(1./XM1(3))
      EP(3)=YO-YP(3)-TAN(ANGLMA(3)+THET1(3)-PAI/2.)*(XO-XP(3))
      PROD(3)=EP(1)*EP(3)
      IF (PROD(3) .LE. 0.) GO TO 780
  760 XC(4)=XC(3)-EP(3)*(XC(2)-XC(3))/(EP(2)-EP(3))
      GO TO 790
  780 XC(4)=XC(1)-EP(1)*(XC(3)-XC(1))/(EP(3)-EP(1))
  790 CALL COORD(I,XC(4))
      YC(4)=Y
      XP(4)=XC(4)*SIN(STAGR(I))+YC(4)*COS(STAGR(I))+SPACE(I)
      YP(4)=-XC(4)*COS(STAGR(I))+YC(4)*SIN(STAGR(I))
```

```
      CALL TANGEN(I,XC(4))
      SL(4)=SLOP
      THET1(4)=SL(4)+STAGR(I)
      XXNU(4)=XNUO+THETA-THET1(4)
      CALL INPRAN(XXNU(4))
      XM1(4)=XM
      ANGLMA(4)=ARSIN(1./XM1(4))
      EP(4)=YO-YP(4)-TAN(ANGLMA(4)+THET1(4)-PAI/2.)*(XO-XP(4))
      IF (PROD(3) .LE. 0.) GO TO 1000
  930 PROD(4)=EP(3)*EP(4)
      IF (PROD(4) .LE. 0.) GO TO 980
  960 XC(5)=XC(4)-EP(4)*(XC(2)-XC(4))/(EP(2)-EP(4))
      GO TO 1060
  980 XC(5)=XC(3)-EP(3)*(XC(4)-XC(3))/(EP(4)-EP(3))
      GO TO 1060
 1000 PROD(4)=EP(1)*EP(4)
      IF (PROD(4) .LT. 0.) GO TO 1050
 1030 XC(5)=XC(4)-EP(4)*(XC(3)-XC(4))/(EP(3)-EP(4))
      GO TO 1060
 1050 XC(5)=XC(1)-EP(1)*(XC(4)-XC(1))/(EP(4)-EP(1))
 1060 XCU=XC(5)
      CALL COORD(I,XCU)
      YCU=Y
      XPP=XCU*SIN(STAGR(I))+YCU*COS(STAGR(I))
      YPP=-XCU*COS(STAGR(I))+YCU*SIN(STAGR(I))
      CALL TANGEN(I,XCU)
      USLOPE=SLOP
      THES=USLOPE+STAGR(I)
      XNUS=XNUO+THETA-THES
      CALL INPRAN(XNUS)
      UMACH=XM
      CALL ISPRES(UMACH,EMACH)
      PRS=PR
      RETURN
      END
```

23145 WORDS OF MEMORY USED BY THIS COMPILATION

```
1               SUBROUTINE COORD(I,XX)
2               COMMON SCOEF(62,10),COEFF(62,10),TP(62,62),TX(62,62),ARSC(62),
3              AX,Y,XNU,SLOP,XM,PR,BETA,USLOPE,PRS,N,NPRO,NSLO,NB,
4              BM(62),STAGR(62),SPACE(62)
5               Y=COEFF(I,1)
6               DO 6150 J=2,NPRO
7               Y=Y+COEFF(I,J)*XX**(J-1)
8         6150  CONTINUE
9               RETURN
10              END

 23073 WORDS OF MEMORY USED BY THIS COMPILATION
```

```
1               FUNCTION TAN(XYZ)
2               TAN=SIN(XYZ)/COS(XYZ)
3               RETURN
4               END

 22787 WORDS OF MEMORY USED BY THIS COMPILATION
```

```
1               FUNCTION ARSIN(XYZ)
2               DEN=SQRT(1./XYZ**2-1.)
3               ARSIN=ATAN(1./DEN)
4               RETURN
5               END

 22850 WORDS OF MEMORY USED BY THIS COMPILATION
```

Appendix 3. Sample Input and Output.

REL. MACH NO. = 1.4 INLET VELOCITY ANGLE = 72. NO. OF BLADES = 38

NO. OF POINTS DOWNSTREAM OF UNINTERCEPTED MACH WAVE = 90

MAXIMUN AXIAL DISTANCE = 10.000 NO. OF SEGMENTS IN AXIAL DIRECTION = 5

J-TH COEFFICIENTS OF I-TH BLADE POLYNOMIAL

COEFF(I,1)	COEFF(I,2)	COEFF(I,3)	COEFF(I,4)	COEFF(I,5)	COEFF(I,6)	COEFF(I,7)	COEFF(I,8)
	I = 1						
0.	1.7633E-01	-5.5500E-02					
	I = 2						
0.	1.7633E-01	-5.5500E-02					
	I = 3						
0.	1.7633E-01	-5.5500E-02					
	I = 4						
0.	1.7633E-01	-5.5500E-02					
	I = 5						
0.	1.7633E-01	-5.5500E-02					
	I = 6						
0.	1.7633E-01	-5.5500E-02					
	I = 7						
0.	1.7633E-01	-5.5500E-02					
	I = 8						
0.	1.7633E-01	-5.5500E-02					
	I = 9						
0.	1.7633E-01	-5.5500E-02					
	I = 10						
0.	1.7633E-01	-5.5500E-02					
	I = 11						
0.	1.7633E-01	-5.5500E-02					
	I = 12						
0.	1.7633E-01	-5.5500E-02					
	I = 13						
0.	1.7633E-01	-5.5500E-02					

```
                I = 14
0.                 1.7633E-01 -5.5500E-02

                I = 15
0.                 1.7633E-01 -5.5500E-02

                I = 16
0.                 1.7633E-01 -5.5500E-02

                I = 17
0.                 1.7633E-01 -5.5500E-02

                I = 18



0.                 1.7633E-01 -5.5500E-02

                I = 19
0.                 1.7633E-01 -5.5500E-02

                I = 20
0.                 1.7633E-01 -5.5500E-02

                I = 21
0.                 1.7633E-01 -5.5500E-02

                I = 22
0.                 1.7633E-01 -5.5500E-02

                I = 23
0.                 1.7633E-01 -5.5500E-02

                I = 24
0.                 1.7633E-01 -5.5500E-02

                I = 25
0.                 1.7633E-01 -5.5500E-02

                I = 26
0.                 1.7633E-01 -5.5500E-02

                I = 27
0.                 1.7633E-01 -5.5500E-02
```

```
                I = 28
0.                 1.7633E-01 -5.5500E-02

                I = 29
0.                 1.7633E-01 -5.5500E-02

                I = 30
0.                 1.7633E-01 -5.5500E-02

                I = 31
0.                 1.7633E-01 -5.5500E-02

                I = 32
0.                 1.7633E-01 -5.5500E-02

                I = 33
0.                 1.7633E-01 -5.5500E-02

                I = 34
0.                 1.7633E-01 -5.5500E-02

                I = 35
0.                 1.7633E-01 -5.5500E-02

                I = 36
0.                 1.7633E-01 -5.5500E-02

                I = 37
0.                 1.7633E-01 -5.5500E-02

                I = 38


0.                 1.7633E-01 -5.5500E-02
```

NO. OF COEFFICIENTS OF POLYNOMIAL REPRESENTING CHORD - DY/DX RELATION = 2

J-TH COEFFICIENTS OF I-TH INVERSE - DY/DX RELATION

SCOEF(I,1) SCOEF(I,2) SCOEF(I,3) SCOEF(I,4) SCOEF(I,5) SCOEF(I,6) SCOEF(I,7) SCOEF(I,8)

I = 1
1.5886E 00 -9.0090E 00

I = 2
1.5886E 00 -9.0090E 00

I = 3
1.5886E 00 -9.0090E 00

I = 4
1.5886E 00 -9.0090E 00

I = 5
1.5886E 00 -9.0090E 00

I = 6
1.5886E 00 -9.0090E 00

I = 7
1.5886E 00 -9.0090E 00

I = 8
1.5886E 00 -9.0090E 00

I = 9
1.5886E 00 -9.0090E 00

I = 10
1.5886E 00 -9.0090E 00

I = 11
1.5886E 00 -9.0090E 00

I = 12
1.5886E 00 -9.0090E 00

I = 13
1.5886E 00 -9.0090E 00

I = 14
1.5886E 00 -9.0090E 00

```
          I = 15
1.5886E 00 -9.0090E 00

          I = 16
1.5886E 00 -9.0090E 00

          I = 17
1.5886E 00 -9.0090E 00

          I = 18
1.5886E 00 -9.0090E 00

          I = 19
1.5886E 00 -9.0090E 00

          I = 20
1.5886E 00 -9.0090E 00

          I = 21
1.5886E 00 -9.0090E 00

          I = 22
1.5886E 00 -9.0090E 00

          I = 23
1.5886E 00 -9.0090E 00

          I = 24
1.5886E 00 -9.0090E 00

          I = 25
1.5886E 00 -9.0090E 00

          I = 26
1.5886E 00 -9.0090E 00

          I = 27
1.5886E 00 -9.0090E 00

          I = 28
1.5886E 00 -9.0090E 00
```

```
          I = 29
1.5886E 00 -9.0090E 00

          I = 30
1.5886E 00 -9.0090E 00

          I = 31
1.5886E 00 -9.0090E 00

          I = 32
1.5886E 00 -9.0090E 00

          I = 33
1.5886E 00 -9.0090E 00

          I = 34
1.5886E 00 -9.0090E 00

          I = 35
1.5886E 00 -9.0090E 00

          I = 36
1.5886E 00 -9.0090E 00

          I = 37
1.5886E 00 -9.0090E 00

          I = 38
1.5886E 00 -9.0090E 00
```

NO. OF POINTS BETWEEN A SHOCK AND UNINTERCEPTED MACH WAVE = 15

I	SPACING BETWEEN THE BLADES	STAGGER ANGLE
1	2.0020E 00	6.5000E 01
2	2.0020E 00	6.5000E 01
3	2.0020E 00	6.5000E 01
4	1.9980E 00	6.5000E 01
5	2.0020E 00	6.5000E 01
6	1.9980E 00	6.5000E 01
7	1.9980E 00	6.5000E 01
8	2.0020E 00	6.5000E 01
9	1.9980E 00	6.5000E 01
10	2.0020E 00	6.5000E 01
11	2.0020E 00	6.5000E 01
12	1.9980E 00	6.5000E 01
13	1.9980E 00	6.5000E 01
14	1.9980E 00	6.5000E 01
15	2.0020E 00	6.5000E 01
16	2.0020E 00	6.5000E 01
17	1.9980E 00	6.5000E 01
18	2.0020E 00	6.5000E 01
19	2.0020E 00	6.5000E 01
20	1.9980E 00	6.5000E 01
21	2.0020E 00	6.5000E 01
22	1.9980E 00	6.5000E 01
23	1.9980E 00	6.5000E 01
24	1.9980E 00	6.5000E 01
25	1.9980E 00	6.5000E 01
26	2.0020E 00	6.5000E 01
27	2.0020E 00	6.5000E 01
28	1.9980E 00	6.5000E 01
29	2.0020E 00	6.5000E 01
30	2.0020E 00	6.5000E 01
31	1.9980E 00	6.5000E 01
32	2.0020E 00	6.5000E 01
33	1.9980E 00	6.5000E 01
34	2.0020E 00	6.5000E 01
35	1.9980E 00	6.5000E 01
36	1.9980E 00	6.5000E 01
37	2.0020E 00	6.5000E 01
38	2.0020E 00	6.5000E 01

SEGMENT NUMBER
1

PROFILE NUMBER	PERIPHERAL DISTANCE	PRESSURE RATIO
1	0.	1.05018
1	0.04274	1.04659
1	0.08548	1.04303
1	0.12822	1.03951
1	0.17095	1.03602
1	0.21369	1.03257
1	0.25643	1.02914
1	0.29917	1.02576
1	0.34191	1.02240
1	0.38465	1.01907
1	0.42739	1.01578
1	0.47013	1.01252
1	0.51286	1.00930
1	0.55560	1.00610
1	0.59834	1.00293
1	0.64108	0.99980
1	0.71482	0.99446
1	0.78776	0.98927
1	0.86156	0.98411
1	0.93623	0.97897
1	1.01181	0.97387
1	1.08830	0.96879
1	1.16574	0.96373
1	1.24414	0.95871
1	1.32352	0.95371
1	1.40392	0.94874
1	1.48536	0.94379
1	1.56787	0.93888
1	1.65147	0.93399
1	1.73620	0.92912
1	1.82209	0.92428
1	1.90918	0.91947
1	1.99750	0.91468
1	2.00200	0.91444

PROFILE NUMBER IS 1 NUMBER OF DIVISIONS ARE 34

BLADE NO. 2

SHOCK POSITION 5.92180

UNINTERCEPTED WAVE POSITION 6.56287

PROFILE NUMBER	PERIPHERAL DISTANCE	PRESSURE RATIO
2	2.00200	1.05018
2	2.04474	1.04659
2	2.08748	1.04303
2	2.13022	1.03951
2	2.17295	1.03602
2	2.21569	1.03257
2	2.25843	1.02914
2	2.30117	1.02576
2	2.34391	1.02240
2	2.38665	1.01907
2	2.42939	1.01578
2	2.47213	1.01252
2	2.51486	1.00930
2	2.55760	1.00610
2	2.60034	1.00293
2	2.64308	0.99980
2	2.71682	0.99446
2	2.78976	0.98927
2	2.86356	0.98411
2	2.93823	0.97897
2	3.01381	0.97387
2	3.09030	0.96879
2	3.16774	0.96373
2	3.24614	0.95871
2	3.32552	0.95371
2	3.40592	0.94874
2	3.48736	0.94379
2	3.56987	0.93888
2	3.65347	0.93399
2	3.73820	0.92912
2	3.82409	0.92428
2	3.91118	0.91947
2	3.99950	0.91468
2	4.00400	0.91444

PROFILE NUMBER IS 2

NUMBER OF DIVISIONS ARE 34

BLADE NO.	SHOCK POSITION	UNINTERCEPTED WAVE POSITION
3	7.92360	8.56487

PROFILE NUMBER	PERIPHERAL DISTANCE	PRESSURE RATIO
3	4.00400	1.05018
3	4.04674	1.04659
3	4.08948	1.04303
3	4.13222	1.03951
3	4.17495	1.03602
3	4.21769	1.03257
3	4.26043	1.02914
3	4.30317	1.02576
3	4.34591	1.02240
3	4.38865	1.01907
3	4.43139	1.01578
3	4.47413	1.01252
3	4.51686	1.00930
3	4.55960	1.00610
3	4.60234	1.00293
3	4.64508	0.99980
3	4.71863	0.99448
3	4.79137	0.98930
3	4.86497	0.98415
3	4.93944	0.97903
3	5.01481	0.97393
3	5.09109	0.96887
3	5.16830	0.96382
3	5.24648	0.95881
3	5.32563	0.95383
3	5.40579	0.94887
3	5.48699	0.94394
3	5.56924	0.93903
3	5.65259	0.93415
3	5.73706	0.92930
3	5.82268	0.92448
3	5.90949	0.91967
3	5.99752	0.91490
3	6.00020	0.91475

PROFILE NUMBER IS 3 NUMBER OF DIVISIONS ARE 34

BLADE NO. 4

SHOCK POSITION 9.92540

UNINTERCEPTED WAVE POSITION 10.56687

PROFILE NUMBER	PERIPHERAL DISTANCE	PRESSURE RATIO
4	6.00020	1.05033
4	6.04306	1.04673
4	6.08591	1.04316
4	6.12877	1.03963
4	6.17163	1.03613
4	6.21449	1.03266
4	6.25735	1.02923
4	6.30021	1.02583
4	6.34307	1.02246
4	6.38593	1.01913
4	6.42879	1.01583
4	6.47164	1.01256
4	6.51450	1.00932
4	6.55736	1.00612
4	6.60022	1.00294
4	6.64308	0.99980
4	6.71682	0.99446
4	6.78976	0.98927
4	6.86356	0.98411
4	6.93823	0.97897
4	7.01381	0.97387
4	7.09030	0.96879
4	7.16774	0.96373
4	7.24614	0.95871
4	7.32552	0.95371
4	7.40592	0.94874
4	7.48736	0.94379
4	7.56987	0.93888
4	7.65347	0.93399
4	7.73820	0.92912
4	7.82409	0.92428
4	7.91118	0.91947
4	7.99950	0.91468
4	8.00400	0.91444

PROFILE NUMBER IS 4 NUMBER OF DIVISIONS ARE 34

BLADE NO.	SHOCK POSITION	UNINTERCEPTED WAVE POSITION
5	11.92199	12.56487

PROFILE NUMBER	PERIPHERAL DISTANCE	PRESSURE RATIO
5	8.00400	1.05018
5	8.04674	1.04659
5	8.08948	1.04303
5	8.13222	1.03951
5	8.17495	1.03602
5	8.21769	1.03257
5	8.26043	1.02914
5	8.30317	1.02576
5	8.34591	1.02240
5	8.38865	1.01907
5	8.43139	1.01578
5	8.47413	1.01252
5	8.51686	1.00930
5	8.55960	1.00610
5	8.60234	1.00293
5	8.64508	0.99980
5	8.71863	0.99448
5	8.79137	0.98930
5	8.86497	0.98415
5	8.93944	0.97903
5	9.01481	0.97393
5	9.09109	0.96887
5	9.16830	0.96382
5	9.24648	0.95881
5	9.32563	0.95383
5	9.40579	0.94887
5	9.48699	0.94394
5	9.56924	0.93903
5	9.65259	0.93415
5	9.73706	0.92930
5	9.82268	0.92448
5	9.90949	0.91967
5	9.99752	0.91490
5	10.00020	0.91475

PROFILE NUMBER IS 5 NUMBER OF DIVISIONS ARE 34

BLADE NO.	SHOCK POSITION	UNINTERCEPTED WAVE POSITION
6	13.92579	14.56687

PROFILE NUMBER	PERIPHERAL DISTANCE	PRESSURE RATIO
6	10.00020	1.05033
6	10.04306	1.04673
6	10.08591	1.04316
6	10.12877	1.03963
6	10.17163	1.03613
6	10.21449	1.03266
6	10.25735	1.02923
6	10.30021	1.02583
6	10.34307	1.02246
6	10.38593	1.01913
6	10.42879	1.01583
6	10.47164	1.01256
6	10.51450	1.00932
6	10.55736	1.00612
6	10.60022	1.00294
6	10.64308	0.99980
6	10.71663	0.99448
6	10.78937	0.98930
6	10.86297	0.98415
6	10.93744	0.97903
6	11.01281	0.97393
6	11.08909	0.96887
6	11.16630	0.96382
6	11.24448	0.95881
6	11.32363	0.95383
6	11.40379	0.94887
6	11.48499	0.94394
6	11.56724	0.93903
6	11.65059	0.93415
6	11.73506	0.92930
6	11.82068	0.92448
6	11.90749	0.91967
6	11.99552	0.91490
6	11.99820	0.91475

PROFILE NUMBER IS 6 NUMBER OF DIVISIONS ARE 34

BLADE NO.	SHOCK POSITION	UNINTERCEPTED WAVE POSITION
7	15.92199	16.56487

PROFILE NUMBER	PERIPHERAL DISTANCE	PRESSURE RATIO
7	11.99820	1.05033
7	12.04105	1.04673
7	12.08391	1.04316
7	12.12677	1.03963
7	12.16963	1.03613
7	12.21249	1.03266
7	12.25535	1.02923
7	12.29821	1.02583
7	12.34107	1.02246
7	12.38393	1.01913
7	12.42679	1.01583
7	12.46964	1.01256
7	12.51250	1.00932
7	12.55536	1.00612
7	12.59822	1.00294
7	12.64108	0.99980
7	12.71482	0.99446
7	12.78776	0.98927
7	12.86156	0.98411
7	12.93623	0.97897
7	13.01181	0.97387
7	13.08830	0.96879
7	13.16574	0.96373
7	13.24414	0.95871
7	13.32352	0.95371
7	13.40392	0.94874
7	13.48536	0.94379
7	13.56787	0.93888
7	13.65147	0.93399
7	13.73620	0.92912
7	13.82209	0.92428
7	13.90918	0.91947
7	13.99750	0.91468
7	14.00200	0.91444

PROFILE NUMBER IS 7 NUMBER OF DIVISIONS ARE 34

BLADE NO.	SHOCK POSITION	UNINTERCEPTED WAVE POSITION
8	17.91999	18.56287

PROFILE NUMBER	PERIPHERAL DISTANCE	PRESSURE RATIO
8	14.00200	1.05018
8	14.04474	1.04659
8	14.08748	1.04303
8	14.13022	1.03951
8	14.17296	1.03602
8	14.21569	1.03257
8	14.25843	1.02914
8	14.30117	1.02576
8	14.34391	1.02240
8	14.38665	1.01907
8	14.42939	1.01578
8	14.47213	1.01252
8	14.51486	1.00930
8	14.55760	1.00610
8	14.60034	1.00293
8	14.64308	0.99980
8	14.71663	0.99448
8	14.78937	0.98930
8	14.86297	0.98415
8	14.93744	0.97903
8	15.01281	0.97393
8	15.08909	0.96887
8	15.16630	0.96382
8	15.24448	0.95881
8	15.32363	0.95383
8	15.40379	0.94887
8	15.48499	0.94394
8	15.56724	0.93903
8	15.65059	0.93415
8	15.73506	0.92930
8	15.82068	0.92448
8	15.90749	0.91967
8	15.99552	0.91490
8	15.99820	0.91475

PROFILE NUMBER IS 8 NUMBER OF DIVISIONS ARE 34

BLADE NO.	SHOCK POSITION	UNINTERCEPTED WAVE POSITION
9	19.92380	20.56487

PROFILE NUMBER	PERIPHERAL DISTANCE	PRESSURE RATIO
9	15.99820	1.05033
9	16.04106	1.04673
9	16.08391	1.04316
9	16.12677	1.03963
9	16.16963	1.03613
9	16.21249	1.03266
9	16.25535	1.02923
9	16.29821	1.02583
9	16.34107	1.02246
9	16.38393	1.01913
9	16.42679	1.01583
9	16.46964	1.01256
9	16.51250	1.00932
9	16.55536	1.00612
9	16.59822	1.00294
9	16.64108	0.99980
9	16.71482	0.99446
9	16.78776	0.98927
9	16.86156	0.98411
9	16.93623	0.97897
9	17.01181	0.97387
9	17.08830	0.96879
9	17.16574	0.96373
9	17.24414	0.95871
9	17.32352	0.95371
9	17.40392	0.94874
9	17.48536	0.94379
9	17.56787	0.93888
9	17.65147	0.93399
9	17.73620	0.92912
9	17.82209	0.92428
9	17.90918	0.91947
9	17.99750	0.91468
9	18.00200	0.91444

PROFILE NUMBER IS 9 NUMBER OF DIVISIONS ARE 34

BLADE NO.	SHOCK POSITION	UNINTERCEPTED WAVE POSITION
10	21.91999	22.56287

PROFILE NUMBER	PERIPHERAL DISTANCE	PRESSURE RATIO
10	18.00200	1.05018
10	18.04474	1.04659
10	18.08748	1.04303
10	18.13022	1.03951
10	18.17296	1.03602
10	18.21569	1.03257
10	18.25843	1.02914
10	18.30117	1.02576
10	18.34391	1.02240
10	18.38665	1.01907
10	18.42939	1.01578
10	18.47213	1.01252
10	18.51486	1.00930
10	18.55760	1.00610
10	18.60034	1.00293
10	18.64308	0.99980
10	18.71682	0.99446
10	18.78976	0.98927
10	18.86356	0.98411
10	18.93823	0.97897
10	19.01381	0.97387
10	19.09030	0.96879
10	19.16774	0.96373
10	19.24614	0.95871
10	19.32552	0.95371
10	19.40592	0.94874
10	19.48736	0.94379
10	19.56987	0.93888
10	19.65347	0.93399
10	19.73820	0.92912
10	19.82409	0.92428
10	19.91118	0.91947
10	19.99950	0.91468
10	20.00400	0.91444

PROFILE NUMBER IS 10 NUMBER OF DIVISIONS ARE 34

BLADE NO.	SHOCK POSITION	UNINTERCEPTED WAVE POSITION
11	23.92380	24.56487

PROFILE NUMBER	PERIPHERAL DISTANCE	SSURE RATIO
11	20.00400	1.05018
11	20.04674	1.04659
11	20.08948	1.04303
11	20.13222	1.03951
11	20.17495	1.03602
11	20.21769	1.03257
11	20.26043	1.02914
11	20.30317	1.02576
11	20.34591	1.02240
11	20.38865	1.01907
11	20.43139	1.01578
11	20.47413	1.01252
11	20.51686	1.00930
11	20.55960	1.00610
11	20.60234	1.00293
11	20.64508	0.99980
11	20.71863	0.99448
11	20.79137	0.98930
11	20.86497	0.98415
11	20.93944	0.97903
11	21.01481	0.97393
11	21.09109	0.96887
11	21.16830	0.96382
11	21.24648	0.95881
11	21.32563	0.95383
11	21.40579	0.94887
11	21.48699	0.94394
11	21.56924	0.93903
11	21.65259	0.93415
11	21.73706	0.92930
11	21.82268	0.92448
11	21.90949	0.91967
11	21.99752	0.91490
11	22.00020	0.91475

NUMBER OF DIVISIONS ARE 34

BLADE NO.	SHOCK POSITION	UNINTERCEPTED WAVE POSITION
12	25.92580	26.56687

PROFILE NUMBER	PERIPHERAL DISTANCE	PRESSURE RATIO
12	22.00020	1.05033
12	22.04305	1.04673
12	22.08591	1.04316
12	22.12877	1.03963
12	22.17163	1.03613
12	22.21449	1.03266
12	22.25735	1.02923
12	22.30021	1.02583
12	22.34307	1.02246
12	22.38593	1.01913
12	22.42879	1.01583
12	22.47164	1.01256
12	22.51450	1.00932
12	22.55736	1.00612
12	22.60022	1.00294
12	22.64308	0.99980
12	22.71663	0.99448
12	22.78937	0.98930
12	22.86297	0.98415
12	22.93744	0.97903
12	23.01281	0.97393
12	23.08909	0.96887
12	23.16630	0.96382
12	23.24448	0.95881
12	23.32363	0.95383
12	23.40379	0.94887
12	23.48499	0.94394
12	23.56724	0.93903
12	23.65059	0.93415
12	23.73506	0.92930
12	23.82068	0.92448
12	23.90749	0.91967
12	23.99552	0.91490
12	23.99820	0.91475

PROFILE NUMBER IS 12

NUMBER OF DIVISIONS ARE 34

BLADE NO.	SHOCK POSITION	UNINTERCEPTED WAVE POSITION
13	27.92199	28.56487

PROFILE NUMBER	PERIPHERAL DISTANCE	PRESSURE RATIO
13	23.99820	1.05033
13	24.04105	1.04673
13	24.08391	1.04316
13	24.12677	1.03963
13	24.16963	1.03613
13	24.21249	1.03266
13	24.25535	1.02923
13	24.29821	1.02583
13	24.34107	1.02246
13	24.38393	1.01913
13	24.42678	1.01583
13	24.46964	1.01256
13	24.51250	1.00932
13	24.55536	1.00612
13	24.59822	1.00294
13	24.64108	0.99980
13	24.71463	0.99448
13	24.78737	0.98930
13	24.86097	0.98415
13	24.93544	0.97903
13	25.01081	0.97393
13	25.08709	0.96887
13	25.16430	0.96382
13	25.24248	0.95881
13	25.32163	0.95383
13	25.40179	0.94887
13	25.48299	0.94394
13	25.56524	0.93903
13	25.64859	0.93415
13	25.73306	0.92930
13	25.81868	0.92448
13	25.90549	0.91967
13	25.99352	0.91490
13	25.99620	0.91475

PROFILE NUMBER IS 13 NUMBER OF DIVISIONS ARE 34

BLADE NO. 14

SHOCK POSITION 29.91999

UNINTERCEPTED WAVE POSITION 30.56267

PROFILE NUMBER	PERIPHERAL DISTANCE	PRESSURE RATIO
14	25.99620	1.05033
14	26.03905	1.04673
14	26.08191	1.04316
14	26.12477	1.03963
14	26.16763	1.03613
14	26.21049	1.03266
14	26.25335	1.02923
14	26.29621	1.02583
14	26.33907	1.02246
14	26.38193	1.01913
14	26.42478	1.01583
14	26.46764	1.01256
14	26.51050	1.00932
14	26.55336	1.00612
14	26.59622	1.00294
14	26.63908	0.99980
14	26.71282	0.99446
14	26.78576	0.98927
14	26.85956	0.98411
14	26.93423	0.97897
14	27.00981	0.97387
14	27.08630	0.96879
14	27.16374	0.96373
14	27.24214	0.95871
14	27.32152	0.95371
14	27.40192	0.94874
14	27.48336	0.94379
14	27.56587	0.93888
14	27.64947	0.93399
14	27.73420	0.92912
14	27.82009	0.92428
14	27.90718	0.91947
14	27.99550	0.91468
14	28.00000	0.91444

PROFILE NUMBER IS 14

NUMBER OF DIVISIONS ARE 34

BLADE NO.	SHOCK POSITION	UNINTERCEPTED WAVE POSITION
15	31.91799	32.56087

PROFILE NUMBER	PERIPHERAL DISTANCE	PRESSURE RATIO
15	28.00000	1.05018
15	28.04274	1.04659
15	28.08548	1.04303
15	28.12822	1.03951
15	28.17096	1.03602
15	28.21369	1.03257
15	28.25643	1.02914
15	28.29917	1.02576
15	28.34191	1.02240
15	28.38465	1.01907
15	28.42739	1.01578
15	28.47013	1.01252
15	28.51286	1.00930
15	28.55560	1.00610
15	28.59834	1.00293
15	28.64108	0.99980
15	28.71482	0.99446
15	28.78776	0.98927
15	28.86156	0.98411
15	28.93623	0.97897
15	29.01181	0.97387
15	29.08830	0.96879
15	29.16574	0.96373
15	29.24414	0.95871
15	29.32352	0.95371
15	29.40392	0.94874
15	29.48536	0.94379
15	29.56787	0.93888
15	29.65147	0.93399
15	29.73620	0.92912
15	29.82209	0.92428
15	29.90918	0.91947
15	29.99750	0.91468
15	30.00200	0.91444

PROFILE NUMBER IS 15

NUMBER OF DIVISIONS ARE 34

BLADE NO.	SHOCK POSITION	UNINTERCEPTED WAVE POSITION
16	33.92180	34.56287

PROFILE NUMBER	PERIPHERAL DISTANCE	PRESSURE RATIO
16	30.00200	1.05018
16	30.04474	1.04659
16	30.08748	1.04303
16	30.13022	1.03951
16	30.17296	1.03602
16	30.21569	1.03257
16	30.25843	1.02914
16	30.30117	1.02576
16	30.34391	1.02240
16	30.38665	1.01907
16	30.42939	1.01578
16	30.47213	1.01252
16	30.51486	1.00930
16	30.55760	1.00610
16	30.60034	1.00293
16	30.64308	0.99980
16	30.71663	0.99448
16	30.78937	0.98930
16	30.86297	0.98415
16	30.93744	0.97903
16	31.01281	0.97393
16	31.08909	0.96887
16	31.16630	0.96382
16	31.24448	0.95881
16	31.32363	0.95383
16	31.40379	0.94887
16	31.48499	0.94394
16	31.56724	0.93903
16	31.65059	0.93415
16	31.73506	0.92930
16	31.82068	0.92448
16	31.90749	0.91967
16	31.99552	0.91490
16	31.99820	0.91475

PROFILE NUMBER IS 16 NUMBER OF DIVISIONS ARE 34

BLADE NO.	SHOCK POSITION	UNINTERCEPTED WAVE POSITION
17	35.92380	36.56487

PROFILE NUMBER	PERIPHERAL DISTANCE	PRESSURE RATIO
17	31.99820	1.05033
17	32.04106	1.04673
17	32.08391	1.04316
17	32.12677	1.03963
17	32.16963	1.03613
17	32.21249	1.03266
17	32.25535	1.02923
17	32.29821	1.02583
17	32.34107	1.02246
17	32.38393	1.01913
17	32.42679	1.01583
17	32.46964	1.01256
17	32.51250	1.00932
17	32.55536	1.00612
17	32.59822	1.00294
17	32.64108	0.99980
17	32.71482	0.99446
17	32.78776	0.98927
17	32.86156	0.98411
17	32.93623	0.97897
17	33.01181	0.97387
17	33.08830	0.96879
17	33.16574	0.96373
17	33.24414	0.95871
17	33.32352	0.95371
17	33.40392	0.94874
17	33.48536	0.94379
17	33.56787	0.93888
17	33.65147	0.93399
17	33.73620	0.92912
17	33.82209	0.92428
17	33.90918	0.91947
17	33.99750	0.91468
17	34.00200	0.91444

PROFILE NUMBER IS 17 NUMBER OF DIVISIONS ARE 34

BLADE NO.	SHOCK POSITION	UNINTERCEPTED WAVE POSITION
18	37.91999	38.56287

PROFILE NUMBER	PERIPHERAL DISTANCE	PRESSURE RATIO
18	34.00200	1.05018
18	34.04474	1.04659
18	34.08748	1.04303
18	34.13022	1.03951
18	34.17296	1.03602
18	34.21569	1.03257
18	34.25843	1.02914
18	34.30117	1.02576
18	34.34391	1.02240
18	34.38665	1.01907
18	34.42939	1.01578
18	34.47213	1.01252
18	34.51486	1.00930
18	34.55760	1.00610
18	34.60034	1.00293
18	34.64308	0.99980
18	34.71682	0.99446
18	34.78976	0.98927
18	34.86356	0.98411
18	34.93823	0.97897
18	35.01381	0.97387
18	35.09030	0.96879
18	35.16774	0.96373
18	35.24614	0.95871
18	35.32552	0.95371
18	35.40592	0.94874
18	35.48736	0.94379
18	35.56987	0.93888
18	35.65347	0.93399
18	35.73820	0.92912
18	35.82409	0.92428
18	35.91118	0.91947
18	35.99950	0.91468
18	36.00400	0.91444

PROFILE NUMBER IS 18

NUMBER OF DIVISIONS ARE 34

BLADE NO.	SHOCK POSITION	UNINTERCEPTED WAVE POSITION
19	39.92380	40.56487

PROFILE NUMBER	PERIPHERAL DISTANCE	PRESSURE RATIO
19	36.00400	1.05018
19	36.04674	1.04659
19	36.08948	1.04303
19	36.13222	1.03951
19	36.17496	1.03602
19	36.21769	1.03257
19	36.26043	1.02914
19	36.30317	1.02576
19	36.34591	1.02240
19	36.38865	1.01907
19	36.43139	1.01578
19	36.47413	1.01252
19	36.51686	1.00930
19	36.55960	1.00610
19	36.60234	1.00293
19	36.64508	0.99980
19	36.71863	0.99448
19	36.79137	0.98930
19	36.86497	0.98415
19	36.93944	0.97903
19	37.01481	0.97393
19	37.09109	0.96887
19	37.16830	0.96382
19	37.24648	0.95881
19	37.32563	0.95383
19	37.40579	0.94887
19	37.48699	0.94394
19	37.56924	0.93903
19	37.65259	0.93415
19	37.73706	0.92930
19	37.82268	0.92448
19	37.90949	0.91967
19	37.99752	0.91490
19	38.00020	0.91475

PROFILE NUMBER IS 19 NUMBER OF DIVISIONS ARE 34

BLADE NO. 20

SHOCK POSITION 41.92580

UNINTERCEPTED WAVE POSITION 42.56687

PROFILE NUMBER	PERIPHERAL DISTANCE	PRESSURE RATIO
20	38.00020	1.05033
20	38.04306	1.04673
20	38.08591	1.04316
20	38.12877	1.03963
20	38.17163	1.03613
20	38.21449	1.03266
20	38.25735	1.02923
20	38.30021	1.02583
20	38.34307	1.02246
20	38.38593	1.01913
20	38.42879	1.01583
20	38.47164	1.01256
20	38.51450	1.00932
20	38.55736	1.00612
20	38.60022	1.00294
20	38.64308	0.99980
20	38.71682	0.99446
20	38.78976	0.98927
20	38.86356	0.98411
20	38.93824	0.97897
20	39.01381	0.97387
20	39.09030	0.96879
20	39.16774	0.96373
20	39.24614	0.95871
20	39.32552	0.95371
20	39.40592	0.94874
20	39.48736	0.94379
20	39.56987	0.93888
20	39.65347	0.93399
20	39.73820	0.92912
20	39.82409	0.92428
20	39.91118	0.91947
20	39.99950	0.91468
20	40.00400	0.91444

PROFILE NUMBER IS 20

NUMBER OF DIVISIONS ARE 34

BLADE NO.	SHOCK POSITION	UNINTERCEPTED WAVE POSITION
21	43.92199	44.56487

PROFILE NUMBER	PERIPHERAL DISTANCE	PRESSURE RATIO
21	40.00400	1.05018
21	40.04674	1.04659
21	40.08948	1.04303
21	40.13222	1.03951
21	40.17495	1.03602
21	40.21769	1.03257
21	40.26043	1.02914
21	40.30317	1.02576
21	40.34591	1.02240
21	40.38865	1.01907
21	40.43139	1.01578
21	40.47413	1.01252
21	40.51686	1.00930
21	40.55960	1.00610
21	40.60234	1.00293
21	40.64508	0.99980
21	40.71863	0.99448
21	40.79137	0.98930
21	40.86497	0.98415
21	40.93944	0.97903
21	41.01481	0.97393
21	41.09109	0.96887
21	41.16830	0.96382
21	41.24648	0.95881
21	41.32563	0.95383
21	41.40579	0.94887
21	41.48699	0.94394
21	41.56924	0.93903
21	41.65259	0.93415
21	41.73706	0.92930
21	41.82268	0.92448
21	41.90949	0.91967
21	41.99752	0.91490
21	42.00020	0.91475

PROFILE NUMBER IS 21 NUMBER OF DIVISIONS ARE 34

BLADE NO.	SHOCK POSITION	UNINTERCEPTED WAVE POSITION
22	45.92580	46.56687

PROFILE NUMBER	PERIPHERAL DISTANCE	PRESSURE RATIO
22	42.00020	1.05033
22	42.04306	1.04673
22	42.08592	1.04316
22	42.12877	1.03963
22	42.17163	1.03613
22	42.21449	1.03266
22	42.25735	1.02923
22	42.30021	1.02583
22	42.34307	1.02246
22	42.38593	1.01913
22	42.42879	1.01583
22	42.47164	1.01256
22	42.51450	1.00932
22	42.55736	1.00612
22	42.60022	1.00294
22	42.64308	0.99980
22	42.71663	0.99448
22	42.78937	0.98930
22	42.86297	0.98415
22	42.93744	0.97903
22	43.01281	0.97393
22	43.08909	0.96887
22	43.16630	0.96382
22	43.24448	0.95881
22	43.32363	0.95383
22	43.40379	0.94887
22	43.48499	0.94394
22	43.56724	0.93903
22	43.65059	0.93415
22	43.73506	0.92930
22	43.82068	0.92448
22	43.90749	0.91967
22	43.99552	0.91490
22	43.99820	0.91475

PROFILE NUMBER IS 22

NUMBER OF DIVISIONS ARE 34

BLADE NO.
23

SHOCK POSITION
47.92199

UNINTERCEPTED WAVE POSITION
48.56487

PROFILE NUMBER	PERIPHERAL DISTANCE	PRESSURE RATIO
23	43.99820	1.05033
23	44.04106	1.04673
23	44.08392	1.04316
23	44.12677	1.03963
23	44.16963	1.03613
23	44.21249	1.03266
23	44.25535	1.02923
23	44.29821	1.02583
23	44.34107	1.02246
23	44.38393	1.01913
23	44.42679	1.01583
23	44.46965	1.01256
23	44.51250	1.00932
23	44.55536	1.00612
23	44.59822	1.00294
23	44.64108	0.99980
23	44.71463	0.99448
23	44.78737	0.98930
23	44.86097	0.98415
23	44.93544	0.97903
23	45.01081	0.97393
23	45.08709	0.96887
23	45.16430	0.96382
23	45.24248	0.95881
23	45.32163	0.95383
23	45.40179	0.94887
23	45.48299	0.94394
23	45.56524	0.93903
23	45.64859	0.93415
23	45.73306	0.92930
23	45.81868	0.92448
23	45.90549	0.91967
23	45.99352	0.91490
23	45.99620	0.91475

PROFILE NUMBER IS 23

NUMBER OF DIVISIONS ARE 34

BLADE NO. 24

SHOCK POSITION 49.91999

UNINTERCEPTED WAVE POSITION 50.56287

PROFILE NUMBER	PERIPHERAL DISTANCE	PRESSURE RATIO
24	45.99620	1.05033
24	46.03906	1.04673
24	46.08192	1.04316
24	46.12477	1.03963
24	46.16763	1.03613
24	46.21049	1.03266
24	46.25335	1.02923
24	46.29621	1.02583
24	46.33907	1.02246
24	46.38193	1.01913
24	46.42479	1.01583
24	46.46764	1.01256
24	46.51050	1.00932
24	46.55336	1.00612
24	46.59622	1.00294
24	46.63908	0.99980
24	46.71263	0.99448
24	46.78537	0.98930
24	46.85897	0.98415
24	46.93344	0.97903
24	47.00881	0.97393
24	47.08509	0.96887
24	47.16230	0.96382
24	47.24048	0.95881
24	47.31963	0.95383
24	47.39979	0.94887
24	47.48099	0.94394
24	47.56324	0.93903
24	47.64659	0.93415
24	47.73106	0.92930
24	47.81668	0.92448
24	47.90349	0.91967
24	47.99152	0.91490
24	47.99420	0.91475

PROFILE NUMBER IS 24

NUMBER OF DIVISIONS ARE 34

BLADE NO.	SHOCK POSITION	UNINTERCEPTED WAVE POSITION
25	51.91799	52.56087

PROFILE NUMBER	PERIPHERAL DISTANCE	PRESSURE RATIO
25	47.99420	1.05033
25	48.03706	1.04673
25	48.07992	1.04316
25	48.12277	1.03963
25	48.16563	1.03613
25	48.20849	1.03266
25	48.25135	1.02923
25	48.29421	1.02583
25	48.33707	1.02246
25	48.37993	1.01913
25	48.42279	1.01583
25	48.46564	1.01256
25	48.50850	1.00932
25	48.55136	1.00612
25	48.59422	1.00294
25	48.63708	0.99980
25	48.71082	0.99446
25	48.78376	0.98927
25	48.85756	0.98411
25	48.93224	0.97897
25	49.00781	0.97387
25	49.08430	0.96879
25	49.16174	0.96373
25	49.24014	0.95871
25	49.31952	0.95371
25	49.39992	0.94874
25	49.48136	0.94379
25	49.56387	0.93888
25	49.64747	0.93399
25	49.73220	0.92912
25	49.81809	0.92428
25	49.90518	0.91947
25	49.99350	0.91468
25	49.99800	0.91444

PROFILE NUMBER IS 25

NUMBER OF DIVISIONS ARE 34

BLADE NO. 26

SHOCK POSITION 53.91599

UNINTERCEPTED WAVE POSITION 54.55886

PROFILE NUMBER	PERIPHERAL DISTANCE	PRESSURE RATIO
26	49.99800	1.05018
26	50.04074	1.04659
26	50.08348	1.04303
26	50.12622	1.03951
26	50.16896	1.03602
26	50.21169	1.03257
26	50.25443	1.02914
26	50.29717	1.02576
26	50.33991	1.02240
26	50.38265	1.01907
26	50.42539	1.01578
26	50.46813	1.01252
26	50.51086	1.00930
26	50.55360	1.00610
26	50.59634	1.00293
26	50.63908	0.99980
26	50.71282	0.99446
26	50.78576	0.98927
26	50.85956	0.98411
26	50.93424	0.97897
26	51.00981	0.97387
26	51.08630	0.96879
26	51.16374	0.96373
26	51.24214	0.95871
26	51.32152	0.95371
26	51.40192	0.94874
26	51.48336	0.94379
26	51.56587	0.93888
26	51.64947	0.93399
26	51.73420	0.92912
26	51.82009	0.92428
26	51.90718	0.91947
26	51.99550	0.91468
26	52.00000	0.91444

PROFILE NUMBER IS 26

NUMBER OF DIVISIONS ARE 34

BLADE NO.	SHOCK POSITION	UNINTERCEPTED WAVE POSITION
27	55.91980	56.56087

PROFILE NUMBER	PERIPHERAL DISTANCE	PRESSURE RATIO
27	52.00000	1.05018
27	52.04274	1.04659
27	52.08548	1.04303
27	52.12822	1.03951
27	52.17095	1.03602
27	52.21369	1.03257
27	52.25643	1.02914
27	52.29917	1.02576
27	52.34191	1.02240
27	52.38465	1.01907
27	52.42739	1.01578
27	52.47013	1.01252
27	52.51286	1.00930
27	52.55560	1.00610
27	52.59834	1.00293
27	52.64108	0.99980
27	52.71463	0.99448
27	52.78737	0.98930
27	52.86097	0.98415
27	52.93544	0.97903
27	53.01081	0.97393
27	53.08709	0.96887
27	53.16430	0.96382
27	53.24248	0.95881
27	53.32163	0.95383
27	53.40179	0.94887
27	53.48299	0.94394
27	53.56524	0.93903
27	53.64859	0.93415
27	53.73306	0.92930
27	53.81868	0.92448
27	53.90549	0.91967
27	53.99352	0.91490
27	53.99620	0.91475

PROFILE NUMBER IS 27 NUMBER OF DIVISIONS ARE 34

BLADE NO.
28

SHOCK POSITION
57.92179

UNINTERCEPTED WAVE POSITION
58.56287

PROFILE NUMBER	PERIPHERAL DISTANCE	PRESSURE RATIO
28	53.99620	1.05033
28	54.03906	1.04673
28	54.08191	1.04316
28	54.12477	1.03963
28	54.16763	1.03613
28	54.21049	1.03266
28	54.25335	1.02923
28	54.29621	1.02583
28	54.33907	1.02246
28	54.38193	1.01913
28	54.42479	1.01583
28	54.46764	1.01256
28	54.51050	1.00932
28	54.55336	1.00612
28	54.59622	1.00294
28	54.63908	0.99980
28	54.71282	0.99446
28	54.78576	0.98927
28	54.85956	0.98411
28	54.93424	0.97897
28	55.00981	0.97387
28	55.08630	0.96879
28	55.16374	0.96373
28	55.24214	0.95871
28	55.32152	0.95371
28	55.40192	0.94874
28	55.48336	0.94379
28	55.56587	0.93888
28	55.64947	0.93399
28	55.73420	0.92912
28	55.82009	0.92428
28	55.90718	0.91947
28	55.99550	0.91468
28	56.00000	0.91444

PROFILE NUMBER IS 28

NUMBER OF DIVISIONS ARE 34

BLADE NO.	SHOCK POSITION	UNINTERCEPTED WAVE POSITION
29	59.91799	60.56087

PROFILE NUMBER	PERIPHERAL DISTANCE	PRESSURE RATIO
29	56.00000	1.05018
29	56.04274	1.04659
29	56.08548	1.04303
29	56.12822	1.03951
29	56.17096	1.03602
29	56.21369	1.03257
29	56.25643	1.02914
29	56.29917	1.02576
29	56.34191	1.02240
29	56.38465	1.01907
29	56.42739	1.01578
29	56.47013	1.01252
29	56.51286	1.00930
29	56.55560	1.00610
29	56.59834	1.00293
29	56.64108	0.99980
29	56.71482	0.99446
29	56.78776	0.98927
29	56.86156	0.98411
29	56.93624	0.97897
29	57.01181	0.97387
29	57.08830	0.96879
29	57.16574	0.96373
29	57.24414	0.95871
29	57.32352	0.95371
29	57.40392	0.94874
29	57.48536	0.94379
29	57.56787	0.93888
29	57.65147	0.93399
29	57.73620	0.92912
29	57.82209	0.92428
29	57.90918	0.91947
29	57.99750	0.91468
29	58.00200	0.91444

PROFILE NUMBER IS 29 NUMBER OF DIVISIONS ARE 34

BLADE NO.	SHOCK POSITION	UNINTERCEPTED WAVE POSITION
30	61.92180	62.56287

PROFILE NUMBER	PERIPHERAL DISTANCE	PRESSURE RATIO
30	58.00200	1.05018
30	58.04474	1.04659
30	58.08748	1.04303
30	58.13022	1.03951
30	58.17296	1.03602
30	58.21569	1.03257
30	58.25843	1.02914
30	58.30117	1.02576
30	58.34391	1.02240
30	58.38665	1.01907
30	58.42939	1.01578
30	58.47213	1.01252
30	58.51486	1.00930
30	58.55760	1.00610
30	58.60034	1.00293
30	58.64308	0.99980
30	58.71063	0.99418
30	58.78937	0.98930
30	58.86297	0.98415
30	58.93744	0.97903
30	59.01281	0.97393
30	59.08909	0.96887
30	59.16630	0.96382
30	59.24448	0.95881
30	59.32363	0.95383
30	59.40379	0.94887
30	59.48499	0.94394
30	59.56724	0.93903
30	59.65059	0.93415
30	59.73506	0.92930
30	59.82068	0.92448
30	59.90749	0.91967
30	59.99552	0.91490
30	59.99620	0.91475

PROFILE NUMBER IS 30 NUMBER OF DIVISIONS ARE 34

BLADE NO.	SHOCK POSITION	UNINTERCEPTED WAVE POSITION
31	63.92380	64.56487

PROFILE NUMBER	PERIPHERAL DISTANCE	PRESSURE RATIO
31	59.99820	1.05033
31	60.04105	1.04673
31	60.08391	1.04316
31	60.12677	1.03963
31	60.16963	1.03613
31	60.21249	1.03266
31	60.25535	1.02923
31	60.29821	1.02583
31	60.34107	1.02246
31	60.38393	1.01913
31	60.42678	1.01583
31	60.46964	1.01256
31	60.51250	1.00932
31	60.55536	1.00612
31	60.59822	1.00294
31	60.64108	0.99980
31	60.71482	0.99446
31	60.78776	0.98927
31	60.86156	0.98411
31	60.93623	0.97897
31	61.01181	0.97387
31	61.08830	0.96879
31	61.16574	0.96373
31	61.24414	0.95871
31	61.32352	0.95371
31	61.40392	0.94874
31	61.48536	0.94379
31	61.56787	0.93888
31	61.65147	0.93399
31	61.73620	0.92912
31	61.82209	0.92428
31	61.90918	0.91947
31	61.99750	0.91468
31	62.00200	0.91444

PROFILE NUMBER IS 31

NUMBER OF DIVISIONS ARE 34

BLADE NO.
32

SHOCK POSITION
65.91999

UNINTERCEPTED WAVE POSITION
66.56287

PROFILE NUMBER	PERIPHERAL DISTANCE	PRESSURE RATIO
32	62.00200	1.05018
32	62.04474	1.04659
32	62.08748	1.04303
32	62.13022	1.03951
32	62.17295	1.03602
32	62.21569	1.03257
32	62.25843	1.02914
32	62.30117	1.02576
32	62.34391	1.02240
32	62.38665	1.01907
32	62.42939	1.01578
32	62.47213	1.01252
32	62.51486	1.00930
32	62.55760	1.00610
32	62.60034	1.00293
32	62.64308	0.99980
32	62.71663	0.99448
32	62.78937	0.98930
32	62.86297	0.98415
32	62.93744	0.97903
32	63.01281	0.97393
32	63.08909	0.96887
32	63.16630	0.96382
32	63.24448	0.95881
32	63.32363	0.95383
32	63.40379	0.94887
32	63.48499	0.94394
32	63.56724	0.93903
32	63.65059	0.93415
32	63.73506	0.92930
32	63.82068	0.92448
32	63.90749	0.91967
32	63.99552	0.91490
32	63.99820	0.91475

PROFILE NUMBER IS 32

NUMBER OF DIVISIONS ARE 34

BLADE NO.	SHOCK POSITION	UNINTERCEPTED WAVE POSITION
33	67.92379	68.56488

PROFILE NUMBER	PERIPHERAL DISTANCE	PRESSURE RATIO
33	63.99820	1.05033
33	64.04106	1.04673
33	64.08392	1.04316
33	64.12677	1.03963
33	64.16963	1.03613
33	64.21249	1.03266
33	64.25535	1.02923
33	64.29821	1.02583
33	64.34107	1.02246
33	64.38393	1.01913
33	64.42679	1.01583
33	64.46965	1.01256
33	64.51250	1.00932
33	64.55536	1.00612
33	64.59822	1.00294
33	64.64108	0.99980
33	64.71482	0.99446
33	64.78776	0.98947
33	64.86156	0.98411
33	64.93623	0.97897
33	65.01181	0.97367
33	65.08831	0.96879
33	65.16574	0.96373
33	65.24414	0.95871
33	65.32352	0.95371
33	65.40392	0.94874
33	65.48536	0.94379
33	65.56787	0.93888
33	65.65147	0.93399
33	65.73620	0.92912
33	65.82209	0.92428
33	65.90918	0.91947
33	65.99750	0.91468
33	66.00200	0.91444

PROFILE NUMBER IS 33 NUMBER OF DIVISIONS ARE 34

BLADE NO. 34

SHOCK POSITION 69.91999

UNINTERCEPTED WAVE POSITION 70.56288

PROFILE NUMBER	PERIPHERAL DISTANCE	PRESSURE RATIO
34	66.00200	1.05018
34	66.04474	1.04659
34	66.08748	1.04303
34	66.13022	1.03951
34	66.17295	1.03602
34	66.21569	1.03257
34	66.25843	1.02914
34	66.30117	1.02576
34	66.34391	1.02240
34	66.38665	1.01907
34	66.42939	1.01578
34	66.47213	1.01252
34	66.51486	1.00930
34	66.55760	1.00610
34	66.60034	1.00293
34	66.64308	0.99980
34	66.71663	0.99448
34	66.78937	0.98930
34	66.86297	0.98415
34	66.93744	0.97903
34	67.01281	0.97393
34	67.08909	0.96887
34	67.16630	0.96382
34	67.24448	0.95881
34	67.32363	0.95383
34	67.40379	0.94887
34	67.48499	0.94394
34	67.56724	0.93903
34	67.65059	0.93415
34	67.73506	0.92930
34	67.82068	0.92448
34	67.90749	0.91967
34	67.99552	0.91490
34	67.99819	0.91475

PROFILE NUMBER IS 34

NUMBER OF DIVISIONS ARE 34

BLADE NO.	SHOCK POSITION	UNINTERCEPTED WAVE POSITION
35	71.92379	72.56488

PROFILE NUMBER	PERIPHERAL DISTANCE	PRESSURE RATIO
35	67.99819	1.05033
35	68.04105	1.04673
35	68.08391	1.04316
35	68.12677	1.03963
35	68.16963	1.03613
35	68.21249	1.03266
35	68.25535	1.02923
35	68.29821	1.02583
35	68.34107	1.02246
35	68.38393	1.01913
35	68.42679	1.01583
35	68.46964	1.01256
35	68.51250	1.00932
35	68.55536	1.00612
35	68.59822	1.00294
35	68.64108	0.99980
35	68.71463	0.99448
35	68.78737	0.98930
35	68.86097	0.98415
35	68.93544	0.97903
35	69.01081	0.97393
35	69.08709	0.96887
35	69.16430	0.96382
35	69.24248	0.95881
35	69.32163	0.95383
35	69.40179	0.94887
35	69.48299	0.94394
35	69.56524	0.93903
35	69.64859	0.93415
35	69.73306	0.92930
35	69.81868	0.92448
35	69.90549	0.91967
35	69.99352	0.91490
35	69.99620	0.91475

PROFILE NUMBER IS 35

NUMBER OF DIVISIONS ARE 34

BLADE NO.
36

SHOCK POSITION
73.91999

UNINTERCEPTED WAVE POSITION
74.56288

PROFILE NUMBER	PERIPHERAL DISTANCE	PRESSURE RATIO
36	69.99620	1.05033
36	70.03905	1.04673
36	70.08191	1.04316
36	70.12477	1.03963
36	70.16763	1.03613
36	70.21049	1.03266
36	70.25335	1.02923
36	70.29621	1.02583
36	70.33907	1.02246
36	70.38193	1.01913
36	70.42479	1.01583
36	70.46764	1.01256
36	70.51050	1.00932
36	70.55336	1.00612
36	70.59622	1.00294
36	70.63908	0.99980
36	70.71282	0.99446
36	70.78576	0.98927
36	70.85956	0.98411
36	70.93424	0.97897
36	71.00981	0.97387
36	71.08630	0.96879
36	71.16374	0.96373
36	71.24214	0.95871
36	71.32152	0.95371
36	71.40192	0.94874
36	71.48336	0.94379
36	71.56587	0.93888
36	71.64947	0.93399
36	71.73420	0.92912
36	71.82009	0.92428
36	71.90718	0.91947
36	71.99550	0.91468
36	72.00000	0.91444

PROFILE NUMBER IS 36

NUMBER OF DIVISIONS ARE 34

BLADE NO.	SHOCK POSITION	UNINTERCEPTED WAVE POSITION
37	75.91799	76.56088

PROFILE NUMBER	PERIPHERAL DISTANCE	PRESSURE RATIO
37	72.00000	1.05018
37	72.04274	1.04659
37	72.08548	1.04303
37	72.12822	1.03951
37	72.17096	1.03602
37	72.21370	1.03257
37	72.25643	1.02914
37	72.29917	1.02576
37	72.34191	1.02240
37	72.38465	1.01907
37	72.42739	1.01578
37	72.47013	1.01252
37	72.51287	1.00930
37	72.55560	1.00610
37	72.59834	1.00293
37	72.64108	0.99980
37	72.71482	0.99446
37	72.78776	0.98927
37	72.86156	0.98411
37	72.93624	0.97897
37	73.01181	0.97387
37	73.08830	0.96879
37	73.16574	0.96373
37	73.24414	0.95871
37	73.32352	0.95371
37	73.40392	0.94874
37	73.48536	0.94379
37	73.56787	0.93888
37	73.65147	0.93399
37	73.73620	0.92912
37	73.82209	0.92428
37	73.90918	0.91947
37	73.99750	0.91468
37	74.00200	0.91444

PROFILE NUMBER IS 37

NUMBER OF DIVISIONS ARE 34

BLADE NO. 38 | SHOCK POSITION 77.32180 | UNINTERCEPTED WAVE POSITION 78.56208

PROFILE NUMBER	PERIPHERAL DISTANCE	PRESSURE RATIO
38	74.00200	1.05018
38	74.04474	1.04659
38	74.08748	1.04303
38	74.13022	1.03951
38	74.17296	1.03602
38	74.21570	1.03257
38	74.25843	1.02914
38	74.30117	1.02575
38	74.34391	1.02240
38	74.38665	1.01907
38	74.42939	1.01578
38	74.47213	1.01252
38	74.51486	1.00930
38	74.55760	1.00610
38	74.60034	1.00293
38	74.64308	0.99980
38	74.71682	0.99446
38	74.78976	0.98967
38	74.86356	0.98411
38	74.93823	0.97897
38	75.01381	0.97367
38	75.09030	0.96879
38	75.16774	0.96373
38	75.24614	0.95871
38	75.32552	0.95371
38	75.40592	0.94874
38	75.48736	0.94379
38	75.56987	0.93888
38	75.65347	0.93399
38	75.73820	0.92912
38	75.82409	0.92428
38	75.91118	0.91947
38	75.99950	0.91468
38	76.00400	0.91444

PROFILE NUMBER IS 38 NUMBER OF DIVISIONS ARE 34

BLADE NO.	SHOCK POSITION	UNINTERCEPTED WAVE POSITION
39	79.92380	80.56468

HARMONICS	SQUARE OF FOURIER COEFFICIENTS	DIFF. DB
1	0.00000001	-65.22817230
2	0.00000000	-67.11970901
3	0.00000002	-60.14904118
4	0.00000004	-56.98303175
5	0.00000001	-61.98793983
6	0.00000000	-66.28487206
7	0.00000001	-60.98696089
8	0.00000001	-62.55872536
9	0.00000000	-79.14916559
	0.00000000	-57.53439760
11	0.00000001	-62.80679893
12	0.00000001	-63.34286213
13	0.00000000	-68.56822777
14	0.00000010	-52.66038513
15	0.00000001	-61.79077435
16	0.00000001	-60.94420767
17	0.00000003	-58.63748312
18	0.00000000	-67.21824551
19	0.00000000	-107.25383282
20	0.00000000	-67.08266449
21	0.00000003	-58.39634929
22	0.00000002	-60.57851362
23	0.00000001	-61.37219572
24	0.00000012	-51.91079950
25	0.00000000	-67.85567093
26	0.00000001	-62.24756813
27	0.00000001	-61.57402783
28	0.00000005	-55.93922091
29	0.00000000	-76.75327015
30	0.00000002	-60.15937948
31	0.00000003	-58.07981253
32	0.00000001	-62.50639486
33	0.00000003	-57.32808447
34	0.00000015	-50.99050713
35	0.00000011	-52.23625040
36	0.00000004	-56.11863327
37	0.00000025	-48.60930729
38	0.01829310	0.

SAMPLE CALCULATIONS

A sample calculation for the spacing error distribution study, A-1 of Table 2, is listed here. The flow data and airfoil shapes are those listed in Table 1.

EMACH = 1.4

THETA = 72

NB = 38

NS = 90

YMAX = 10.0

NSEG = 5

NPRO = 3

NSLO = 2

MMM = 15

ISOP = 1

SPACG(I) = see A-1 of Table 1

ISTAGR = 2

STAGR(I) = 65.0

IBSURF = 2

COEFF(I,1) = 0

COEFF(I,2) = 0.17633

COEFF(I,3) = -0.0555

SCOEF(I,1) = 1.58855

SCOEF(I,2) = -9.009

In the output, first the input data are printed out. After that, the pressure distribution at a given axial distance upstream of the rotor will be given. "SEGMENT NUMBER N" designate the pressure distribution at an axial distance equal to YMAX × N/NSEG. Next the pressure distribution will be given blade after blade. "PROFILE NUMBER" is not equal to blade number. For example, the pressure distribution at profile number 1 means the pressure distribution between the shock waves emanating from the second and the third blades. "PERIPHERAL DISTANCE" is measured from the intersection of the bow shock emanating from the second blade and the axial distance upstream of rotor in question. "PRESSURE RATIO" is the ratio of static pressure to the static pressure at infinity. The peripheral position of the shock and unintercepted Mach wave are printed under the heading of "SHOCK POSITION" and "UNINTERCEPTED WAVE POSITION". The origin of these positions are the leading edge of the second blade. After the printout of pressure profiles, the harmonic content of the pressure distribution are given. "HARMONICS" designates the harmonics of shaft frequency. "SQUARE OF FOURIER COEFFICIENTS" is the (amplitude of N-th harmonics × 2π)^2. Sound power level of the harmonics, the BPF as base, is listed under the heading of "DIFF. DB".

NASA-Langley, 1971 —— 12